Investigation of Rain Effect on MIMO Systems at Microwave and Millimeter wave bands

Student Name: Kirubel Abiyu

A thesis submitted to the department of Electronics and Communication Engineering

School of Electrical Engineering and Computing

Presented in Partial Fulfillment of the Requirement for the Degree of Masters in Electronics and Communication Engineering

Office of Graduate Studies

Adama Science and Technology University

Adama

July, 2019

Investigation of Rain Effect on MIMO Systems at Microwave and Millimeter wave bands

Student Name: Kirubel Abiyu Tiruneh

Advisor: Dr. Feyisa Debo Diba (Ass. Prof)

A thesis submitted to the department of Electronics and Communication Engineering

School of Electrical Engineering and Computing

Presented in Partial Fulfillment of the Requirement for the Degree of Masters in Electronics and Communication Engineering

Office of Graduate Studies

Adama Science and Technology University

Adama

July, 2019

Approval of Board of Examiners

We, the undersigned, members of the Board of Examiners of the final open defense by______ ____ ____have read and evaluated his thesis entitled "____ ____" and examined the candidate. This is, therefore, to certify that the thesis has been accepted in partial fulfillment of the requirement of the Degree of ………………………………………………………………..………………

Supervisor /Advisor	Signature	Date
Chairperson	Signature	Date
Internal Examiner	Signature	Date
External Examiner	Signature	Date

DECLARATION

I hereby declare that this MSc thesis is my original work and has not been presented for a degree in any other university, and all sources of material used for this thesis have been duly acknowledged.

Name: ____

Signature: ____

This MSc thesis has been submitted for examination with my approval as thesis advisor;

Name: ____

Signature:____

Date of submission:……………………….

ACKNOWLEDGEMENTS

I would like to take this opportunity to express my heartfelt thanks for my supervisor, Dr. Feyisa Debo. I thank him for his unreserved support, openness to discussion and calming influence. Thank you for tolerating me when I had trouble with my work. Without him, it would not have been possible to be here now.

I would like to thank Adama Science and Technology University Electrical Engineering and Computing Department, the instructors, the school dean and the chair person for all the effort that has been put to run this program successfully.

I would also like to thank my colleagues at work place who covered for me without complain when I had to go away for research related tasks. Special thanks to Eyerusalem Tadesse, a dear friend at work, without whose persistence I could not have started this altogether.

CONTENTS

List of Tables

Table of Figures

List of Acronyms

CBSMs	Correlation Based Stochastic Models
CCIR	Consultative Committee for International Radio Communication
CF	Cumulative Frequency
CSIT	Channel State Information at The Transmitter
DSD	Drop Size Distribution
ECMWF	European Centre For Medium-Range Weather Forecast
ERA	Environmental Risk Assessment
EXCELL	Exponential Distributed Rain Rate Rain Cell Model
GBSMs	Geometry Based Stochastic Models
GPCC	Global Precipitation Climatology Centre
GUI	Graphical User Interface
HYCELL	Hybrid Rain Cell Model
I.D.	Independent Identically Distributed
ITU	International Telecommunication Union
ITU-R P	International Telecommunication Union Recommendation Publication
JWD	Joss-Waldvogel Distrometer
KBSM	Kronecker Based Stochastic Model
LP	Laws and Parsons Drop Size Distribution Model
MIMO	Multi Input Multi Out Put

MP	Marshall- Palmer Drop Size Distribution Model
NMA	National Metrology Agency
RCS	Rain Cell Size
RH	Rice-Holmberg Rain Rate Prediction Model
RMSE	Root Mean Square Error
RSL	Received Signal Level
Rx	Receiver
SG	ITU's Study Group
SISO	Single Input Single Output
Tx	Transmitter
VCR	Virtual Channel Representation
WRC	World Radio Conference

Abstract

The rapid growth of bandwidth, data rate and availability requirements is pushing for deployment of new schemes that can meet these requirement. MIMO systems deployment in microwave and millimeter wave bands looks to be a hugely promising approach in this regard. However, these spectra are highly affected by precipitation phenomena. So, it is imperative to deal with the performance limits of MIMO systems under rain, the principal degradation mechanism in these ranges of frequency and the dominant precipitation mechanism in Ethiopia.

In the process of assessing the effect of rain on millimeter and microwave MIMO systems, the research work has tried to model the 1-minute integration time rain fall rate statistics of various locations in Ethiopia based on as much information as it was possible to gather locally. The deficiency of some widely used rain rate prediction approaches in relation to Ethiopia’s climate has been shown. Hence, a new improved rain rate integration time conversion method, based on 1-minute rain rate data from Jimma, has been used with good results. New $R_{0.01}$ value for Jimma, Bahirdar, Addis Ababa and Mekele were calculated as 122.9, 130.49, 71.8 and 74.64 mm/h. In relation to this the worst-case rain cell size has been calculated.

The distribution of rain drops, which are the agents of attenuation and scattering effects of rain, has been researched. Drop size distribution models have been compared for use in the research work for some locations in Ethiopia. The inaccuracy of models devised for temperate region of the world, which ITU uses for global attenuation prediction, has been shown. Tropical drop size distribution models, which better represent locations within Ethiopia than temperate models, have been used for attenuation calculation and determination of the propagation parameters; extinction, absorption, scattering coefficient and the anisotropy factor. In line with that new specific attenuation values are calculated based on adapted drop size distribution models. As large as 20dB/Km of difference was found between ITU's prediction and local data.

The effect of rain on MIMO link capacity has been investigated. The system capacity performance has been compared under different scenarios. It has been shown that, while system performance like attenuation degrading system capacity increase with rain rate, there are circumstances where rain can also cause enhancements to capacity. It is demonstrated that these

rain rates, described as “best rate” rates, differ for varying distribution models and the signal to noise ratio of the link.

Finally, the research concludes by indicating future research areas related to this research work. The field of study could be fine-tuned by furthering the study on variability of rain rate along a signal path (spatial distribution of rain rate), effect of non-sphericity of rain drops and effect of antennal linkage on MIMO performance. The use of channel state information for mitigation has been recommended.

CHAPTER ONE

1. Introduction

1.1. Background of the study

The communication industry is witnessing relentless expansion of interest in the wireless branch. This mode of communication has attracted attention of all kinds of users and service providers. Its far-reaching impact could easily be seen by the proliferation of mobile phone users throughout the world. Simply put, the importance and the influence of wireless communication in the day to day lives of the public can't be over emphasized judging from the fact that our mobile devices have become an integral part of our daily routine.

The proliferation of new applications based on wireless network of sensors such as smart homes, automated highways and factories are but a few examples of the upcoming uses wireless communication. Nevertheless, there are still technical challenges that need solving before we could benefit the full advantages of wireless communication.

One of the limiting factors of wireless communication has been scarcity of frequency bandwidth [1, 3]. In a move to alleviate this problem there have been efforts to use higher frequency bands, millimetric and microwave spectrum with multiple antennas at the transmit and receive stations. For instance, the World Radiocommunications Conference WRC15 identified a number of frequency bands between 24 and 86GHz as candidate frequencies for future cellular networks [4]. Sure, the problems of bandwidth and data rate can ideally be solved with the introduction of these bands of frequency into the realm wireless communication. In addition, there are other benefits to be gained in these ranges of frequency. Some of these benefits include smaller component size, narrow beam widths, smaller antennas. But there is a catch.

The propagation medium plays a huge part in these sections of frequency bands and has to be given sufficient design consideration if the aforementioned benefits of the microwave and millimetric band are to be ripped. Because the propagation medium contains many components whose effects get pronounced at these range of frequencies [1, 5]. These constituents of the medium which can be rain, snow, water vapor and other gases in the atmosphere are generally called fade phenomena. These are broadly classified as clear air and precipitation mechanisms. Some of these mechanisms are absorption, scattering, refraction, diffraction, multipath, scintillation and frequency dispersion [3, 6]. These negatively affect the reliability and quality of service of communication systems by affecting parameters of signal. The affected parameters are the signal amplitude, phase, polarization, frequency, bandwidth and angle of arrival [3, 6]. The most significant factor that affects the transmission of signals at these bands are scattering and attenuation.

The primary aim of a communication system is to guarantee certain level of availability and quality of service [2, 13]. So, it becomes apparent that in order to guarantee certain level of quality of service and reliability, the factors affecting the signal transmission should be modeled/predicted as accurately as possible. This will help eliminate design errors that lead to dysfunctional system with low availability and high BER. The application of fade mitigation techniques comes into play here. Fade mitigation techniques generally are used to enable the system to continue delivering service to customers even when higher than normal fade attenuation is happening.

MIMO systems are one of the enabling technologies of future high-speed wireless networks. Hence, the capacity of these frequency bands to support MIMO communication and the effect of rain (since it is the dominant factor in the propagation and could be said the prevalent form of precipitation all over Ethiopia) should be researched and made available to the network designer and academicians alike.

There has been only limited number of studies conducted and this area remains unexplored. The research work presented in this research aims to bridge this gap by modeling MIMO system that could be applied considering the peculiarities of rain profiles. The model developed can be used to prepare rain fade mitigation techniques to counteract negative effects of rain on communication links. Rain being the most fundamental form of precipitation fade mechanism in most part of Ethiopia, the research will try to model the propagation medium under rainy conditions.

1.2. Statement of the problem

The area of wireless communication has seen and is continuing to entertain an ever-increasing data rate and reliability (system availability) demands as the type and size of content shared by users increase. Needless to say, the allotted bandwidth is already congested. Thus, service providers are forced to look for other means to meet these high data rate and bandwidth requirements [7].

Since higher frequencies can satisfy the need for increased data rate, naturally communication research attention to investigation into the practical usability of these untapped frequency range [6]. Couple this with additional advantage of MIMO systems, even greater capacity limits can be attained. However, the effect of rain in the millimeter and microwave ranges limit the performance of MIMO systems. And this depends on the peculiarity of the location. The geographic location of a particular link has close relationship with the frequency and intensity of rain phenomena that cause fades. MIMO systems designed in a temperate region couldn't work effectively say in tropical areas for the reason explained above.

So, it was imperative to make this study taking into all local weather factors into consideration. This included determination of proper rain rate profile of the area, DSD profile, attenuation prediction and stochastic MIMO channel modeling which by themselves qualify as research ideas. The study also suggested ways to mitigate rain fades and effective utilization of transmission power based on available channel information.

1.3. Objectives,

1.3.1. General objective

The general objective of the study has been the study of rain fall effects on a millimeter and microwave-based MIMO system. It aims to establish performance limits that can be guaranteed under particular rain rate and drop size distribution of a given location. Peculiarities of Ethiopian climate have been taken into consideration in the assessment.

1.3.2. Specific objective

The study had to answer the following research questions to fully characterize millimeter/microwave MIMO systems under rainy conditions. It is based on answers (findings regarding) to these questions in a step by step manner has led to the formulations made by the research. The list below describes the specific research questions that were addressed in different phases of the research work.

- Determination of rain rate exceeded for 0.01% the time. The determination of $R_{0.01\%}$ required data collection filtering and statistical analysis. The best approach for conversion of rain integration time from 15 minutes to 1-minute was applied.
- Calculation of rain cell sizes to know the extent of rain traversed communication path. This helped to determine the range of application of calculations.
- Owing to lack drop size measurement, finding a proper drop size distribution that could describe rain phenomena in Ethiopian locations. Some prominent DSD models have been compared.
- Stochastic MIMO channel modeling. Selection of models that serve purpose of this particular study from among number of options was considered.
- And finally, simulation of performance of MIMO channels using an appropriate simulation tool.

1.4. Significance of the study

Researchers like Diba Feyisa [8] has modeled radio wave propagation under precipitation and clear air circumstances based LOS SISO links in the millimeter and microwave range. He has put forward important findings regarding single input single output configuration. There are other similar works on millimeter and microwave links in Africa by Sumbiri et al [9], Alonge A. A. and Afullo T. J [10], Odedina M. O and Afullo T. J [11], Ojo J. S et al [12].

To the knowledge of the researcher study of performance of MIMO systems under Ethiopia's peculiar rain distribution and climate has not been conducted. So, the potential of MIMO systems remains unexplored.

This research work thus will bridge the gap in this area. It is a material that can be used as a stepping stone for future endeavors in propagation studies conducted in the microwave and millimeter range of spectrum. Service providers alike can use the procedure outline for rain rate prediction, attenuation calculation for power budget determination and system performance limits in terms of available capacity. By clearly showing how system capacity is affected as function of rain rate, frequency and drop size concentration, the study helps prepare fade mitigation techniques.

1.5. Limitations of the study

As has been described the primary purpose of the research work has been the study of effect of rain on MIMO systems. There are assumptions which have been taken in order to reach that specific target. Without these assumptions it would not have been able to conclude the research work within these pages. So, in a view to narrow the focus of the research work, the following limitations have been taken into consideration.

- Spherical shape of rain drops has been assumed. This choice has implications about depolarization effect of rain drops which by itself is a huge research topic.
- Owing to lack of DSD measurements the research had to use some tropical DSD models.
- Owing to lack of 1-min integration time rain rate data for locations other than Jimma, rain rate conversion procedure based on 1-min rain data from Jimma has been used. Although this approach produced better estimation results than some global models, it still needs to be refined with local rain rate measurement data.
- Effect of linkage between elements of antenna array has not been considered.
- The MIMO system considered is based on fixed links. Issue of mobility is left for future researches.

CHAPTER TWO

2. Literature Review

2.1. Introduction

The efforts to meet customers' data rate, band width and availability requirements have been intensified in a move to keep up with the demands. Ways to exploit the untapped frequency spectrum in the millimeter and microwave range are being studied relentlessly. One of the major limiting influences posed happens to come from the interaction of precipitation particles. Rain is the major culprit that reduces the capacity of links on millimeter and microwave bands by causing attenuation and scattering [3, 6].

MIMO systems have emerged as an attractive technological breakthrough alternative to use the same frequency to increase availability of service or data rate without expenditure of additional power. So, investment into study of ways to exploit the rich potential MIMO holds will pay huge dividends. The effects of rain on MIMO links have to be researched in a way that considers the peculiarity of rain distribution of the area. This will help service providers to be on terms promises they make to their customers. Another advantage of such studies is that they will help in finding the right fade mitigation techniques.

The purpose of this section is to present a review of research works conducted in areas related to propagation of millimeter and microwave EMW through rain. The subject matter is a combination of studies on many supporting ideas which are, to name a few, establishing dependable rain rate statistics of the area in question, determination of extent of rain coverage, modeling of the drop size concentration, determination of propagation factors like attenuation, scattering, MIMO system modeling.

This literature review gives a comprehensive review of important works that have been accomplished in a view to lay the foundation for this research work. Modeling approaches deemed fit for this current work are indicated explicitly.

2.2. Rain rate distribution

A common requirement of any precipitation media propagation study is a rain distribution profile of a location obtained with fast response rain gauges. One-minute integration time rain fall rate data is a conventional threshold [13, 14]. The problem is rainfall rate data sampled with such short time are a scarcity because most meteorological bureaus need not collect such short-time sampled rainfall data for obvious reason that it is the volume of the rain fall over a period is usually the most important parameter. Therefore, the rain fall databases usually are filled with higher integration time data, of 5-min at best and 1-hr or longer at worst [14]. So, it is imperative to have a good approach in place for rain rate integration time conversion for scenarios where local 1-min rain intensity data is not available.

2.2.1. Rian rate integration time conversion

R. Crane [14] and Ajayi and Ofoche [1] demonstrated that longer integration times hide higher rain rate samples and thereby alter the distribution profile. Figure 2-1 demonstrated loss of data inherent in higher integration time rain rate distributions. The researchers employed fast response (fastest being 10s) rain gauges between September , 1979 and December , 1981 in Ile Ife, Nigeria . The figure shows the rain fall rate CD plots for various integration times, 10sec, 1-min, 2-min, 5-min, 10-min, 20- min. This has led to researches on methods to be able to infer shorter integration time data from longer available rain fall rate data. many works have been published that describe various methods of integration time conversion [6].

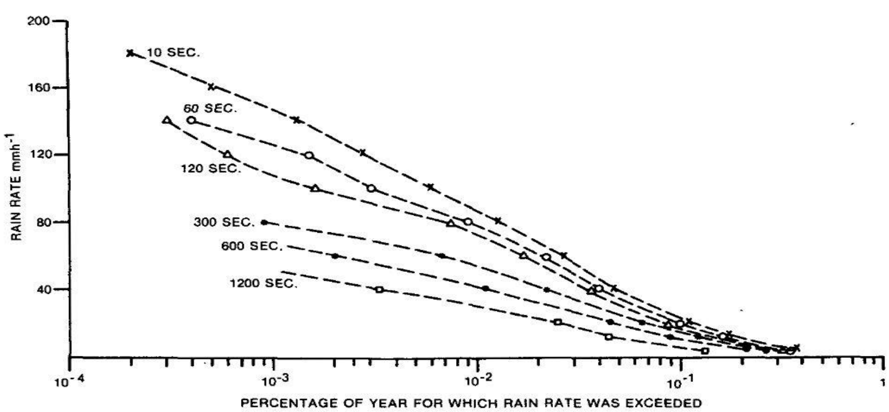

Figure 2-1. Showing loss of data by higher integration time rain gauges [1]

In trying to find the equivalent short integration time rain rate data from higher integration time data, different approaches have been proposed [6, 15]. Capsoni et al [16] classified these methods in three broad categories. These are known as physical, analytical and empirical methods.

The first class of the methods try to incorporate physical rain formation process by means of parameters into the model to capture the peculiarity of the location. The Rice-Holmberg [17], Dutton-Dougherty-Martin Models [18], EXCELL [19] and Lavergnat-Golé [20] models fall into this category. Most of the physical approaches need understanding or the physical rain formation process . As there are many factors involved the number of variable parameters under consideration become too many to apply to our situation. It has to be mentioned, though, that the method of Rice-and-Holmberg lends itself for simplest of manipulations basing the rain rate calculation procedure on two parameters as shown in the formulae below in equation (2-1).

$$P(\%) = \frac{T_1(R)}{87.66} \qquad (2\text{-}1)$$

where

$T_1(R) = M(0.03\beta \exp(-0.03R + 0.2(1-\beta)[\exp(-0.258R) + 1.86\exp(-1.63R)])$ and P(%) is a probability estimate of 1-min integration time rain rate, M the mean yearly rain fall accumulation and β, the thunderstorm ratio of the yearly rain fall accumulation thought of as comprising thunderstorm (M_1) and other type (M_2) of rain fall. Rice and Holmberg [17] gave contour maps indicating yearly mean rainfall accumulation and the value of β all over the world. Ethiopia is represented as having values of 500mm and 1000mm yearly rain accumulation(M) as shown in Figure 2-2and 0.2 as the value of β. Feyisa [7] used this model in conjunction with Chebil [21] model to predict the rain fall cumulative distributions of various locations in Ethiopia in the absence of recoded data.

Analytical approaches try to find a mathematical model for a probability function that could describe the rain rate distribution of the area. The model proposed by Moupfouma [22] is probably the most renowned analytical rain rate distribution model. Its fame has to do with the fact that it includes local climatic influence by its parameters. In his previous work Moupfouma,[23], proposed a semi empirical prediction model for cumulative distribution given in (2-2). The model resembles gamma distribution at higher rain rates and log-normal at lower rates.

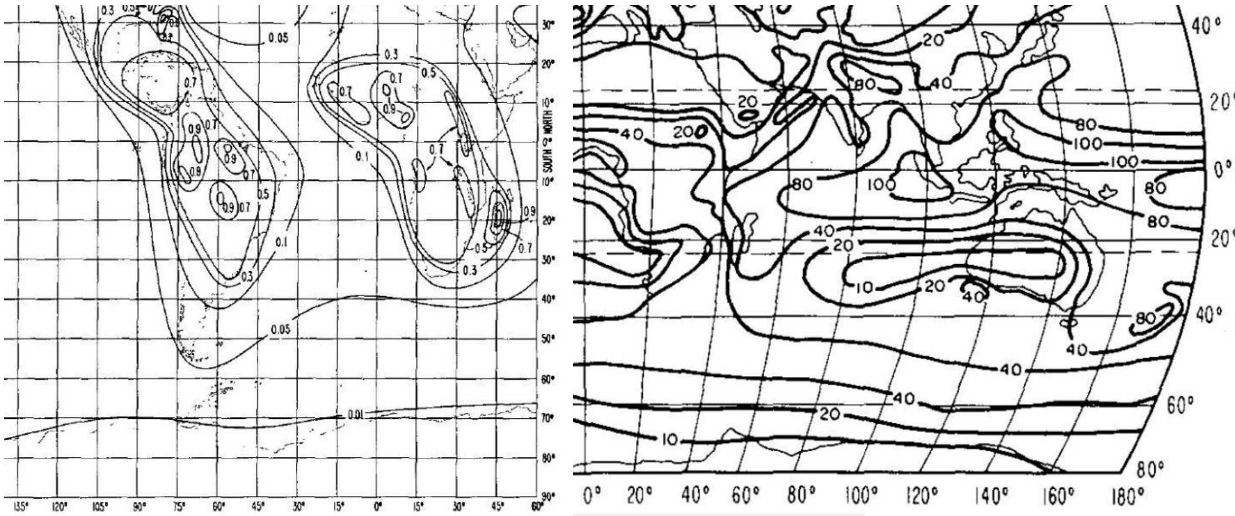

(a) (b)

Figure 2-2.(a);values of β,(b); thunderstorm accumulation M contour lines [17]

$$P(R \geq r) = \frac{a}{r^b} \times e^{-u \times r} \tag{2-2}$$

The new model is based on available rain rate $R_{0.01\%}$ and was approved and incorporated by the ITU-R to predict cumulative rain rate distributions for all kinds of weather. It is given by;

$$P(R \geq r) = 100 \left(\frac{R_{.01}+1}{r+1}\right)^b e^{u(R_{.01}-r)-ln\,10^4} \tag{2-3}$$

with

$$b = \left(\frac{r}{R_{.01}} - 1\right) ln\left(1 + \frac{r}{R_{.01}}\right), \tag{2-4}$$

Where u is a climate parameter depending on the integration time, can thus be expressed according to the climate as follows;

For equatorial (tropical and sub-tropical) localities

$$u(r) = \frac{ln\,10^4}{R_{.01}} e^{(-\lambda(\frac{r}{R_{.01}})^\gamma} \tag{2-5}$$

with

$\lambda = 1.066$ and $\gamma = 0.214$ for tropical regions

The model also gave a different expression and set of values to be used for temperate regions There is need of determining six variables (a, b and u) for each integration time during the conversion process. This means, complete knowledge about the distribution of rain rate in the two contrasting integration times is necessary, which was not available for this work.

The third group of rain rate integration time conversion approach known as empirical method. Empirical models describe the relationship between equiprobable rain rates of two different integration time measurements by a simple mathematical model. The mathematical model more often is expressed by a power or exponential law shown in (2-6). The simplicity of the model has led to the widespread use of this model in rain rate conversion attempts the world over [15].

$$R_1(P) = aR_T(P)^b \qquad (2\text{-}6)$$

where R_1 and R_T are rain rates at equiprobable probability P; a and b and coefficients of conversion to be determined empirically. Authors like [6, 13, 24] have used the above model of rain rate conversion.

The prediction method used by ITU-R P.837-6 [13] was formulated based on two weather parameters. The first is the total monthly rainfall data generated from the GPCC Climatology (V 2015) database over land and from the European Centre for Medium-Range Weather Forecast (ECMWF) ERA Interim re-analysis database over water. The second is monthly mean surface temperature data in Recommendation ITU-R P.1510 [25]. There is a software package with GUI implemented using MATLAB that one can make conversions from user input higher integration time data to 1min data. The publication presents global coefficients for power law conversion from 5, 10, 20, 30 min integration time rain rate data in to 1-min integration time equivalent. These coefficients are given in Table 2-1.

Table 2-1.Global regression coefficients by ITUR-P.387-6 for power law conversion [13]

T(min)	5	10	20	30
A	0.986	0.919	0.68	0.564
b	1.038	1.088	0.68	0.564

Ajayi and Ofoche [1] applied the power law relationship to convert fast response gauge rain data into higher integration time equivalent. The researchers obtained coefficient for the power law conversion method between different integration times starting from 10s to 1, 2, 5, 10 and 20 minutes for Ile- Ife, Nigeria. The coefficients are displayed in Table 2-2.

Table 2-2. Coefficients for $R_{\tau} = aR_{T}^{b}$ τ = 10 s,1min,2min and T=1,2,510,20 min [1].

T (min)	τ = 10 s		τ = 1min		τ= 2min s	
	a	b	a	b	a	b
1	1.174	0.992	-	-	-	-
2	1.026	1.046	0.872	1.055	-	-
5	1.155	1.091	0.991	1.098	1.138	1.039
10	2.076	1.011	1.797	1.016	2.011	0.960
20	5.012	0.846	4.311	0.853	4.602	0.805

The other approach starts by defining a conversion factor, which is the dividend between rain rates of the two integration times at equal probability of exceedance. Then these factors are fitted as an exponential or power law functions of the percentage probability. The set of equations below define the method.

$$CF(P) = \frac{R_1(P)}{R_T(P)}, \quad (2\text{-}7)$$

$$CF(P) = aP^b, 0 < P < 1. \quad (2\text{-}8)$$

$$CF(P) = aP^b + c(e^{dP}), 0 < P < 1 \quad (2\text{-}9)$$

The equation in (2-8) was proposed by B. Segal [26] and (2-9) by Chebil J. and Rahman T. A. [21]. The choice a particular approach is decided in the chapter 3.

2.3. Rain cell size determination

Accurate calculation of attenuation statistics requires complete knowledge not only about the intensity and distribution of those agents but also about the length of the link's span traversed. In particular, the size of rain cells is of great importance in the study of attenuation characteristics of millimeter and microwave transmissions. Rain rate measured by rain gauges is generally assumed to be a result of moving rain cells. There have been several attempts made to get mathematical description of the rain cell size by [19, 27-29], each justifying use of certain assumptions based on the geographic area in question. A summary the models derived by the above authors is discussed next.

Capsoni C. et al [27] emphasized the difference of effects of light rain regime and intense shower events on radio wave propagation, thus drawing attention to the need to clear distinction between stratiform and convective form of rain. Radio communication group SG3, while developing ran statistics conversion model, employed the EXCELL rain cell model to describe the shape and size of rain cell structure and the rotational symmetry and exponential spatial distribution of rain intensity. A distinction was made between stratiform and convective forms of rain. This formulation could be summarized in the following expression defined in terms of peak rain rate (R_M) and the equivalent rain cell diameter, ρ_o, the distance from the center of the cell to where the intensity falls below R_M/e.

$$R(\rho) = R_M e^{-\frac{\rho}{\rho_o}} \qquad (2\text{-}10)$$

where ρ is distance from the center.

The above rain cell model defined in (2-11) implies that rain cells extend to infinity. A new model addressing this problem was proposed by Capsoni and Luini [30]. It introduced the "lowered EXCELL" model by incorporating a limiting rain rate value R_{low} which is the minimum rain rate achievable at a max radius ρ_{max} after which the cell ceases to exist (R(p)=0). This formulation is given below:

$$(R_M + R_{low})e^{\frac{\rho}{\rho_o}} - R_{low} \quad \rho \leq \rho_{max} \qquad (2\text{-}11)$$

$$R(\rho) = 0 \qquad \rho > \rho_{max} \qquad (2\text{-}12)$$

Although the wind velocity v_{700} at an altitude equivalent to 700 hPa isobar (around 3000 m above the ground) can be taken as a good estimation of the rain cell translational speed, the rain cell structure is subject both to both translation and to morphological modifications. Capsoni and Luini [30] in an earlier paper suggested a wind speed corresponding to 600hPa isobar (4000-4200m of altitude). Discrimination of rain cell types is made based on the cause behind translational speed, either morphological evolution (stratiform) or wind (convective). The study also showed the dependence of translational speed on integration time confirming formation of clear morphological rain cell structures as the integration time lengthens. The dependence of translational speed on integration time T was formulated in the following expression:

$$v_{conv}(T) = \frac{v_{700}}{k_1(T)} \qquad (2\text{-}13)$$

$$v_{strat}(T) = k_2(T)v_{conv} \qquad (2\text{-}14)$$

Dependence of $k_1(T)$ and $k_2(T)$ on integration has been given based on the rainfall statistics database gathered from 6 locations, i.e., Montreal (Canada) and Prague (Czech Republic) in the cold region; Spino d'Adda (Italy) and a site in Florida (USA) in the temperate region; Ji-Paranà (Brazil) and Chorillos (Colombia) in the tropical region.

$$k_1(T) = 0.185T^{0.498} + 0.768 \qquad \textit{for } 5<T<60 \textit{ minutes} \qquad (2\text{-}15)$$

$$k_2(T) = -0.017T^{0.746} + 0.69 \qquad \textit{for } 5<T<60 \textit{ minutes} \qquad (2\text{-}16)$$

It is now a common practice to assume to classify rain rate values from 10 to 15mm/h as stratiform type.

P. O. Akuon and T. J. O. Afullo [31] applied the "synthetic storm" technique and assumed circular rain cells in determining the rain cell size in three regions in south Africa. The use of an average advection velocity, despite the continuous change in drop size implying varying advection velocity, was employed in translating the point rain rate data into distance series data.Advection velocities of 6m/s and 10m/s were used for rain rate categories R<12 mm/h and R>12mm/h respectively . The researchers used the method pointed out by Goldhirsh and Julius [29] to extract the power law relationship between the rain rate and rain cell size. P. O. Akuon and T. J. O. Afullo [24] presented a method to extract rain cell size from point rain rate data. This approach is detailed in the methodology section 3.3.

2.4. Rain drop size distribution

The rain drop size distribution (DSD, quantity symbol N) represents the probability density of equivolumetric drop diameter D being in the unity volume(m-3). The product N(D) dD gives the number of rain drops of the diameter between D and D+dD in the unity volume. Only rain drops of diameters below 7 mm can exist for physical reasons [32], [33]. Ross Gunn and Gilbert D. Kinzer [34],in their study titled “the terminal velocity of fall for water droplets in stagnant air”, state that mechanically stable rain droplet size doesn’t exceed a diameter of about 6mm. The pioneering work by Laws and Parsons [33] indicated the rapidly dwindling contribution of smaller diameter droplets to the total distribution of drop sizes as the rain rate increase.

To study propagation characteristics of microwave and millimeter wave transmissions through rain, one requires drop size distribution models for the area in study. Such models have been touted as a convenient means for attenuation and scattering analysis. There are only limited number of droplet size measurements generally. The cost of the device is a big hampering issue. Different devices with varied principle of measurement have been used by researchers. A videodistrometer is the most advance and user friendly version to date [32]. An electromechanical distormeter developed by Joss-Wadvogel is a widely used source of raw DSD data. T

here are occasions where optical measuring devices were used for the same purpose.

There are a number of models in use worldwide. Among these the most renowned and earliest models are the Marshall and Palmer [35], Laws and Parsons [33], of Joss et al and Ulbrich [36]. The Laws and Parsons model was the standard model in practice. It was accepted by International Radio Consultative Committee (CCIR) for the calculation of specific attenuation. The M-P model was applied by numerous researchers as well [37-40]. The next sections are dedicated to concise review of the major models for rain drop size distribution that are being used by radio science researchers.

2.4.1. Marshall Palmer DSD

In 1947, Marshall and Palmer [35] carried out an experiment to measure the size and number ofdrops in rain and produced analytical expression. The experimental setup included dyed filter paper. The expression gives the drop concentration as a function of rain drop diameter interval and rain rate. It is given in (2-17).

$$N(D) = N_0 exp(-\Lambda D), \quad (2\text{-}17)$$

where

$N_0 = 8000 m^{-3} mm^{-1}$ and $\Lambda = 4.1R^{-0.21}$

The original researchers have pointed out that the above negative exponential model fails to match experimental data at lower diameter range . The researchers acknowledged that the model overestimates below drop diameter of 1.5mm.

Another pioneering work that has to be mentioned alongside MP model is the work of Laws and Parsons [33]. The researchers studied the drop size distribution to understand the effect it had on soil erosion . The researchers used a technique that included used of flour . Some of the conclusions and recommendations made by LP are;

- The median drop size doesn't show significant change with change of rain rate. A 400-fold increase in rain rate only resulted in the median drop size jumping to the third higher drop size class.
- The largest drop size for even the most intense rain fall is around 7mm in diameter.

One key observation from (2-17) is that, the above negative exponential model is a monotonically decreasing function of drop size . This means the effect of small sized rain drops on any attenuation or scattering study is going to be pronounced even if measurement statistics doesn't support it.

As pointed out earlier the above model has found widespread application in attenuation and scattering calculations to this day, especially it is very popular with temperate bound wave propagation studies.

2.4.2. Gamma distribution

The MP DSD model can be seen as a special case of gamma distribution when the factor p is set to zero. Given here

$$N(D) = \Lambda_1 D^p exp(-\Lambda_2 D^q) \quad (2\text{-}18)$$

. where $\Lambda_2 = aR^{-b}$, $N(D)$ is the number of drops per unit volume per unit diameter of interval($m^{-3}mm^{-1}$), D is the drop diameter and a, b, p, q and Λ_1 are to be derived from experimental data.

[1, 41, 42] have confirmed the inability of the negative-exponential distribution in describing small diameter range and generally drop size distributions in non-temperate regions of the world. There have been few experimental works in Africa in relation to drop size distribution modeling by Ajayi and Olsen [43] and Sumbiri et al [42]. The next section presents a very concise discussion of two prominent works that have been used in this research work for comparison purpose.

2.4.3. Modified Gamma Distribution (Butare)

Sumbiri et al [42] showed deficiency of some DSD models in describing rain phenomena in tropical region. This work is based on Joss-Waldvogel type distrometer, RD-80, measurements at the coordinates , 2°36’53.88” S, 29°44’31.53” E Butare , Rwanda . The DSD samples were classified according to rain fall regime grouping based on rainfall rate as drizzle (0.1mm/h ≤ R <5 mm/h), widespread (5mm/h ≤ R <10 mm/h), shower (10 mm/h ≤ R <40 mm /h) and thunderstorm (R > 40 mm /h). In this work the researchers have compared different DSD models to fit the experimental data. The tested models are M-P, Weibull, lognormal and gamma distributions.

Sumbiri et al [42] found varied performance from all the models. It was reported that at rain rate of 1.53mm/h the lognormal model falls below the measured data in the drop diameter range of 0.359-0.913mm while the Weibull distribution appeared the best in these rain rate regimes. In the next class of rain rate i.e., widespread, Weibull, gamma and M-P models were observed to overestimate diameter range 0.359-1mm. lognormal model appeared the best. At samples taken in the shower regime the lognormal fitted the measured data well. But in the thunderstorm case, lognormal only assumes the shape of the actual distribution failing to fit to the data. Neither did the other models.

To overcome the above scenario, Sumbiri et al [42] considered making modification to the lognormal distribution with additional parameters so that it will work for low as well as high rain rate regimes. The researchers proposed a model which is given below in equation (2-19).

$$N(D) = \frac{N_T}{C\sigma D\sqrt{2\pi}} exp\left\{-\frac{1}{2}\left(\frac{ln\,D_i - \mu}{\sigma}\right)^2\right\}\{1 + \alpha\, exp(-D_i)\} \qquad (2\text{-}19)$$

where μ is the mean of lnD, σ, the standard deviation, and N_T is the total number of drops of all sizes α is the modification parameter.

The researchers used method of Maximum Likelihood Estimation to find input fit parameters. And then the researchers applied least square regression method to find expression for the parameters as a function of rain rate. The researchers came up with the following expressions . which are similar to that of Ajayi [1]except for the new modification factor which is given as a power law function of rain rate R.

$$\mu = A_\mu + B_\mu\, ln\, R \qquad (2\text{-}20)$$

$$\sigma^2 = A_\sigma + B_\sigma\, ln\, R \qquad (2\text{-}21)$$

$$\alpha = a_\alpha R^{b_\alpha} \qquad (2\text{-}22)$$

The total drop concentration parameter N_T was forced to satisfy the rainfall-DSD relationship given by;

$$R = \frac{3.6\pi}{1000}\int_0^\infty D^3 v\,(D_i)N(D_i)dD \qquad (2\text{-}23)$$

where R is the rain rate(mm/h) (derived from rain gauge measurement)

v is the terminal falling velocity

N(D) is the drop size distribution

D is the equivolumetric drop radius

Rearranging for N_T;

$$N_T = \frac{R}{6\pi\times10^{-4}\sum_{i=1}^{N} D^3 f(D_i)v(D_i)\Delta D} \qquad (2\text{-}24)$$

Sumbiri et al [42] reported that, generally speaking, the modified distribution model performed better than the other four models. This comparison was done in terms of RMSE and CHI goodness of fit tests. In the drizzle regime Weibull DSD brought comparatively minimal RMSE and Chi test results. The widespread regime saw two models compete with the lognormal getting the upper hand only slightly. For shower events the new model and lognormal recorded nearly same RMSE scores. In the thunderstorm case, the new model trumps all the other ones. Based on these observations concluded that the new model gives a better representation of DSD in the area of Butare, Rwanda.

One other key observation from the above work is that the performance of the M-P distribution model. It can easily be seen that the M-P DSD is the least fitting distribution model with the worst scores in both tests at all of the regimes. This result is in conformity with those reported by [1] which will see shortly.

2.4.4. Ajay's Log-normal model

Ajayi, G. O. and Olsen, Roderic [1] proposed a lognormal DSD model for all types of rain rates, i.e., drizzle to thunderstorm , for data taken from Ile Ife, Nigeria (7.5^{o}N, 4.5^{o}E). The research employed a distrometer system to record the number and size of rain drops . The system had an electromechanical sensor and a processor that classified the drops into 20 classes in the range [0.3 mm-5.3mm] of diameter size. The lognormal DSD is given in equation (2-25).

$$N(D) = \frac{N_T}{\sigma D\sqrt{2\pi}} exp\left\{-\frac{1}{2}\left(\frac{ln\, D-\mu}{\sigma}\right)^2\right\} \quad (2\text{-}25)$$

where μ is the mean of lnD, σ, the standard deviation, and N_T is the total number of drops of all sizes.

The researchers used moment regression method by method of moments [44]to estimate values of the above three parameters . Without going into the derivation , only the results and the important findings will be discussed in this particular work. Below are given the expressions for the three parameters.

$$N_T = a_0 R^{b_0} \quad (2\text{-}26)$$

$$\mu = A_\mu + B_\mu\, ln\, R \quad (2\text{-}27)$$

$$\sigma^2 = A_\sigma + B_\sigma\, ln\, R \quad (2\text{-}28)$$

Wide range of rain rate values were used, 0.23, 1.1, 2.3, 14, 30, 64, 75, 146 mm h^{-1}.

The following expressions are the result of the regression;

$$N_T = 108R^{.363} \tag{2-29}$$

Using the second and third moments,

$$\mu = -0.195 + 0.199\, ln\, R \tag{2-30}$$

$$\sigma^2 = .137 - 0.013\, ln\, R \tag{2-31}$$

And using the fifth and sixth moments,

$$\mu = -0.137 + 0.192\, ln\, R \tag{2-32}$$

$$\sigma^2 = .109 - 0.01\, ln\, R \tag{2-33}$$

The reported results of comparison of the new model against the M-P distribution can be seen in Figure 4-14. The lognormal models gave a very good distribution fit against the measured drop sizes at both ends of the rain rate spectrum.

According to the above work, the M-p distribution was reported to overestimate the small diameter range for all ranges of rain rates. It had a better performance when considering larger drop size region for low rain rates (<5mm /h). For higher rain rates , the performance of the M-P distribution was claimed to be worse . Similar fitting results were expected of the L-P distribution.

2.5. Propagation of millimeter and microwaves through rain

2.5.1. Introduction

As outlined in the previous sections, the ever-increasing demand for bandwidth, data rate and availability has overcrowded the frequency region below 10GHz. The upper spectrum range are being studied and experimented with to be able to support those demand together with deployment of MIMO systems which make advantage of spatial diversity to use the available spectrum to support greater data rates. These frequency ranges, however suffer heavily from precipitation events like snow, rain, hail and so on. Rain, especially happens to be the greatest cause of attenuation at these millimeter and microwave frequencies. The reason for this is that the sizes rain drops, which make up any rain event, become suddenly comparable to the wavelength of the transmission at millimeter and microwave frequencies [45, 46] Raindrops absorb and scatter radio waves, leading to signal attenuation and reduction of the system availability and reliability. The severity of rain impairment increases with frequency and varies with regional locations [47]. The performance of MIMO systems under these conditions has to be studied so that necessary adjustments are made during design phase to guarantee availability for 99.99% of the time.

It is obviously crucial to make as accurate a prediction as possible about the rain attenuation along a line of sight link system [48]. There are two major methods for the prediction of rain attenuation on microwave paths: the empirical method and the physical method. The former is dependent on experimental attenuation measurement record archives from a given region of interest. The physical method, on the other hand, tries to replicate, through mathematical analysis, the physical behavior manifested in attenuation scenarios [49, 50]. All of the input may not be available when trying physical modeling, so researchers and theoreticians alike turn to empirical approach.

There have been many studies carried out throughout the world on characteristics microwave and millimeter wave propagation through rain. There also have been results of attenuation studies conducted in Ethiopia . The purpose of this section is to summarize various theoretical and practical approaches of attenuation studies . The research work develops the concept of attenuation through rain as it moves to modeling of MIMO systems. This will serve as a stepping stone for our study of the effect of rain in the performance of millimeter and microwave MIMO systems. The section also highlights the prominent scattering theories. These theories are used as bases for attenuation calculation expressions used as standard in world telecom governing authorities.

2.5.2. Specific attenuation due to rain

Rain falling in the path of an electromagnetic transmission link causes reduction of received power by means of scattering and absorption. The scattering reduced voltage levels as the incident wave reflects off from rain drops in number of directions including the original path but with reduced strength as part of it goes astray which may or may not rejoin the destination with delay. Absorption is a more straight forward attenuation mechanism which absorbs parts of the impending energy which is converted into heat, hence ending up wasted. Scattering will be dealt in greater detail in Mie scattering calculations section, but now the research work presents models adopted for specific attenuation calculation based on rain rate information, specifically $R_{0.01}$.

2.5.2.1. Specific attenuation calculation based on long term rain fall

ITU-R P.530-16 [51] proposes a method of calculating the rain attenuation over a distance, d. The recommendation suggests availability of long-term statistics of local rain fall rate. In cases where there is no long-term rain fall rate statistics of a given location refers to use of procedure outlined in [52] to obtain the desired rain fall rate at a given probability level. The formulations have clear expressions and parameter values for different polarizations.

There have been studies confirming the applicability of the various standard attenuation estimation procedures devised by the ITUR committees. Most of these sites affirming the use of ITUR's procedures for rain rate and attenuation determination are, understandably, found in the temperate part of the world. However, numerous works have been conducted across different parts of the world that refute attenuation outputs obtained by using ITU and recommend improvements. A few of such cases are discussed in these literature survey.

Sujan Shrestha and Dong-Yu Choi [53] in ”Rain attenuation statistics over millimeter wave bands in South Korea” detailed the experiment conducted to measure attenuation and rain fall rate over link distance of 3.2 and 0.1 km at 38 and 75GHz respectively in Icheon, South Korea. The climate in Icheon region is cold and temperate in which summers are much rainier than winters with average rainfall of 1296 mm/year South Korea. The rain rate and attenuation data were recorded for a period of three years from 2013 to 2015. The researchers employed an optical distrometer, OTT Parsivel, to collect rain intensity data. The optical distrometer is reported to have validity of 99 .95% of the time. The attenuation level(dB) was calculated by subtracting received signal level (RSL)during rain from clear sky RSL.

The researchers compared their outcome with attenuation results obtained using other models in [54-57]. Comparison also was made between outcome of the experimental setup and that of ITU-R P.530- 16 [51] prediction. The researchers showed that while that of [51] and experimental data agreed on the 38GHz attenuation data. [58] reported ITU attenuation prediction success in Japan. However, there was huge difference between the two when it came to the 75GHz link reaching up to 20dB in the former study. The reason for such discrepancy was predicted to have been lack of consideration for true drop size concentration. The researchers proposed a modification to attenuation prediction model of ITUR 530 16 by incorporating new terms that depend on the rain rate values at any desired percentage level of exceedance.

$$A_{\%\,predicted} = A_{0.01}\, C_1 p^{\,-(C_2+C_3\,log_{10}\,p)} + a_1 R_{\%p}^4 + a_2 R_{\%p}^3 + a_3 R_{\%p}^2 + a_4\, R_{\%p} + a_5 \qquad (2\text{-}34)$$

where $A_{\%\,predicted}$ is the estimated attenuation level for level exceedance %p

$A_{0.01}$ is the attenuation exceeded for 0.01% of the time as predicted by ITU R 530-16

$C_{1,2,3}$ are coefficients given by ITU R 530-16 for estimation of attenuation at exceedance level p other than 0.01%

$R_{\%p}$ is the corresponding 1-min integration time rain rate of the locality

$a_{1,..,4}$ are coefficients of the fourth order polynomial that best fits the deviation between the experimental and ITUR530-16.

Parshotam Sharma et al [59] developed statistics of practical attenuation measurements over terrestrial microwave link . The setup was done at Amritsar , India at 28.75GHz . The setup included a tipping bucket type rain gauge to keep track of the rain rate as the attenuation measurement go on simultaneously . The researchers compared the results of ITUR and the experimental result . The researchers found significant differences between the two sets of data , affirming the need to reevaluate the ITUR models.

Another experimental approach at attenuation statistics was carried out by Z. X. Zhou et al [60]. The study carried out measurements in the frequency range from 15 to 38GHz in Singapore's tropical region. Up on comparison with CCIR's prediction, it was reported that the CCIR model underestimates the attenuation level in the percentage levels between .01% and .5%. The paper concluded that the drop size distribution used for CCIR model formulation was completely different to what prevails in Singapore's tropical region.

This approach has been used by many researchers [8, 9, 31] to estimate specific rain attenuation parameters in Africa. Diba [8]calculated the specific attenuation of some major cities in Ethiopia based on R-H estimate of $R_{0.01}$. The non-uniformity of rain in the path is incorporated in the effective path, d_{eff}, factor. Having mentioned some works carried out based on ITU's models, it is time to briefly present the formulations , recommendation and procedures given by the world governing body. ITUR recommendations give explicit expressions used to calculate estimation of rain attenuation for any location based on R. the expressions have clear dependence on polarization and frequency. These expressions are given below:

$$\gamma_R = kR^{\alpha} \qquad (2\text{-}35)$$

where the coefficients k and α are functions of frequency defined as follows for vertical and horizontal polarizations.

$$log_{10} k = \sum_{j=1}^{4}\left(a_j exp\left(-\left[\frac{log_{10} f - b_f}{c_j}\right]^2\right)\right) + m_k \, log_{10} f + c_k \qquad (2\text{-}36)$$

$$\alpha = \sum_{j=1}^{5}\left(a_j exp\left(-\left[\frac{log_{10} f - b_f}{c_j}\right]^2\right)\right) + m_k \, log_{10} f + c_a \qquad (2\text{-}37)$$

Where:

f: frequency in GHz

k: either k_H or k_V

α: either α_H or α_V

The values of α and k determined by experiment are given in tabular form. The specific attenuation exceeded for 0.01% of the time is found by a mere substitution of R by the long-term statistics derived $R_{0.01\%}$. Attenuation value exceeded for 0.01% of the time is then obtained simply by multiplying the specific attenuation by the effective communication distance d_{eff} as given

below.

$$A_{0.01} = \gamma_R d_{eff} = \gamma_R dr \qquad (2\text{-}38)$$

where is the reduction factor r given as:

$$r = \frac{1}{0.477 d^{0.633} R_{0.01}^{0.073\alpha} f^{0.13} - 10.579\left(1 - exp(-0.024d)\right)} \qquad (2\text{-}39)$$

where f is frequency in GHz and α is the exponent used in the determination of the specific attenuation γ and

r = 2.5 if r < 0.4.

The other approach, a more direct one, used in attenuation calculation is made by considering the interaction of rain drops and quantifying the effect of absorption and scattering. The next section considers a brief review of this approach.

2.5.2.2 Specific attenuation calculation based on scattering theory

The specific rain attenuation at any point in space depends upon the rain rate which itself can be parameterized by number of variables. These are shape and size of rain droplets, ambient temperature, rain cell size, magnetic permeability and permittivity of drops as well as medium. The absorption and scattering phenomena in rain can be seen as the integration of the effect of all the rain drops that make up the path. The parameter associated with attenuation here is known as extinction cross-section. Most of the attenuation calculations that are based on the above concept make the following assumptions;

1. Rain drops are of spherical shape.
2. The effects of individual drops are additive to the whole result.

The specific attenuation $\gamma(dB/Km)$is given by equation

$$\gamma(dB/Km) = 4.343 \times \int_0^\infty Qext(D,\lambda,m)N(D)dD \qquad (2\text{-}40)$$

Where

Q_{ext} is the extinction cross section,

D is the drop diameter

λ is wavelength of transmission

m is the complex refractive index of water drop, a function of temperature and frequency

N(D) drop size distribution($m^{-3}mm^{-1}$)

The attenuation over a path of length l, A, is simply this specific attenuation integrated over the path length as given here;

$$A = \int_0^l \gamma dl \qquad (2\text{-}41)$$

Q_{ext} and other propagation constants will be briefly discussed in the subsequent sections. [11, 61]

are among many researchers that applied this approach to calculate specific attenuation . M. Sekine et al [61] obtained a good agreement between measured and calculated data using the above equations with Weibull DSD in the range 8GHz to 312.5GHz.

2.6. MIMO Channel Models

2.6.1. Introduction

MIMO systems, simply defined as the systems containing multiple transmitter antennas and multiple receiver antennas, are seen as one of breakthrough technologies in the digital communication [62], [63]. The remarkable Shannon capacity gains available from deploying multiple antennas at both the transmitter and receiver of a wireless system, has generated great interest in recent years. Theoretical results show that a MIMO systems' channel capacity has the potential to increase linearly with the number of antennas [62, 64]. All these capacity gain promises are possible because of the inherent nature of MIMO in using multipath propagation to the benefit of the user. That is, if presence of multipaths in uncorrelated channel offers multiple subchannels while correlated channel denies just that. The increase in data rates possible through parallel channels is called spatial multiplexing. These increases are gained without using additional transmit power or spectral bandwidth.

Apart from faster data transmission, high reliability can be offered by MIMO systems. This is achieved by sending same information bearing signals into multiple antennas. This will increase reliability of the system because the signal has a pool of paths to arrive at the destination. It is not likely all the different MIMO paths will be in deep fade at the same time [65].

The MIMO system performance, besides coding and signal processing techniques, depends on the communication channel. Characterization of the channel is crucial step to understand and exploit the potential bene fits offered by MIMO systems. The main purpose of this research work being the study of the effects of rain on MIMO links, the research investigated number of channel modeling approaches that characterize propagation of EMW in such conditions.
This section presents the literature survey on relevant MIMO channel modeling approaches. There are different approaches used to model the MIMO channels and modeling approaches. Broadly speaking the models can be classified as physical and analytical models. Analytical models have

advantages of providing mathematical expressions that describe the channel matrix. These types of models are useful to assess the effect of correlation on performance parameters. According to [66], there is another type of classification of MIMO channel modeling approach. Those are correlation-based stochastic models (CBSMs) and geometry-based stochastic models (GBSMs). The CBSM are future classified into classic i.i.d. Rayleigh fading channel model and correlated channel models. Correlated channel models include the Kronecker-based stochastic model (KBSM), which treats the transmit and receive correlation matrices independent of each other and the Weichselberger [67] model and the virtual channel representation (VCR) that take the mutual coupling effect of transmit and receive antenna system in to consideration in the channel model derivation [68]. Correlation based MIMO channel models are of low complexity and lend themselves for easy performance calculation tractability.

In this section, MIMO system models that have been in practice are presented. The advantage and disadvantage the models will be explained. Based on the surveyed literature, selection of appropriate model used in this research work is done. Three prominent MIMO system modeling approaches are reviewed. The performance of the models under different circumstances, as conducted by number of researchers, is also presented.

The mathematical description of any MIMO system with N transmit and M receive antennas starts with the following expression:

$$y = Hx + n \qquad (2\text{-}42)$$

where

$H \in C^{MxN}$, $y \in C^{Mx1}$ $x \in C^{Nx1}$ and $n \in C^{Mx1}$is gaussian distributed circularly symmetric noise sample. The transmitter is constrained in its total power, i.e., $E[x^H x] \leq P_{tot}$.

The advantage of MIMO methods depends on the ability to use the new dimension, space; additional to the usual two dimensions, space and time. The spatial correlation between all pairs of transmit-receive channel is given by a $MNxNM$ positive semi definite matrix R defined [66] below in equation (2-44) followed by expressions for transmit and receive correlation matricesR_t and R_r:

$$R = E[vec(H)vec(H^H)] \qquad (2\text{-}43)$$

$$R_t = E[H^H H] \text{ and} \qquad (2\text{-}44)$$

$$R_r = E[(HH^H)^H] \quad (2\text{-}45)$$

Full correlation matrices are traceable only when the number of antennas is small. As the number of antennas grow the number of parameters that need to specified increases rapidly, MN^2. This would make the interpretation of each element of R difficult [66, 69].

The above model requires full knowledge of the spatial correlation between every pair of channel links. As a remedy to the above scenario, different authors developed channel models. Recently, it has been reported in [70, 71] that for indoor NLOS environments, the MIMO channel correlation matrix **R***H* can be approximated as a Kronecker product of the correlation matrix at the transmitter **RTx** and the correlation matrix at the receiver **RRx**. These models are the famous Kronecker model[reference], the virtual channel representation and the eigenbeam model [66, 69]. Each approach is based on different assumptions.

The remaining portions of this section are devoted to discussions on the modeling perspective, advantage offered by the particular model, assumptions made in arriving at the model and limitations of the model.

2.6.2. The Kronecker model

To solve the problem created by too many arguments in the full correlation matrix of (2-43), define it in terms of the receive and transmit correlation matrices R_r and R_t respectively in proposed by Da Shuan et al [72] and given in equation (2-48).

The relaxation means the correlation between any two pairs of transmit-receive elements is the product of the correlations as seen from the transmit and receive sides, respectively. One of the main strengths of this MIMO stochastic model is that it relies on a small set of parameters to fully characterize the communication scenario. These are the power gain of the MIMO channel matrix and two correlation matrices describing the correlation properties at both ends of the transmission links [71].

Kronecker based models are more" suitable for widely separated antennas such as massive MIMO systems with distributed antennas than co-located antenna arrays" [68]. The following two assumptions are the building blocks of the above model of the full correlation matrix.

- Independence of the transmit and receive correlation matrices. In scenarios with sufficiently rich multipath scattering, it is reasonable to assume spatial stationarity, that is, that the correlation between the fading signals received at two antenna elements only depends on the element distance but not on the exact location, at least for small dislocations. Then correlation matrix of the signals as seen from the receive side will be the same, no matter which of the transmit elements is used. Then the transmit and receive correlation matrices can be defined as follows:

$$\mathbf{R}_{\mathrm{Tx}} = \frac{1}{N}\,\mathrm{E}\left[\left(\mathbf{H}^{H}\mathbf{H}\right)^{T}\right. \tag{2-46}$$

$$\mathbf{R}_{\mathrm{Rx}} = \frac{1}{M}\,\mathrm{E}\left[\mathbf{H}\mathbf{H}^{H}\right] \tag{2-47}$$

- The cross-channel correlation matrix should be the product of corresponding transmit and receive correlations.

$$R = R_r \otimes R_t \tag{2-48}$$

where the $\otimes$ denotes the Kronecker product given in [appendix].

There are literature based on experiment that argue in favor of the above model [71, 73]. The first requirement can be fulfilled if the inter antenna spacings are spaced so that there is minimal coupling between closely placed antennas [66, 74]. Correlation between signals exist unless some distance is kept between antenna pairs. E.Bonek [75], showed that correlation index lower than 0,7 is obtained when the antenna spacing is in the order of 70 wavelengths for the broad side and 15-20 wavelengths in the inline case. Da- Shan et al [72] have indicated that as long as certain minimum distance is maintained between the antennas, correlation introduced will be low enough that fades associated with two different antennal elements can be considered independent. Considering the above assumptions, the channel matrix of the Kronecker model is given by equation (2-49):

$$H = R_r^{1/2} H_w R_t^{1/2} \tag{2-49}$$

where H_w is an i.i.d. random matrix whose entries are zero mean complex-normal distributed.

The channel matrix could also be expressed in terms of eigenbases of the receive and transmit correlation matrices. Denoting the eigen bases as U_{Rr} and U_{Rt} and the eigen vectors as u_{Rm}at, u_{Rn}. Similarly, the eigen values of R_r and R_t being Λ_{Rr} and Λ_{Rt} whose square roots are represented by λ_{Rr} and λ_{Rt}.

2.6.3. The virtual channel representation model (VCR)

This model was devised to solve the problem of interdependence of transmit and receive antennas which was ignored by the above model. Arbitrary coupling was allowed in this model. The product assumption on the cross-correlation matrix was relaxed between transmitter and receiver [64, 71, 74, 76] independently neglecting statistical inter dependence between the two. The virtual representation captures the essence of physical modeling without its complexity, provides a tractable linear channel characterization and offers a simple and transparent interpretation of the effects of scattering and array characteristics on channel capacity and diversity [77]. It describes the channel with respect to fixed spatial basis functions defined by fixed virtual angles that are determined by the spatial resolution of the arrays.

There are times where this approach can serve well. [74, 78] have shown that practical indoor MIMO channels cannot be modeled in this approach and this will result in underestimation of capacity performance The VCR models the MIMO channel by predefined discrete Fourier Transform (DFT) matrices instead of one-sided correlation matrices []. "The transformed matrix can be modeled as an elementwise product of a virtual channel power matrix and an i.i.d. Gaussian random matrix. Therefore, unlike the Kronecker model, the non-separable channel statistics are preserved" [79].

2.6.4. The Weichselberger model

The Weichselberger model reduces to the virtual channel representation by forcing the eigenbases to be DFT matrices; and it reduces to the Kronecker model by forcing the coupling matrix to be of rank one. As stated by Weichselberger et al "The purpose of the new model is threefold. We want to

- alleviate the restriction imposed by the "Kronecker model "and describe the joint spatial structure of the channel as the "virtual channel representation" does

- alleviate the restriction imposed by the “virtual channel representation” and adopt the spatial eigenbases to the channel as well as to the array configuration (including array geometry, element characteristics and element polarizations) as the “Kronecker model” does;
- formulate a model that includes both the “Kronecker model” and the “virtual channel representation” as special cases.”

So, the parameters for the Weichselberger model represent the coupling matrix, and the eigen bases of the transmit and receive correlation matrices [80].

Materializing the above concept, one-sided spatial correlation matrices of link end A (or B) have the same eigenbasis that is defined by the unparameterized one-sided correlation matrix $\boldsymbol{R}_A$ (or $\boldsymbol{R}_B$) [67].

$$R_A = U_A \Lambda_A U_A^H \qquad (2\text{-}50)$$

$$R_B = U_B \Lambda_B U_B^H \qquad (2\text{-}51)$$

Where Λ_B and Λ_A are real valued diagonal matrices with non-negative entries. Their eigenvalues may differ.

CHAPTER THREE

3. Methodology

3.1. Introduction

In this section the step by step detailed approach used to assess the effect of rain on MIMO channels is presented. The performance assessment is made based on capacity of channels under assumption of perfect CSIT and no CSIT. But before considering the calculation of channel capacity under these circumstances, the determination of input parameters like rain rate, propagation constants and channel models has to be cleared.

The methodology section of the thesis is organized as follows. The first section deals with the establishment of the rain distribution profile of the system deployment area. Here, the various approaches considered will be presented. Techniques applied to find 1-min integrated rain rate data are stated. In the subsequent and related section, the procedure used o fine the ever-important rain rate figure $R_{0.01\%}$ is presented. Next in "Rain cell size determination" section the concise step by step procedure used to calculate the maximum possible rain cell diameter form the rain rate is given. Subsequent sections present the attenuation calculation procedure applied in the work together with the formulation of Mie scattering theory. Finally, formal derivation of the channel matrix is given together with the derivation of the transmit and receive correlation matrices.

3.2. Rain fall data measurement and processing

Accurate representation of rain distribution profile of an area is a compulsory prerequisite for design engineers. It is the knowledge of the rain spatial and temporal distribution of rain that allows designers to allow room for additional margins to combat deep fades to prevent network outage at times of intense rain fall. Rain rate distribution profile can be collected from rain gauges normally. But only fast sampling rain gauge data can qualify as an input to propagation studies. There is scarcity of such data in Ethiopia. The only available information related to weather phenomena are obtained from NMA. rain rate data kept by NMA is of 15-min integration time. data from NMA, with proper integration time conversion, has been used in this research work as presented in the next section. 1-minute integration time data, from weather station installed at Jimma University has also been employed as well.

3.2.1. Rain rate integration time conversion

This is an important step in any propagation study in relation to rain. It is a means of extracting shorter integration time rain rate values (with higher intensity) from longer integration equivalent time series rain rate records (lesser intensity). Conversion methods reviewed in the literature review section 2.2.1 have been compared. Specially the approaches used by [31], [26], [20] are compared to find the best fit method. This is reported in section 4.3.

3.2.2. Determination of $R_{0.01}$

Ensuring 99.99% system availability the design of microwave/millimeter wave links requires knowledge about the worst-case fade levels. For fade levels related to rain, this is possible by considering the rain rate exceeded for 0.01% of the time in a year, commonly known as $R_{0.01}$. This requirement is stated by [51]. $R_{0.01}$ should be of 1-min integration time. There are two approaches to determine $R_{0.01}$. The first approach includes integration time conversion techniques and it was discussed.

In the previous section 3.2.1, the best practices used by researchers to get 1-min rain rate data have been discussed. It is obvious that some of the methods are concerned directly with the calculation of $R_{0.01\%}$. Rice and Holmberg [17] used some parameters like the annual rain accumulation in a bid to localize the parameters . This approach is only recommended when there is no local rain fall data. When there is a locally measured rain fall rate data, statistical approach is followed to arrive at $R_{0.01\%}$. The review of second approach is presented here as the study had got locally measured rain rate data with 1- minute integration time. Given one has the raw rate intensity data, this a very quick and simple method of arriving at $R_{0.01\%}$. The procedure is briefly outlined in [81].

The procedure is based on the fact that a minute accounts for 1/525,949.2 th (0.00019%) of a year. This means the approximately 53 minutes of outage in a year would count as 0.01 percentage . In other words, the rain rate exceeded for 0.01% of the time is the 53rd recording when the 1minute integration time rain rate is sorted in the descending order. Formal definition of the above procedure is:

- Filter rain rate raw data and remove recordings with blank reading. Different measuring device have different means of communicating times when there was no recording for some reason, so the particular equipment's setting and syntax should be followed.

- Sort the rain rates in an ascending order
- Assign cardinal numbers n for the rain rate values like n = 1,2, 3…, Nr
- Determine the number of non-zero recordings, Nr.
- Calculate the percentage for each r>0mm/h recoding by the following formula

$$P(\%) = \frac{Nr-n}{no\ of\ minutes\ in\ a\ year} x100\% \qquad (3\text{-}1)$$

- Read the rain rate value along $P(\%) = 0.01$, which is the value of $R_{0.01\%}$

$P(\%)$is the cumulative distribution of rain rate.

The RH given in equation produce $R_{0.01\%}$ values as a function of mean yearly rain accumulation M. The accuracy of this model is compared against measurement results in the section 4.

3.3. Rain cell size determination

In this work the guide line summarized by Akuon, P. O and Afullo, T. J. O [24] for determination of rain cell diameter is used. It should, however, be noted that the resulting expression of rain cell size only gives the maximum possible cell size at the given rain rate. The procedure is described below:

1. Sorting of time-series rain rate records beginning from earliest to the most recent entry.
2. Integration time conversion from 1hr to 1min equivalent rates.
3. Determination of rain rate distribution trend by classification data into categories based on lower bounds of, 3, 5, 12, 20 mm/h. Here the distinction between stratiform and convective type of rain events should be clearly defined. This classification will determine the advection velocity that will be assigned in the next stage of the procedure.
4. Determine the distance of each rain event. Multiplying the advection velocity by the time each event took. The result will be statistics of rain cell size.
5. The output distance data for each class are then processed statistically to find their cumulative probability distribution. The equiprobable distances in the classes are plotted against the respective lower bounds of rain rates at the 0.01%.

It should be noted that the above procedure is based on rain rate data of 1hour integration time, but works the same for other integration time rain data also as long as the integration time conversion step is observed carefully.

3.4.Rain drop size distribution

If rain rate measurements in Ethiopia are scarce, then DSD measurement are nonexistent. To fill this gap, DSD models that have been devised for African countries have been studied. Since the $R_{0.01\%}$ figures are similar to what is found in Ethiopia , especially Jimma and Bahirdar , the researcher believed the DSD models for these areas could be used without loss of peculiarity . The result of the other widely used DSD model of MP is compared with the two tropical models to show how system parameters are affected by the choice of a particular DSD model.

3.5. Determination of specific attenuation

One of the approaches used to calculate the specific attenuation of locations in Ethiopia is the practice recommended by world governing body, ITU as surveyed in section 2.5.3. The research work made comparison of this and the method detailed below in section 3.6 to get the true attenuation values for some major cities.

3.6. Mie scattering calculations

As we move up the frequency spectrum ladder, millimeter and microwave range, we face new challenges in the form of attenuation. The attenuation can be caused by structures like concrete walls, glass surfaces or generally anything that stand in the way between the transmitter and receiver. Rain, being one of the most important attenuation mechanisms for line of sight wireless communications , its interaction with these frequency range should be studied. The importance of rain at these frequencies is due to the fact that rain drops (which measure anywhere between 0.01 to 0.7cm [45, 46] and wavelength of the transmission begin to have comparable dimensions . This makes for greater interaction possibilities at these frequencies than at lower frequencies . Drop sizes larger than .7cm are not considered in the calculation because as stated in [34], such drops would not be mechanically stable and will eventually disintegrate into smaller droplets. The loss in power of an incident wave happens in two forms. These are scattering and absorption . In this section the mathematical description of scattering is reviewed and foundation laid for scattering calculations made in the results section of the thesis. The phenomena of rain drop interaction of a wave front can be seen in the Figure 3-1 below.

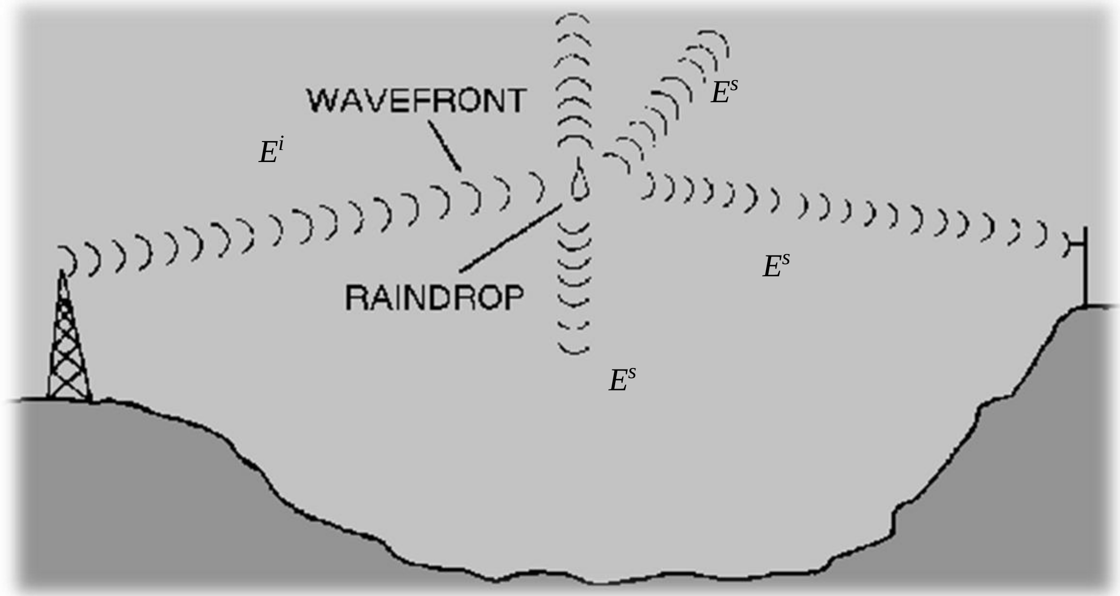

Figure 3-1. Interaction of a rain drop with a wave front [82].

The scattered wave E^s is given by:

$$E^s = E^i . f\left(K_1, K_2\right). r^{-1}. e^{jk_0 r}\Big) \quad (3\text{-}2)$$

where E^sstands for the intensity of the scattered wave(V/m), E^i, the incident wave and $K_i$are the direction vector of scattered and incident wave. The type of scattering modeling used depends on the relative size of the interacting bodies, i.e., waves and droplets.

Rayleigh theory calculates scattering function for situations where the drop size is smaller than the wavelength which is in the order of tens at frequencies below 3GHz[46],i.e., $\frac{\pi D}{\lambda} \ll 1$. The application of the Rayleigh approach becomes obsolete above 5GHz [32]. Our range of interest is the millimeter and microwave band where the drop sizes are. So, the research work focuses on the other scattering theory formulated to deal with just that. This theory is widely known as Mie scattering theory. Scattering function for Mie scattering is given by:

$$f = \frac{j\lambda^3}{\pi^3 D^2} \left[\sum_{n=1}^{\infty} (2n + 1) \left(a_n + b_n\right)\right]^* \quad (3\text{-}3)$$

where a_n, b_n are Mie coefficients . The derivation of these coefficients , which are functions of the relative refractive index of water, is given in Bohren and Hoffman [83].

$$a_n = \frac{\mu m^2 j_n(mx)[x j_n(x)]' - \mu_1 j_n(x)[mx j_n(mx)]'}{\mu m^2 j_n(mx)\left[x\, h_n^{(1)}\right]' - \mu_1\, h_n^{(1)}(x)[mx j_n(mx)]'} \quad (3\text{-}4)$$

$$b_n = \frac{\mu_1 j_n(mx)[x j_n(x)]' - \mu j_n(x)[mx j_n(mx)]'}{\mu_1 j_n(mx)\left[x\, h_n^{(1)}\right]' - \mu\, h_n^{(1)}(x)[mx j_n(mx)]'} \quad (3\text{-}5)$$

Where m is the refractive index of water with respect to the ambient medium, μ_1 and μ are the permeability of the sphere and the ambient medium respectively. $h_n^{(1)}$ and j_n are the spherical Henkel and Bessel functions of order n. The two functions and their relationships and the derivatives are given in

$$h_n^{(1)} = j_n(z) + i y_n(z) \quad (3\text{-}6)$$

The spherical Bessel and Henkel functions are expressed in terms of the first and second order Bessel functions J_n and Y_n.

$$j_n(x) = \sqrt{\frac{\pi}{2x}} J_{n+0.5}(x) \quad (3\text{-}7)$$

$$y_n(x) = \sqrt{\frac{\pi}{2x}} Y_{n+0.5}(x) \quad (3\text{-}8)$$

Propagation coefficients are determined from these coefficients. These propagation coefficients in turn determine various parameters of electromagnetic wave propagation through rain. These are the absorption depth (τ_a), scattering depth (τ_s), optical depth (τ_o), and anisotropy factor (a_p). Absorption and scattering depths determine represent power attenuation due to absorption and scattering. The optical depth refers the total attenuation. The anisotropy factor represents the average of the cosine of the scattering angle.

Calculation of the above propagation parameters is possible after definition of the corresponding cross sections $C_{ext}, C_{sca}, C_{abs}$ (or efficiencies $Q_{ext}, Q_{sca}, Q_{abs}$).

$$Q_{ext} = \frac{C_{ext}}{G} \quad (3\text{-}9)$$

where G is the cross-sectional area of the spherical rain drops πr^2.

The extinction or cross section can be thought of as the ratio of the sum of absorbed and scattere energies to the incident average power density [84].

Bohren and Huffman [83]derived the expression for $C_i, i = ext, sca, abs$ as follow.

$$C_{sca} = \frac{2\pi}{k^2}\sum_{n=1}^{\infty}(2n+1)(|a_n|^2+|b_n|^2) \quad (3\text{-}10)$$

$$C_{ext} = \frac{2\pi}{k^2}\sum_{n=1}^{\infty}(2n+1)Re(a_{n+}b_n) \quad (3\text{-}11)$$

$$C_{abs} = C_{ext} + C_{sca} \quad (3\text{-}12)$$

where k is the wave number $2\pi/\lambda$.

The detailed derivations of can be found in [83]. These Mie scattering derivations are accepted means of calculating propagation constants and have been used in numerous researches [11], [85], . [41], [61], [86] and [87] to mention a few. These and many others conducted and proved the applicability of Mie scattering theory to characterize propagation of millimeter and microwave transmissions through rain.

The calculation of the total cross section representation of a certain rain phenomena takes the following form as described by [40, 88]:

$$T_i = 0.25\pi\int_0^{\infty} D^2 Q_i(D)N(D)dD\ ;\ i = \quad ext, sca, abs \quad (3\text{-}13)$$

$$T_{sca}.\text{ap}=0.25\pi\int_0^{\infty} D^2 < costeta > Q\text{sca}(D)N(D)dD \quad (3\text{-}14)$$

MATLAB routines and functions were written to calculate the total cross sections based on the Mie scattering formulations which make use of the Bessel functions.

3.7. MIMO system modeling

As clearly stated in the limitation of the study, the main purpose of this research work is to study the effect of rain fall on millimeter and microwave MIMO systems without considering effects like polarization and antenna linkage. So, our choice of MIMO channel model is the correlation based Kronecker model. Here the expressions of the channel matrix H and transmit and receive correlation matrices are formulated as stated in [40]. Formulas used for capacity calculation will be expressed as derived in by Shannon. MATLAB routines and functions were written based on these mathematical expressions to simulate the performance of MIMO channel under variety of parameters. These parameters are;

- Frequency
- Rain rate
- Number of transmit and receive antennas
- Antenna separation distance
- Drop size distribution models
- Signal-to-noise ratio

Directly to the derivation of the MIMO channel matrix and correlation matrices which are the building blocks of the Kronecker model. Assuming randomly distributed scatterers and a point X illuminating on an object at distance D. consider two such points on the distant object O1 and O2 with h1 and h2 as channel coefficients between X and the two points respectively . The expectation of the channel coefficients is given in [38] and [40] as:

$$E(h_i) = \sqrt{\rho_0}\alpha e^{-j\frac{2\pi}{\lambda}d_{Oi,X}}\ i = 1,2 \qquad (3\text{-}15)$$

and

$$E\left(h_i h_j^H\right) = \alpha^2 e^{-j\frac{2\pi}{\lambda}\left(d_{Oi,X}-d_{Oj,X}\right)}\left(\rho_0 + \rho_s e^{-j\frac{-d_{oi,oj}^2}{l_0^2}}\right) \qquad (3\text{-}16)$$

where $\alpha = \frac{\lambda\sqrt{\eta}}{4\pi D}$ is the large scale propagation factor

η is product of receiver and transmitter antennas

$d_{oi,oj}$ is the distance between pair of points i and j

ρ_0 is the term representing the total power lost due to absorption and scattering

ρ_s is the term representing power attenuation due to scattering

$l_0 = \sqrt{\frac{3\lambda^2 a_p(1-e^{-\tau_s})}{\pi^2\tau_s}}$

a_p is the anisotropy factor representing the average of cosine of the scattering angle

τ_s is the scattering depth.

The quantities τ_s, τ_a $\tau_o$and a_p are defined in the previous section 3.6.

For the sake of ease of mathematical manipulation both uniform antenna arrays are assumed to be placed the transmitter at the origin and the receiver parallel to the transmitter D distance away. The distance between any pair of transmitting and receiving antenna is given as $d_{m,n}^2 = (x_m - x_n)^2 + (y_m - y_n)^2$. In this case $x_m - x_n = D$ $d_{m,n}^2 = D^2 + (y_m - y_n)^2$

Since D>>$y_{m,n}$ the following approximation can be replaced in place of

$$d_{m,n} \sim D + \frac{(y_m + y_n)^2}{2D} \tag{3-17}$$

$$= D + \frac{1}{8D}\left((2m-1-M)^2 d_r^2 + (2n-1-N)^2 d_t^2\right) - \frac{1}{4D}(2m-1-M)(2n-1-N) d_r d_t \tag{3-18}$$

Combining (3-16) and (3-18) the channel coefficients for the channel matrix H can be written as:

$H = (h_{m,n}) \in C^{MxN}$ where

$$h_{m,n} = e^{-j\frac{2\pi D}{\lambda}} . e^{-j(\emptyset_m + \emptyset_n)} . e^{j\frac{S(2m-1-M)(2n-1-N)}{2}} \tag{3-19}$$

$$\emptyset_n = \frac{\pi(2n-1-N)^2 d_t^2}{4\lambda D} \tag{3-20}$$

$$\emptyset_m = \frac{\pi(2m-1-M)^2 d_r^2}{4\lambda D} \tag{3-21}$$

$$S = \frac{\pi d_r d_t}{\lambda D} \tag{3-22}$$

Following similar procedure to calculate the correlation matrices $E(HH^H)$. It is easy to see that each entry of $E(HH^H)$ is a summation of the contribution of the correlation of all possible one receiver and all transmit antennas combination which is given analytically as follows.

$$E\left(\sum_{n=1}^{N} h_{m,n} h_{m,n'}^H\right) = \sum_{n=1}^{N} E\left(h_{m,n} h_{m,n'}^H\right) \tag{3-23}$$

$$= a^2 \rho_0 \sum_{n=1}^{N} h_{m,n} h_{m,n\prime}^H + a^2 \rho_s e^{-\frac{(m-m\prime)^2 d_r^2}{l_0^2}} \sum_{n=1}^{N} h_{m,n} h_{m,n\prime}^H \tag{3-24}$$

$$\sum_{n=1}^{N} h_{m,n} h_{m,n\prime}^H = e^{-j(\emptyset_m - \emptyset_{m\prime})} \frac{\sin\left(SN(m-m\prime)\right)}{\sin\left(S(m-m\prime)\right)} \tag{3-25}$$

Assigning the expression in (3-25) as R_r, $E(HH^H)$ can be given as

$$E(HH^H) = a^2 \rho_0 R_r + a^2 \rho_s \varphi_r \blacksquare R_r \tag{3-26}$$

where ■ represents the element by element matrix product (Hadamard Product) and

φ_r is C^{MxM} where $\varphi_r\,(m,m') = e^{-\frac{(m-m\prime)^2 d_r^2}{l_0^2}}$.

The transmit correlation matrix $E(H^H H)$ is similarly derived as a correlation between all pairs of transmit and receive channels as a summation of correlation of a single transmit antenna with all receive antennas.

$$E(H^H H) = a^2 \rho_0 R_t + a^2 \rho_s \varphi_t \blacksquare R_t \qquad (3\text{-}27)$$

where

$R_t \in C^{NxN}$ with $R_t(n,n') = e^{-j(\emptyset_n - \emptyset_{n\prime})} \frac{\sin(SN(n-n\prime))}{\sin(S(n-n\prime))}$

$\varphi_t \in C^{NxN}$ with $\varphi_t\,(n,n') = e^{-\frac{(n-n\prime)^2 d_t^2}{l_0^2}}$

The channel model is constructed in such a way that signal arriving at the receiver is seen as a combination of directly attenuated term and scattered part. Since the distance D is much larger than dr or dt all scattered terms can be represented by a single variance term. Recalling the Kronecker model defined in (2-49) the channel model is formulated as follows.

$$H_{MXN} = H_d + \beta A^{1/2} H_{i.i.d} B^{1/2} \qquad (3\text{-}28)$$

where

$H_d = \sqrt{\rho_0}.\,a.\,H$ is the directly attenuated term

$\beta = \sqrt{\rho_s}.\,a$ is the variance of all indirectly scattered terms

$A = \frac{1}{N}\varphi_r \blacksquare R_r$ is the term representing the receive correlation matrix

$B = \frac{1}{M}\varphi_t \blacksquare R_t$ is the term representing the transmit correlation matrix

It is easy to notice that all the expressions are some function of the rain phenomena. The channel model reduces to the directly attenuated term only in case of no rain. This showed validity of the channel model devised by [40].

3.8. MIMO channel capacity

Channel capacity (C) is the highest rate at which information can be sent with arbitrarily low probability of error [89]. From the very beginning , the research work has assumed narrow band channel where the channel matrix , which is defined by the propagation parameters , remains constant for the period of transmission. So, it is reasonable to associate C with a fixed H. Besides, the work assumes the following constraint on transmitter power [90]:

$$E(xx^H) \leq P \qquad (3\text{-}29)$$

Equivalently,

$$tr(E(x^H x)) \leq P \qquad (3\text{-}30)$$

where tr denotes the matrix operation trace.

C is defined in terms of mutual information $I(x{:}\,y)$ which is given as [90, 91]:

$$I(x{:}\,y) = H(y) - H(y|x) = H(y) - H(n) \qquad (3\text{-}31)$$

where $H(.)$ denotes the entropy operator.

The channel capacity as defined in [89] can be obtained by maximizing the mutual information in (3.8). Assuming a zero mean complex input vector the covariance matrix defined as

$$E(xx^H) = Q \qquad (3\text{-}32)$$

$$E(yy^H) = HQH^H + I_r \qquad (3\text{-}33)$$

The mutual information is thus given as

$$I(x{:}\,y) = log_2 det(\, I_r + HQH^H) \qquad (3\text{-}34)$$

For SISO system (MIMO with 1 antenna) system is given as:

$$C(1) = log_2 det(\, 1 + P_{tot}|H|^2/N_0\, W)\ bps/Hz \qquad (3\text{-}35)$$

Calculating the capacity of MIMO channels takes two forms [92]. The first approach is practical when the transmitter doesn't have information about the channel. Under such circumstances the transmitter simply divides the total power into the number of available antennas [89]. We will go through the derivation of this quantity. It should be noted here that the channel is assumed to be known at the transmitter.

We start the derivation by establishing the singular value decomposition of the channel matrix H. This is given as [63]:

$$H = UDV^H \tag{3-36}$$

where D is MxN non negative diagonal matrix with diagonal elements square root of eigenvalues of HH^H. U and V are MxM and NxN unitary matrices. $UU^H = I_{MxM}$ and $VV^H = I_{NxN}$. The eigenvalues of $HH^H$are defined as

$$HH^H A = \lambda A,\ \ A \neq 0 \tag{3-37}$$

A is an $Mx1$ vector associated with the eigenvalues λ, called an eigenvector. So,

$$y = Hx + n \tag{3-38}$$

Can be written as

$$y = UDV^H x + n \tag{3-39}$$

Multiplying all sides by U^H the following expression results;

$$y' = Dx' + n' \tag{3-40}$$

where $y' = U^H y$, $x' = V^H x$, and $n' = U^H n$. Obviously, the nature of U^H is that the preceding operations only have scaling effect on y, x and n.

Since D is diagonal element y' can be described as a weighted sum of the input vector x as follows:

$$y_i{}' = \sqrt{\lambda_i} x_i{}' + n_i{}' \tag{3-41}$$

Since at most only $\min(M, N)$ of the diagonal elements of D are non-zero the above equation can be simplified like

$$y_i' = \sqrt{\lambda_i} x_i{}' + n_i', i = 1,2, \dots, r \tag{3-42}$$

$$y_i' = n_i', i = r + 1, r + 2, \dots, M \tag{3-43}$$

where $r = rank(H)$.

The above result implies a new way of looking at MIMO channels and the potential associated with them. It suggests that MIMO channels can be thought of as consisting of r uncoupled parallel subchannels with each subchannel assigned to a channel gain amounting to singular value of the channel matrix [63, 93]. Since r is at most $\min(M, N)$ any MIMO configuration is able to support

r parallel sub channels. This idea is showed in Figure 3-2.

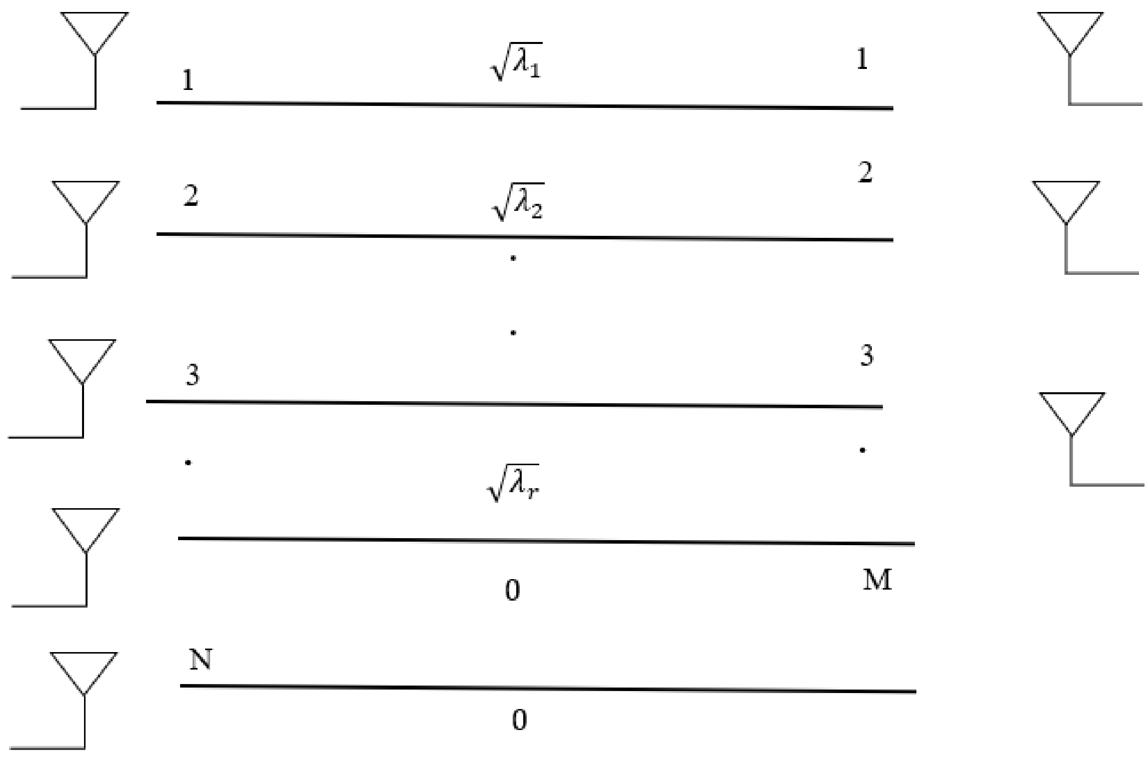

Figure 3-2. Block diagram of an equivalent channel for N>M.

The above decomposition of the MxN channel into r parallel sub channels means the total capacity is the sum of individual SISO capacities of (3-9). Thus, the channel capacity is given as:

$$C = W \sum_{i=1}^{r} log_2(1 + \frac{P_i}{\sigma^2}), \qquad (3\text{-}44)$$

Where W is the bandwidth of each subchannel and $P_i = \lambda_i / N$,

So when the final expression of channel capacity when there is no CSIT in terms of the eigenvalues of HH^H is given as follows [62, 94]:

$$C = W \sum_{i=1}^{r} log_2(1 + \frac{\lambda_i P}{N\sigma^2}) \qquad (3\text{-}45)$$

where P is the total transmitter power.

The above method of transmission appears to be wasteful of transmit power, dividing equally among all antennas. It doesn't give consideration the state of the subchannels. All channels, no matter how much the fade level they are experiencing get equal share of the power P [63] [93]. There is another approach which aims to use the transmit power in an effective way. Channel capacity could be improved if the status of the channel is known beforehand. Channels that are known to be in good condition are assigned larger power and vice versa [62]. Why waste premium transmit power when you know it wouldn't reach the other side?

The allocation of transmitter power when there is perfect CSIT is accomplished using a technique known as "water filling/pouring" [40, 62, 90, 93]. The power allocation is based on the following equation:

$$P_i = \left(\mu - \frac{\sigma^2}{\lambda_i}\right)^+, \quad i = 1, 2, \dots, rank(H) \qquad (3\text{-}46)$$

where $(.)^+$ denotes maximum of the two arguments.

The threshold μ is determined in such a way that the total power assigned to each sub channel doesn't exceed total transmitter power P.

$$\sum_{i=1}^{rank(H)} P_i = P \qquad (3\text{-}47)$$

The capacity in this case is given as:

$$C = W \sum_{i=1}^{r} log_2\left(1 + \frac{P_i}{\sigma^2}\right) \qquad (3\text{-}48)$$

The channel capacity is thus maximizing by allocating the transmit power wisely.

The next chapter is where the results found in the course of the research work are discussed. It

CHAPTER FOUR

4. Result and discussion

4.1. Introduction

This is the section of the thesis where the findings of the research study are discussed. Because the subject matter selected for study is a result of cumulative influence of a number of factors, the thesis' portion included not only the assessment of performance parameters of the end target, MIMO systems, but also all about factors contributing to the final formulations. Detailed discussion of the following topic is presented; determination of rain rate exceedance values, specific attenuation, propagation coefficients, MIMO channel matrix and calculation of MIMO performance parameters (channel capacity and SNR). The rest of this chapter presents those points as ordered above.

4.2. Determination of $R_{0.01}$

The approaches used to obtain rain rate exceedance values were discussed in section 3.2. here the results are plotted and relative mismatch (error) magnitude as calculated by

$$\%\, error = \frac{measured\ vlue - predicted}{measured\ value}. \qquad (4\text{-}1)$$

The first model to be discussed is the computation method recommended by ITU-R P.837-7, the latest in the series ITU-R P.837. Two options are provided by the publication. The first method can be programmed into MATLAB routine using digital monthly temperature , location coordinate (latitude and longitude pairs) maps provided for the purpose of estimation of the rain rate exceedance values at any given probability was used. The program has GUI enabled version where the user can enter location details and measured values at higher integration time. The software outputs plot of the estimated 1-min integration time rain rate together with the input rates. The predicted values are presented in Table 4-1. The same results could be seen plotted against percentage probability values in Figure 4-1. The error in prediction of measured and estimated values are given for the city of Jimma in Table 4-2 for which, as explained earlier, it was possible to get 1-min integrated rain rate values. Both the ITU-R 837-7 and R-H models overestimate the rain rat values in the probability exceedance range between 0.5 and 1% with error percentage values of 61.14, 78.5, 21.21 and 21.21% respectively for the two approaches. Network design calculations based on estimation methods like the two are bound to be erroneous. To correctly model the rain rate distribution, fast integration time rain gauge networks should be installed. Improved expressions for conversion between higher integration time to 1-min rain rate data are needed. In the next section 1-min rain rate prediction method is proposed for a number of Ethiopian cities based on 1-min integration time rain data obtained from the Davis Vantage weather station installed at Jimma University.

Table 4-1. ITU R-P837-7 rain rate prediction values for 8 cities in Ethiopia.

%p	Jimma	Addis Ababa	Mekele	Dire Dawa	Bahirdar	Adama	Arbaminch	Kombolcha
1	5.89	3.28	1.42	2.94	4.09	2.55	3.23	3.11
0.8	7.25	3.98	2.02	3.82	4.92	3.2	4.03	3.93
0.5	10.64	5.72	3.56	6.07	6.98	4.83	6.04	6.02
0.08	32.92	17.01	14.51	21.43	20.22	15.73	19.41	20.09
0.02	63.39	32.32	30.39	43.07	38.05	30.84	37.87	39.71
0.01	**84.77**	**43.01**	**41.81**	**58.44**	**50.48**	**41.5**	**50.88**	**53.59**
0.009	88.45	44.85	43.79	61.09	52.61	43.34	53.12	55.99
0.005	111.27	56.25	56.16	77.63	65.82	54.76	67.04	70.89
0.001	197.86	99.37	104	140.98	115.73	98.28	120.05	127.79

Notice: the values in bold are the $R_{0.01\%}$ estimate values.

Table 4-2. Percentage errors of estimation of ITU and RH models.

%p	Jimma (1-min)	ITU	R-H	%error (ITU)	%error(RH)
1	3.3	5.89	4	-78.5	-21.21
0.5	6.6	10.63	8	-61.14	-21.21
0.1	34.5	29.26	16	15.17	53.62
0.08	41.4	32.91	19	20.49	54.10
0.05	58.2	41.65	26	28.43	55.32
0.01	122.9	84.76	76	31.02	38.16
0.008	133.1	92.69	83	30.35	37.64
0.002	200.5	155.73	131	22.32	34.66

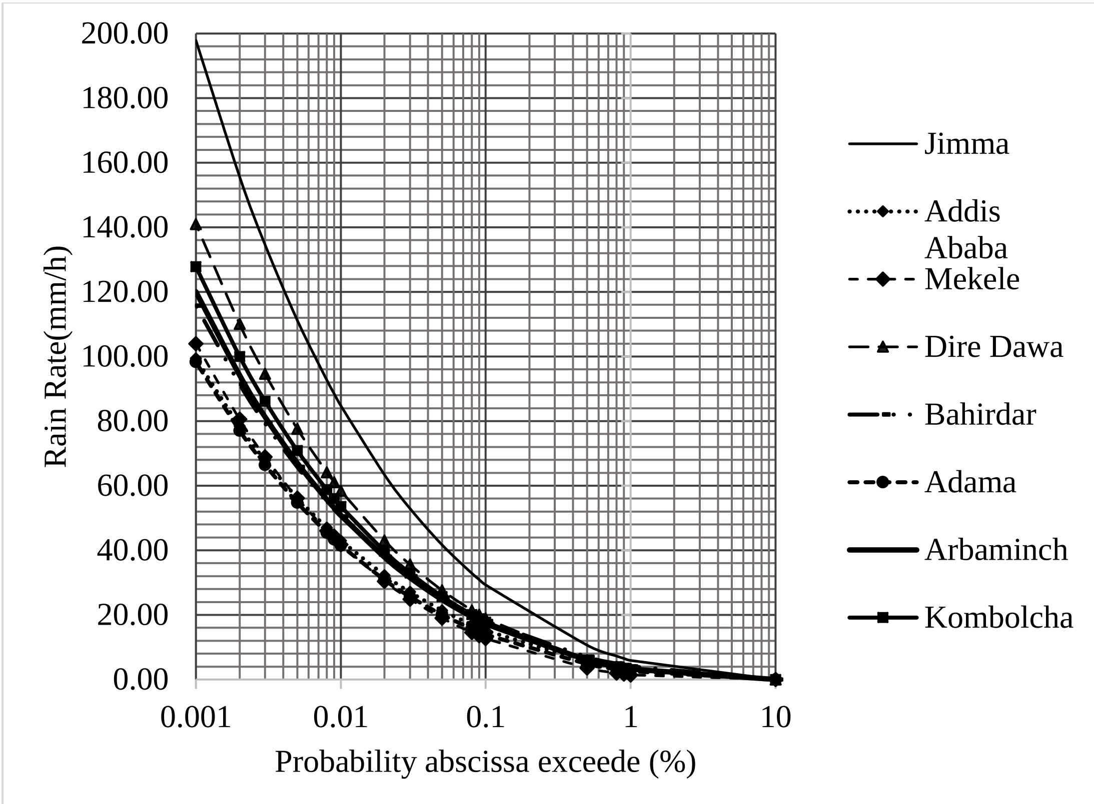

Figure 4-1. ITU R-P 837-7 predicted rain rate values.[52]

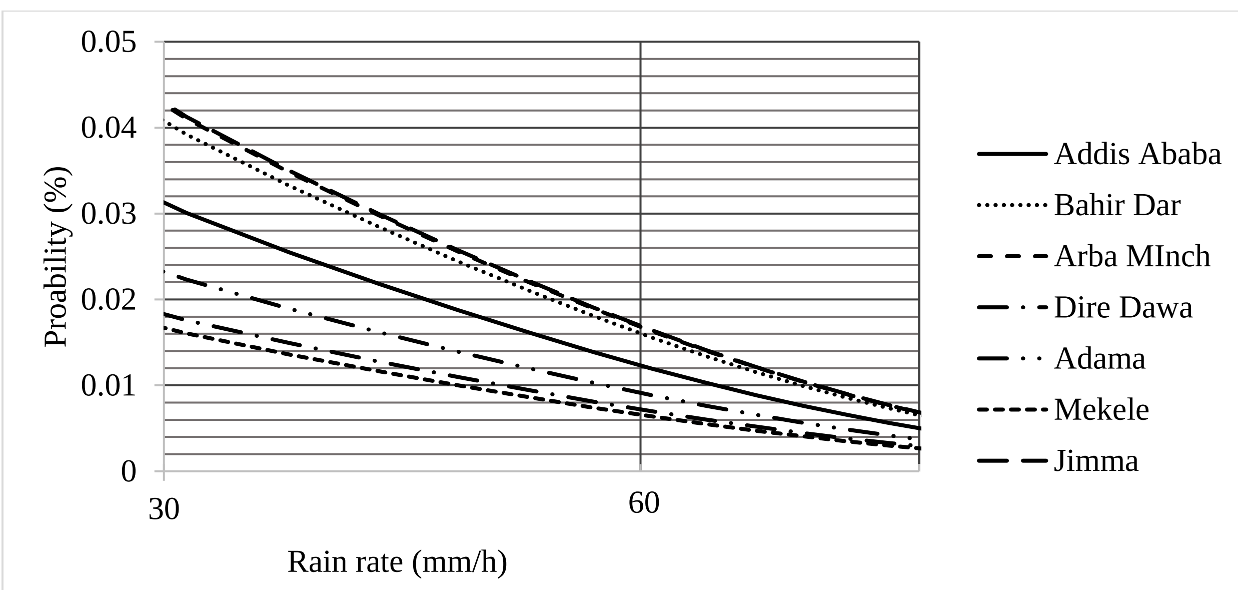

Figure 4-2. RH estimates of cumulative distribution of rain. [17]

4.3. Rain rate integration time conversion

Before proceeding to integration time conversion, the cumulative distribution of rain for Jimma was done based on available measured data. This can be seen in Figure 4-3. It is this distribution that serves as a reference point to develop conversion technique.

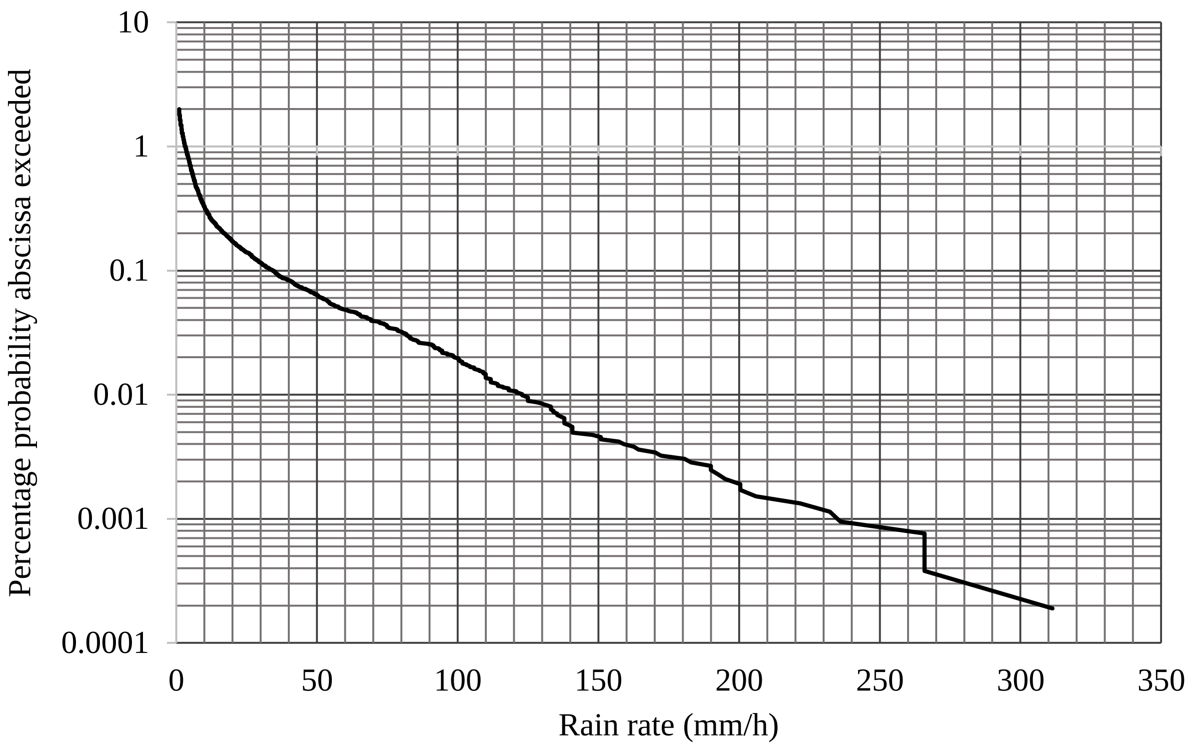

Figure 4-3. 1-min rain rate data and CDF for Jimma. $R_{0.01\%}$=122.9mm/h.

The first conversion method used for integration time conversion was the power law equation defined in (2.6). Our starting point for any conversion calculation is the Jimma 1-min rain rate distribution. Coefficients a and b were determined and these were used for other locations since only 15-min integration time for the other locations were available for this research work. The result of regression and fitting are presented in Figure 4-4. The correlation coefficient is also shown on the figure. A value of 0.978 can be improved using other methods. The research work showed that a correlation coefficient higher than the value above is obtained using the conversion factor approach. An RMSE value of 15.58 is also indicative of high mismatch between the data points. Due to lack of measured 1-min data for other locations in Ethiopia the research has used the result of integration time conversion for Jimma site to other cities as well. The results of the two approaches, i.e., the power law and the conversion factor methods, are presented. Due to the similarity in the rain process across these locations the work reasoned that the method doing well for Jimma site could as well give a better estimation result than other estimation methods.

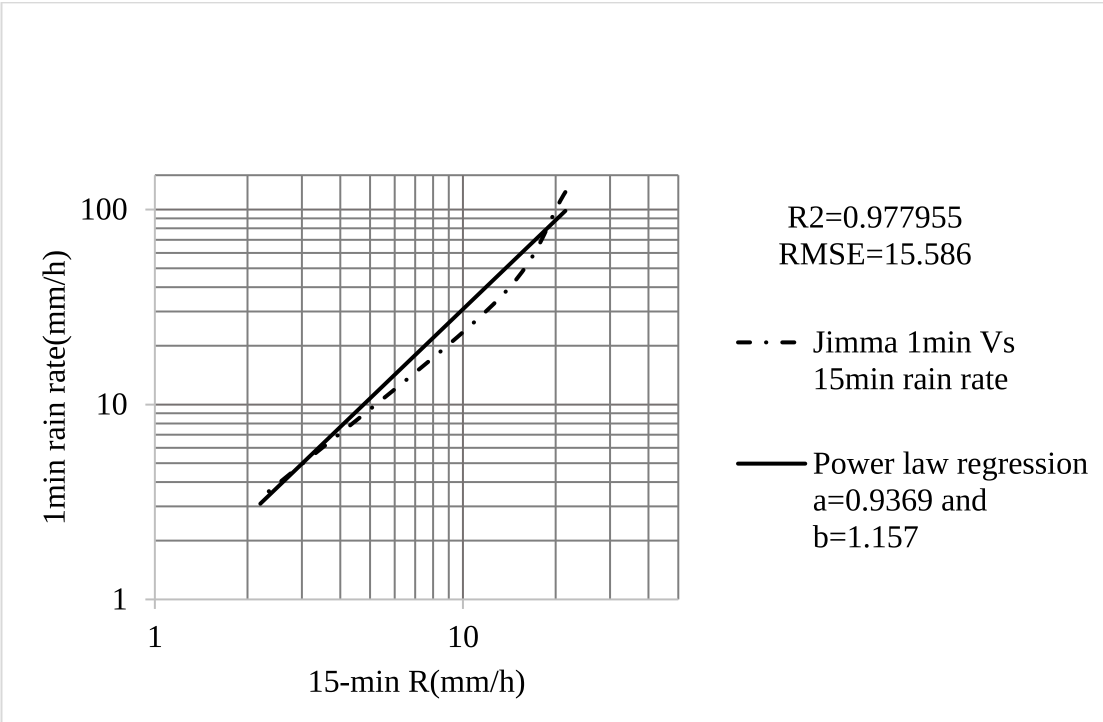

Figure 4-4. Power law regression fitting, 1-min Vs 15-min measured rain rate (Jimma).

The following table shows the estimation results.

Table 4-3. 1-min rain rate power law estimate based on results for Jimma data

1-min rain fall estimation(mm/h)				
Bahirdar	Adama	Arbaminch	Dire Dawa	Kombolcha
113.36	75.16	68.92	48.58	91.55
33.18	19.91	16.03	10.76	35.60
3.31	2.28	2.09	1.39	10.76

The 1-min probability exceedance levels were fitted against the 15-min data (both are measured set of rain rate data) for Jimma city to find the conversion coefficients a and b for power law method defined by $R(p)_1 = CF * R(p)_{15}$, where $CF = aP^b$. First the conversion factor CF is fitted against the probability levels as shown in Figure 4-5.

The second method clearly shows better estimation ability than the first one. As it is shown in Figure 4-6 ,both the correlation coefficient and the RMSE showed drastic reduction. The new RMSE of 2.66 is a huge improvement over 15.58. The correlation coefficient , 0.9995 is also close to unity, clearly indicating how close the measured and fitted data are.

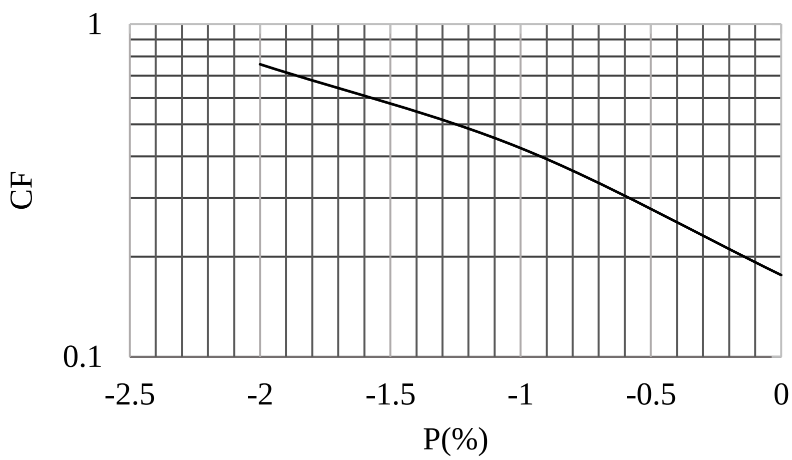

Figure 4-5. $CF=aP^b$ for $0.001<p<1$(a=1.451607, b= -0.29051)

This CF values are then used to calculate the estimated 1-min rain rate values as R_1=C F(p). R_{15}.

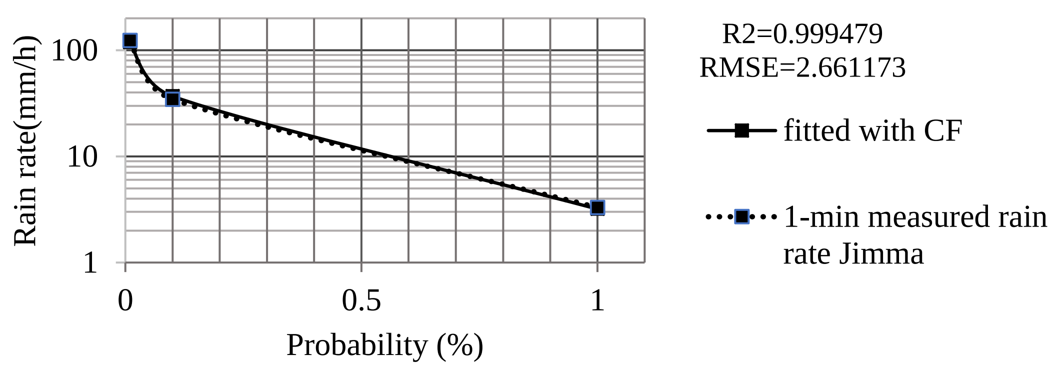

Figure 4-6. Regression fitting for Jimma. Integration time conversion with $CF(p)=aP^b$

There similarity in rain formation and orographic process between locations with in Ethiopia's territory. Integration time conversion coefficients based on rain rate data from Jimma should produce better estimation results than say the ITU models which are based on temperate climate rain data. The estimated 1-min rain rate values for selected cities is given below in Table 4-4.

Table 4-4. Conversion factor $R_{0.01\%}$ estimate based onJimma (m=measured, e=estimated)

City	Jimma			Addis Ababa		Bahir Dar		Mekele		Arbaminch	
%p	m (τ =1min)	m(τ=15min)	e (τ =1min)	m (τ =15min	e (τ =1min)	m (τ =15min)	e (τ =1min)	m (τ =15min)	e (τ =1min)	m (τ =15min)	e (τ =15min)
0.01	**122.9**	**21.5**	**118.88**	**13**	**71.88**	**23.6**	**130.49**	**13.5**	**74.64**	**17**	**94.00**
0.1	34.5	13	36.823	5.5	15.579	10.5	29.74	5.8	16.42	6.5	18.41
1	3.3	2.2	3.19	1.5	2.17	2.3	3.33	1.4	2.03	1.7	2.46

4.4. Rain cell size calculation

According to the method outlined in 3.3, the rain events were classified into bins and velocity assigned and distance statistics result fitted against rain rate to get the expression for rain cell diameter as a function of rain rate. here the results are presented as follows.

Figure 4-7 shows the cumulative probability of distance of each rain class. It can be seen that as the rain rate increases the distance covered by the rain even decreases. This confirms out intuitive understanding that light rain regimes tend to last longer and cover wide area while more intense forms of rain tend to be short lived thus affecting only a specific area.

According to power law regression result, the rain cell diameter is given by:

$$D = 53.927R^{-0.86979}Km \qquad (4\text{-}1)$$

The regression fitting procedure is shown in Figure 4-8. The rain rate $R_{0.01\%}$ is 122.9mm/h. This gives a diameter of about 0.9Km. Deep fades, when they occur, encompass 1Km of an area.

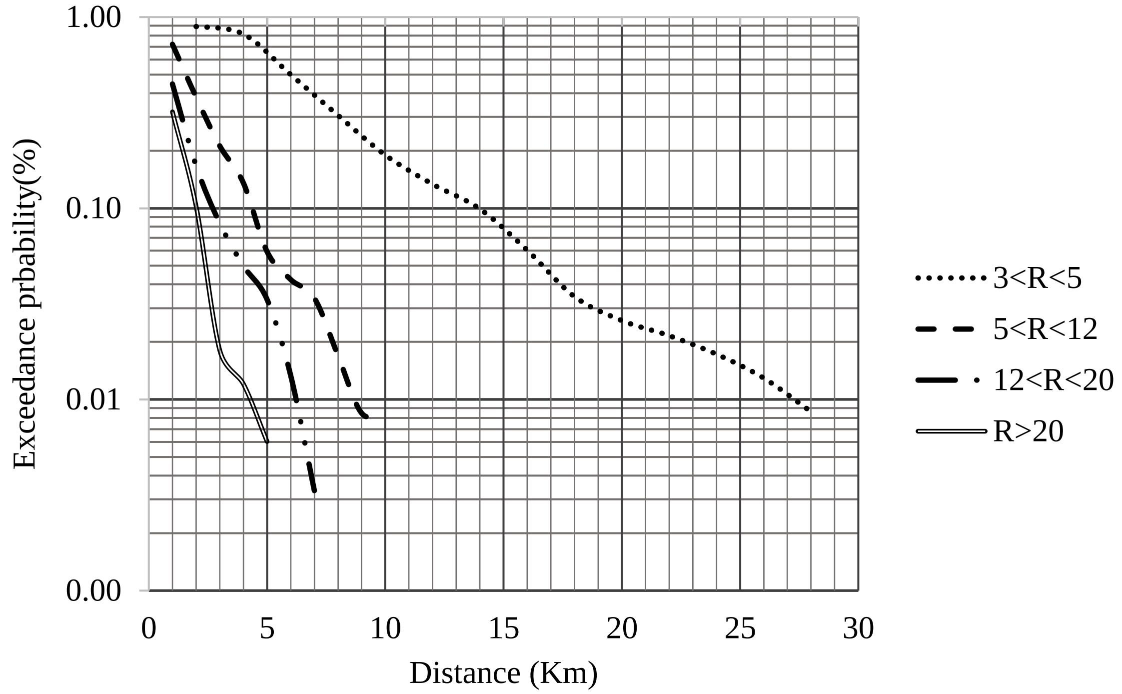

Figure 4-7. Cumulative distribution of rain cell diameter.

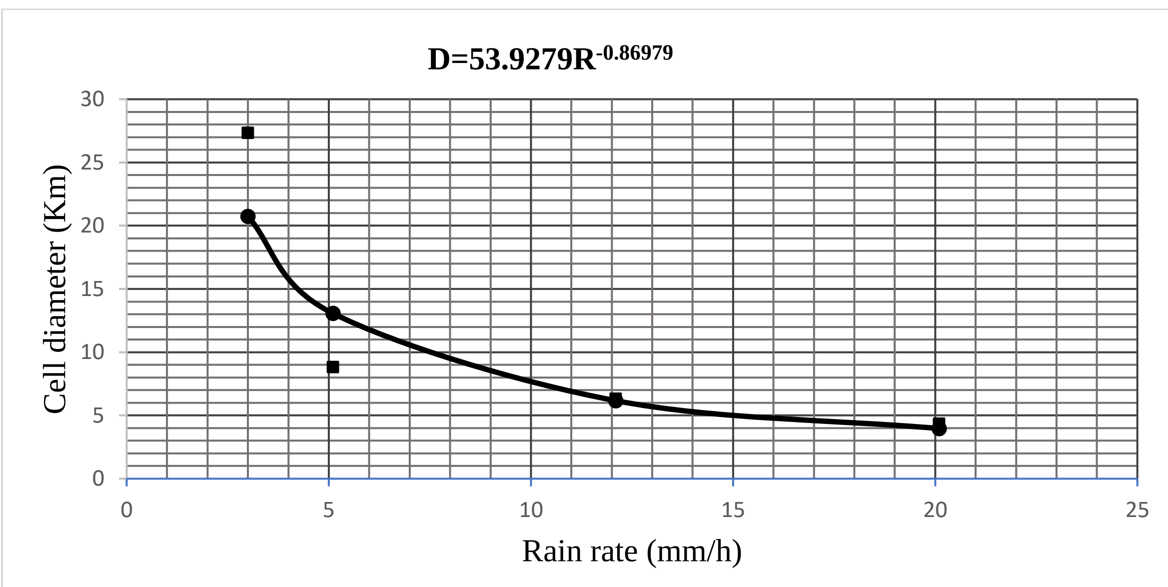

Figure 4-8. Rain cell diameter vs rain rate for Jimma

4.5. Drop size distribution

In this section the comparison of the candidate DSD functions are compared. The peculiarities of the distributions are investigated.

Let's discuss the Marshall-Palmer distribution first. Described by the negative exponential function of (2-17), this DSD model has found applications in many research works and standards accepted worldwide. The logarithmic plot of MP DSD at rain rates 0.23, 1.1, 14 and 64mm/h is shown in Figure 4-9. The general trend of the doesn't change from one rain rate to the next. It is a monotonically decreasing function of the drop diameter D. This means in all scenarios the small diameter sized drops have the highest degree of effect on the propagating electromagnetic wave. Despite its famed use to date, even the original researchers who proposed the DSD model have indicated that the model overestimated the concentration below drop diameter of 1.5mm [35]. The researchers have referred to another work [33] for a better description of small size diameter drop concentration. Laws and Parsons' measurement showed a median in the region of 2-3mm.

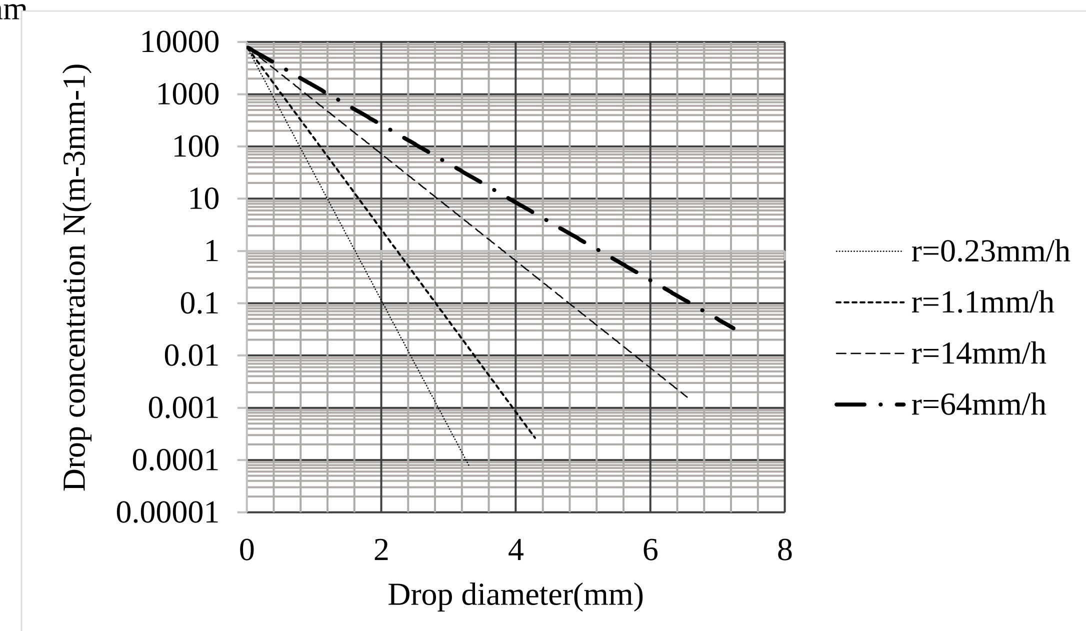

Figure 4-9. Marshall-Palmer DSD concentration (log scale) plot at different rain rates.

The next models are discussed to get representative model for the tropical region from among widely used models. It is clear that the tropical region is markedly different from the temperate region in terms of seasonality, intensity and orographic process involved in the rain formation process. These models are known as the lognormal model of Ile Ife and modified lognormal distribution of Butare whose expression are given in equations (2-25) and (2-19) respectively. As the Ile Ife model is earlier in its conception, it is discussed first. The model is the result of method of moments fitting of experimental DSD data in Nigeria, Ile Ife by Ajayi and Olsen [43]. Figure 4-10 shows what was missing from the above MP model. It does indicate a moving median as the rain rate increase affirming the fact that intense rain fall events are associated with larger size droplets.

Figure 4-11 is a logarithmic scale plot of the lognormal distribution. Not only do the two plots show the agreement of the lognormal model to results various drop size concentration measurement campaigns but also seems to be truncated above the drop diameter size of 7mm. It has been stated that drop diameters beyond 7mm don’t hold stable for long and disintegrate into smaller diameter drops.

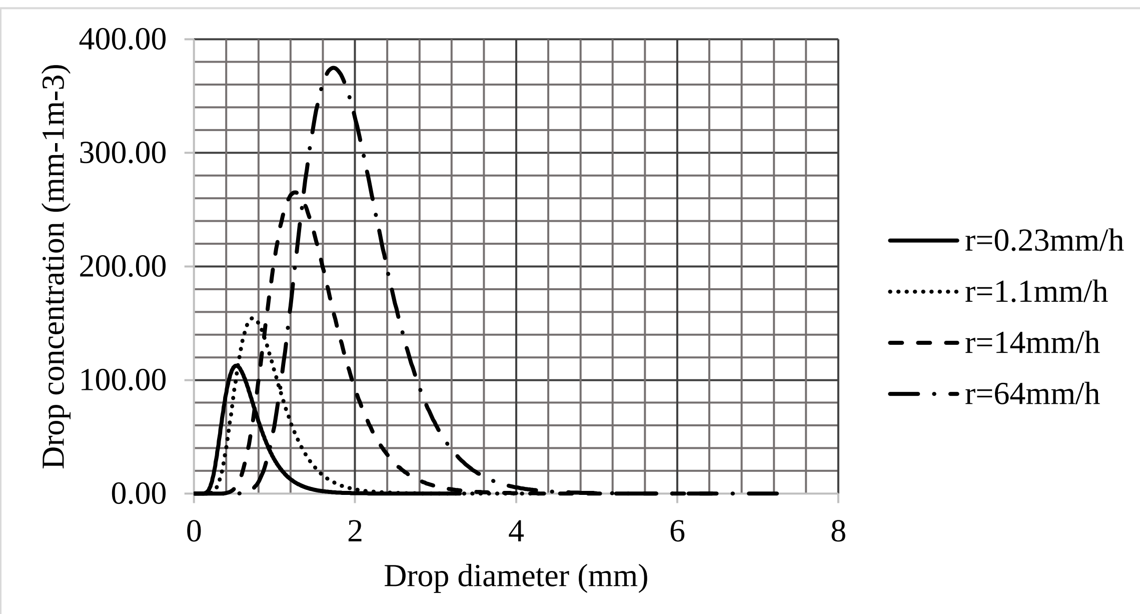

Figure 4-10. Lognormal DSD of ILe Ife as modeled by Ajayi and Olsen [43]

The second model in discussion, defined for another tropical location, Butare, Rwanda, is the modified log normal DSD model. The expression is given in equation (2-19). It is defined in piece wise manner among four rain regimes, i.e., drizzle, widespread, shower and thunderstorm. The drop size concentration is plotted at the same rain rates on Figure 4-12. It has the general trend shown by the lognormal model in Figure 4-10. A huge difference exists around the drop size concentration around r=0.23mm/h.

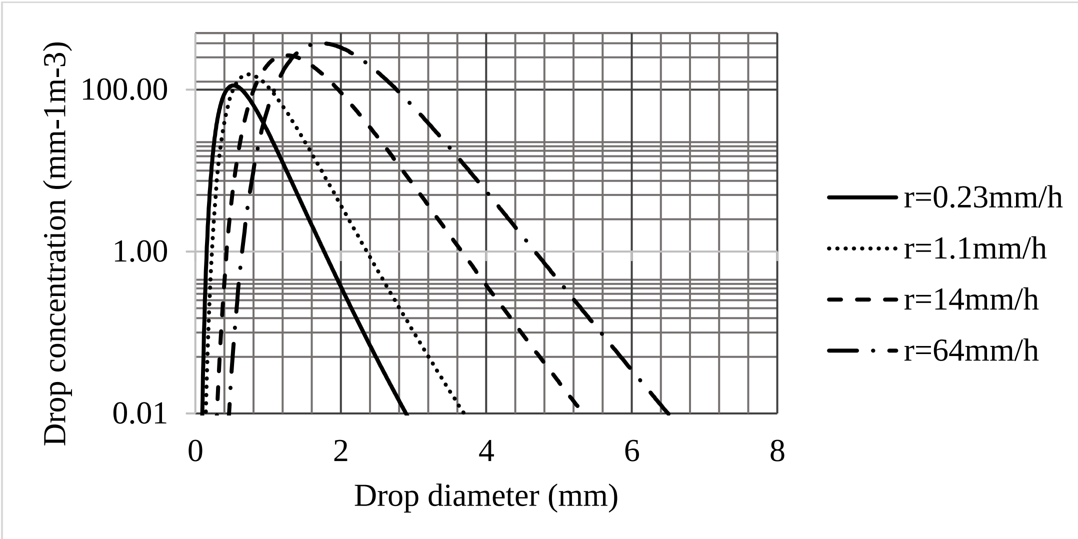

Figure 4-11. Log scale plot of drop size concentration of Ajayi's lognormal DSD model

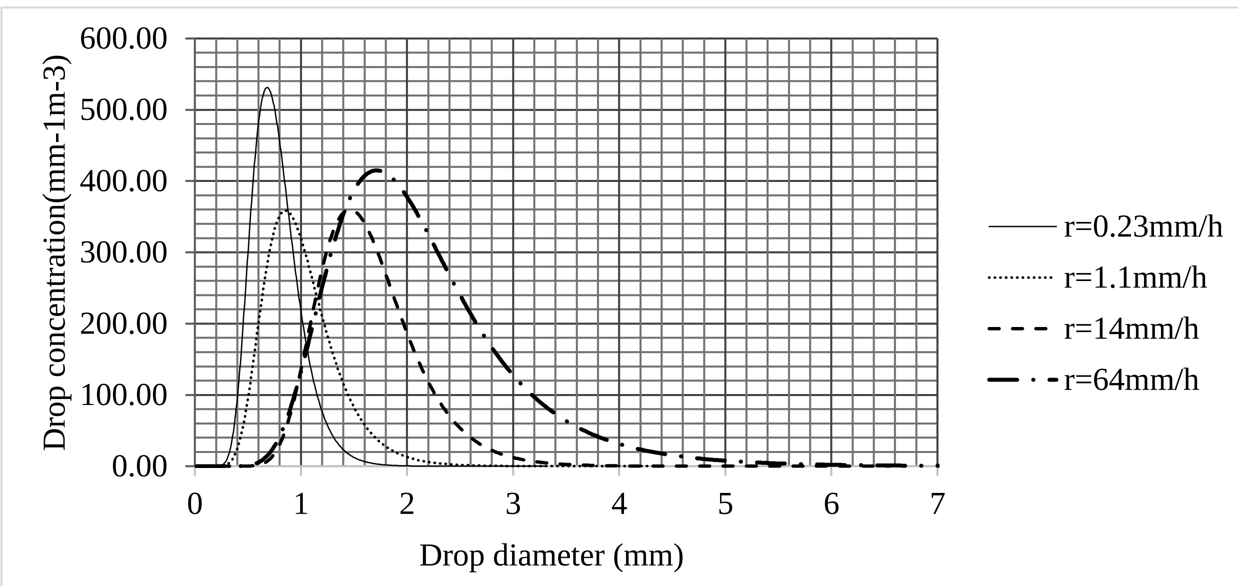

Figure 4-12. Sumbiri's modified log normal DSD plot for rain rates 0.23, 1.1, 14, 64mm/h.

The other difference visible as the rain rate increase on the log scale plot of Figure 4-13 is the modified lognormal model doesn't seem to take into consideration the physical stability of droplet sizes above 7mm. As the rain rate increases, the number of larger drop size contributing to the total DSD increases contrary to what can be seen in the lognormal model of Ile Ife.

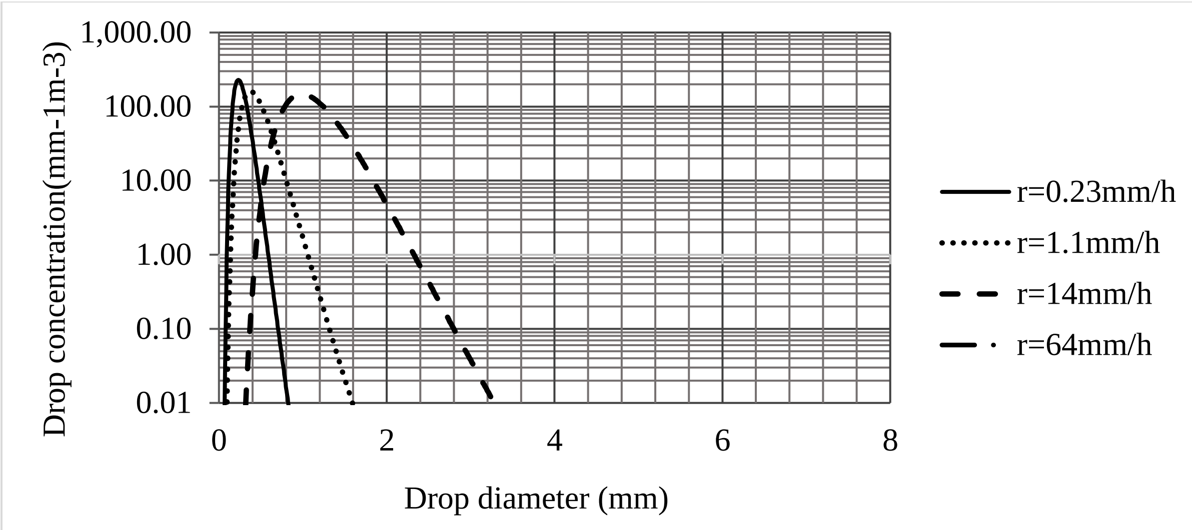

Figure 4-13. Log scale plot of the modified drop size distribution.

To help see the difference of the three DSD model the research work give a plot of the above three models in the same figure ate equal rain rates in Figure 4-14.

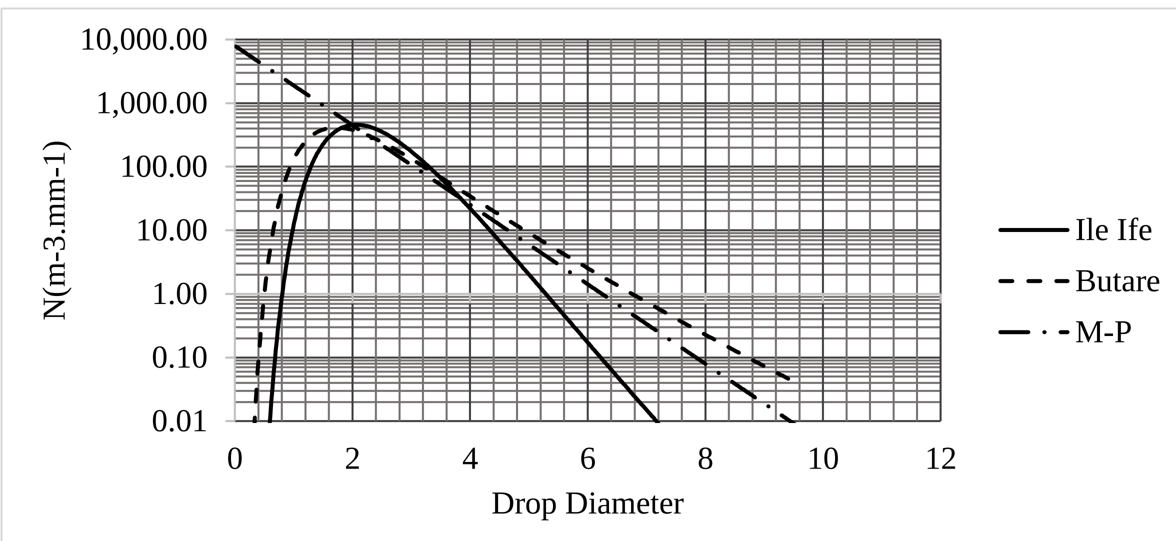

Figure 4-14. Comparison of DSD models at r=146mm/h.

It can be seen that even at rain rate of 146mm/h, the lognormal model of Ajayi has hold its relevance in terms of the droplet sizes. The number of droplets with size bigger than 7mm are radically reduced. The other two models, MP and modified lognormal model continue to entertain that region of diameter despite physical meaninglessness.

4.6. Propagation coefficients ($T_{ext}, T_{abs}, T_{scat}, a_p$)

In this section the result of propagation coefficients calculations is presented. As a functions of system variables such as temperature, frequency, drop size and drop size concentrations, the dependency of propagation constants on these parameters are discussed. The results will be discussed in terms of the impact of rain intensity . Here the research work presents the dependence of Mie efficiencies ($Q_{abs}, Q_{scat}, < costeta >$) on temperature and frequency. The effect of a single drop as a function of temperature and frequency.

4.6.1. $\mathbf{Q_i}$ Vs frequency

The interaction of drop lets with EMW highly dependent on the frequency of transmission. The size of the drops and the wave length become comparable in the frequency region which is our topic of interest. The following series of figures show how the efficiencies vary as a function of frequency. First, let's see what the efficiencies look like at different frequencies.

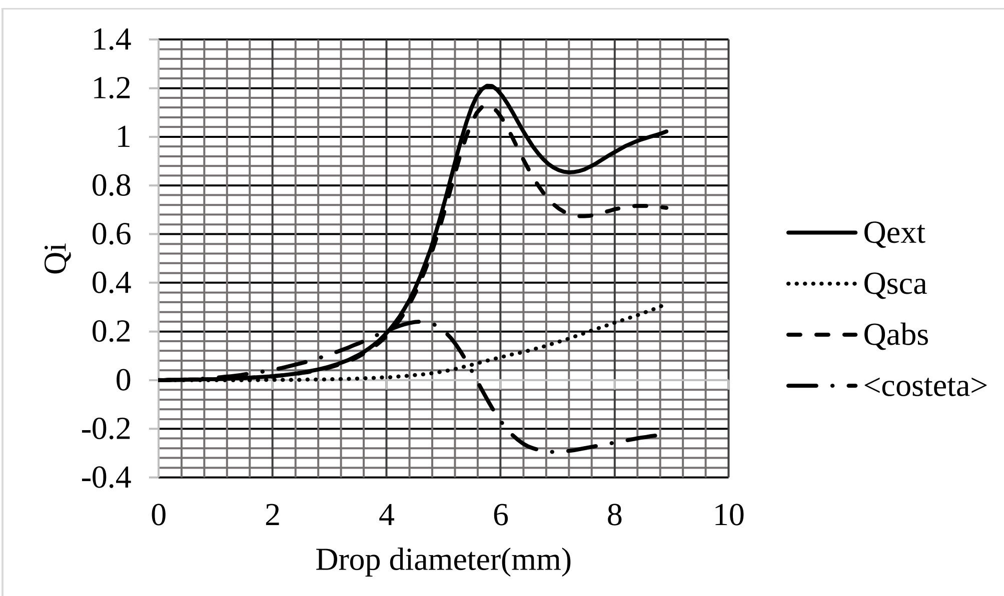

Figure 4-15. Qi Vs drop diameter at 6Ghz.

Figure 4-15, Figure 4-16, Figure 4-17 and Figure 4-18 show the contribution of drop size to the efficiencies which determine the propagation coefficients. Starting from 6GHz and going up the maximum contribution from among the drop diameters becomes higher for small sized drops. At 6GHz the highest contribution happens to be around drop diameter of 6mm and as the frequency

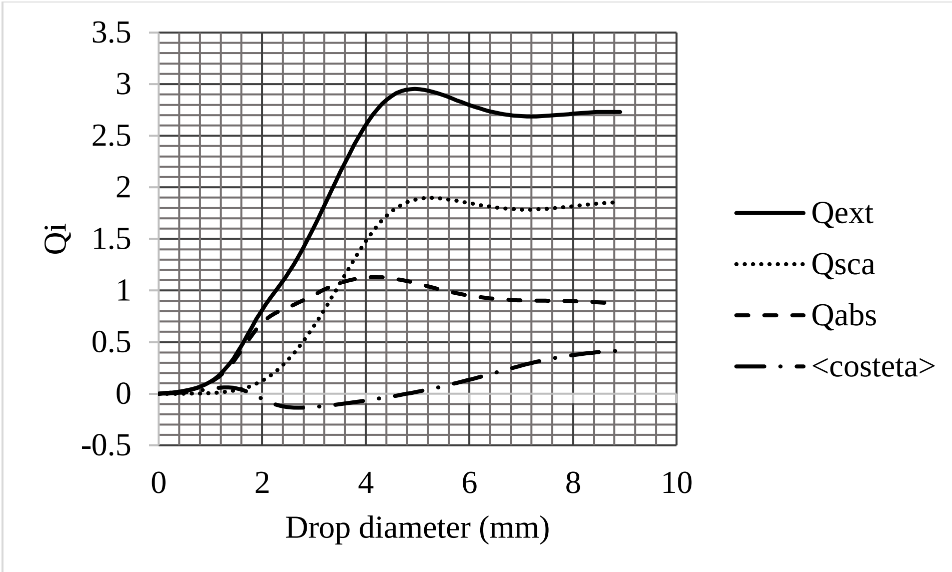

Figure 4-16. Qi Vs drop diameter at 21GHz.

increases (and the wavelength decreases correspondingly) the height of contribution begins to drift into the smaller diameter region.

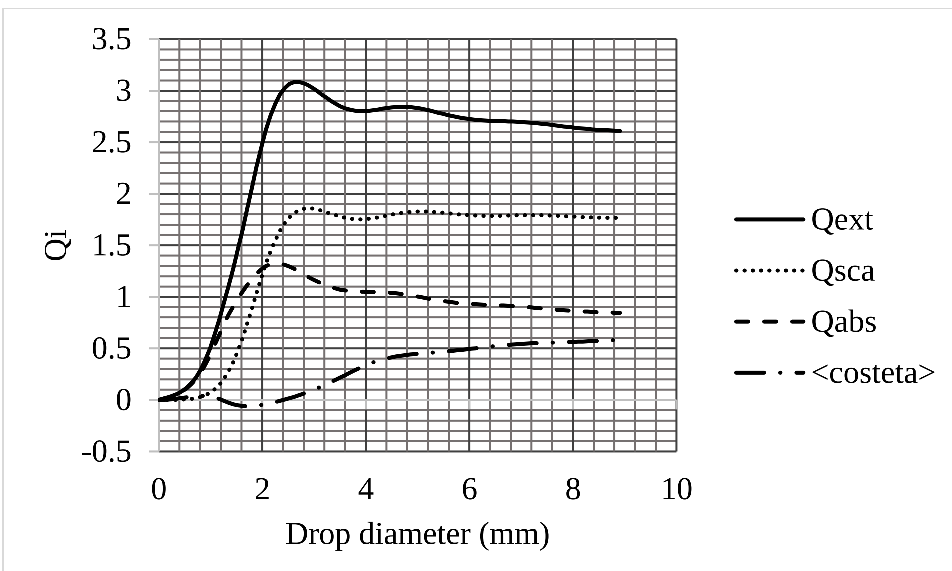

Figure 4-17. Qi vs drop diameter at 38GHz.

Finally, at f=90GHz the drop diameter in the region of 1-2mm has the highest contribution. Figure 4-19 shows the logarithmic scale plot.

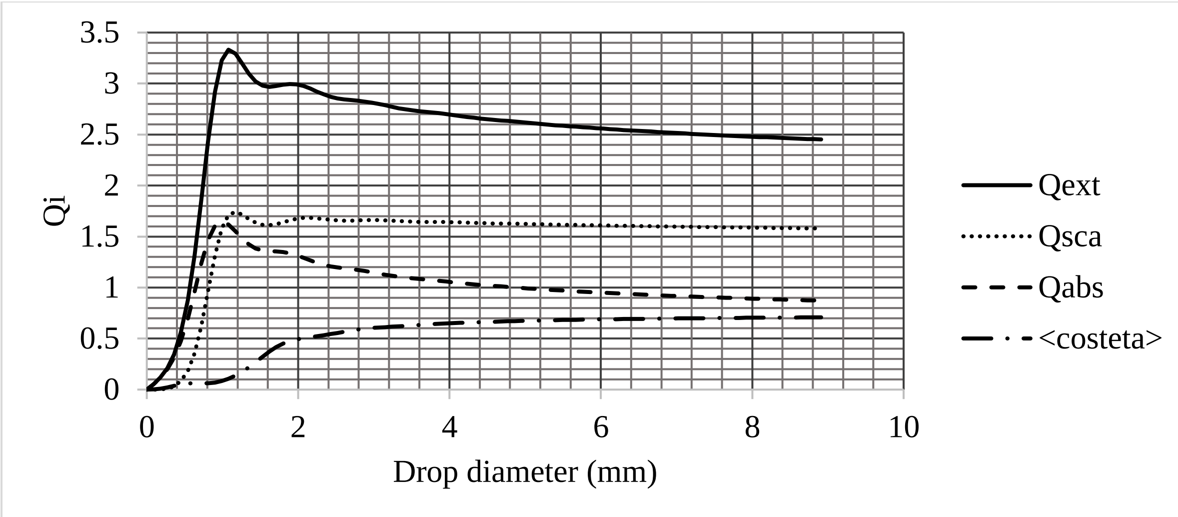

Figure 4-18. Qi vs drop diameter at 90GHz.

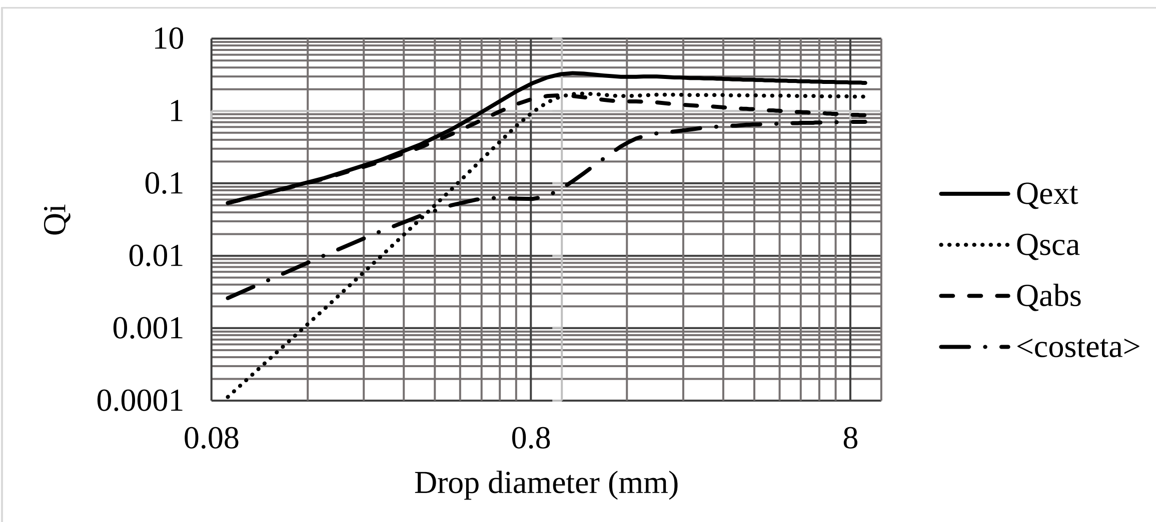

Figure 4-19. Logarithmic plot of Qi vs diameter at 90GHz.

4.6.2. Q_i Vs temperature

The temperature affects the complex refractive index of water. Propagation studies made in temperate regions cannot reflect the exact figure in the tropical region where the ambient temperature not as cool as one would expect. The following illustrations demonstrate the effect of temperature on the efficiencies.

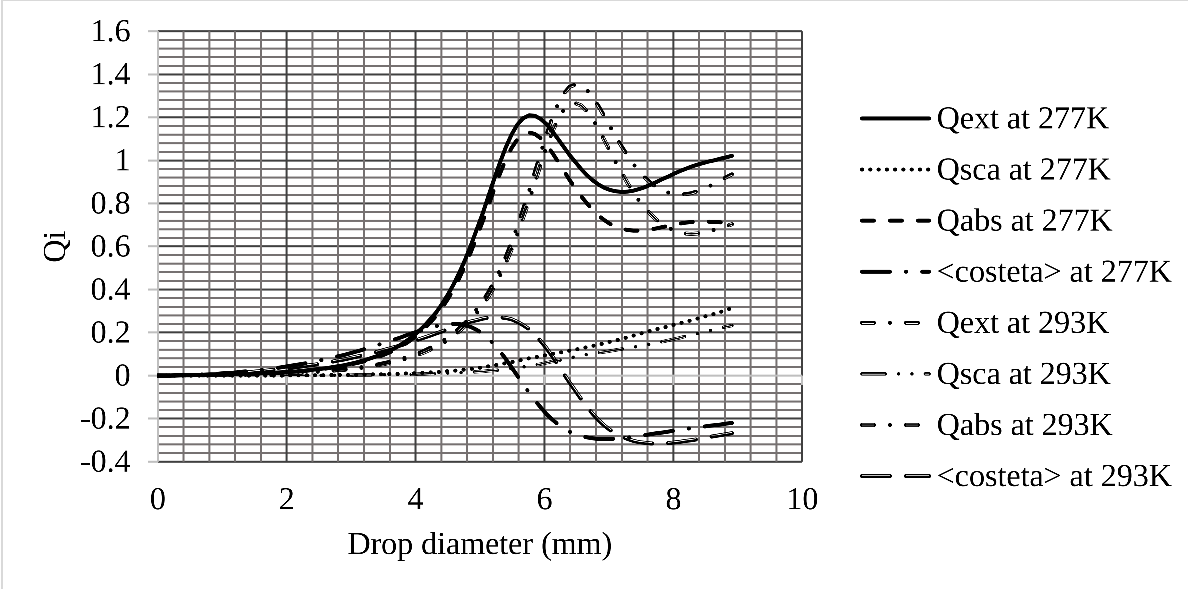

Figure 4-20. Comparison of Qi vs drop diameter at 277K and 293K at 6GHz.

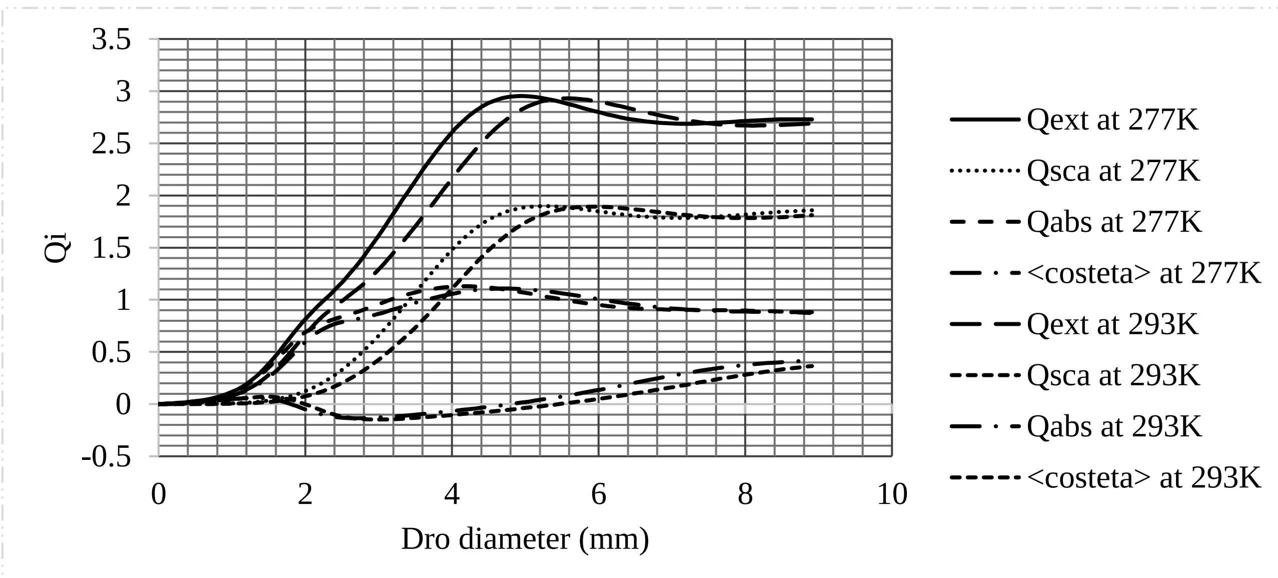

Figure 4-21. Comparison of Qi vs diameter at 277K and 293K at 21GHz.

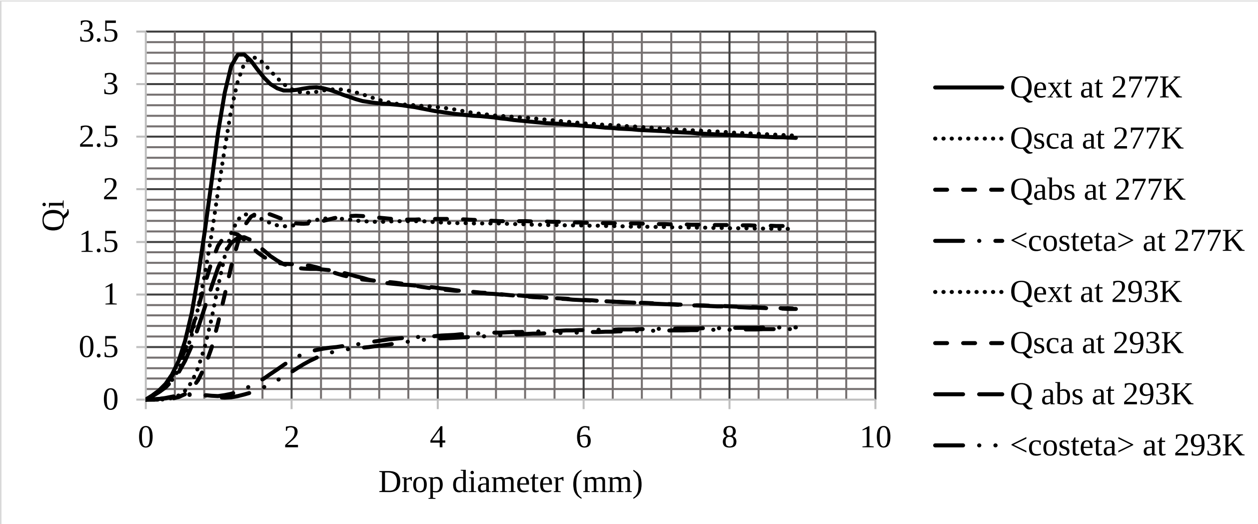

Figure 4-22. Comparison of Qi vs diameter at 277K and 293K at 75GHz.

The effect of temperature could be seen in Figure 4-20, Figure 4-21, Figure 4-22. The Qi plot has moved to the right showing decrease in the contribution of smaller droplets. The effect however seems to be overshadowed by increase in frequency.

Having seen the effect temperature and frequency on the magnitude of the frequencies, it is time to assess the effect of multitude of droplets, as is the case during rain fall.

4.6.3. T_{i} vs rain rate

As the whole research work centers around rain and its effect on propagation of EMW, it is worthwhile to look at how the scattering cross sections are affected by rain. The calculation of cross sections is done by equation (3-13) and the average of the scattering angle by equation (3-14). As the equations reveal explicitly the quantities are dependent on the particular DSD model employed for the calculation . In section 3.4, the research work has shown how the different DSD models fare against actual DSD measurements . The following figures show the dependence of the cross sections on the rain rate. The case for the three DSD models , i.e., MP, Ajay's lognormal and Butare's modified lognormal, are compared and illustrated. This section is important because all the propagation parameters like the absorption depth , extinction depth and anisotropy factor which determine the channel matrix all depend on the rain rate and the chosen DSD profile of the area . Let' s start the discussion by showing how $\boldsymbol{T_i}$ varies as a function of rain rate ate different frequencies using the much-famed MP drop size distribution model.

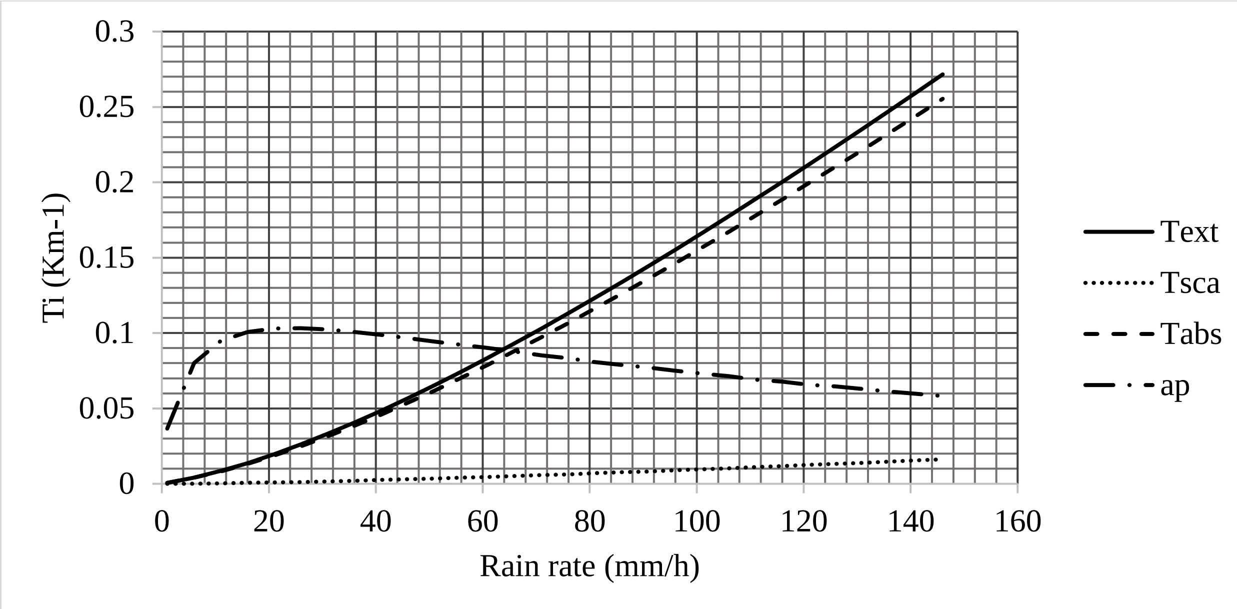

Figure 4-23. *T*i vs rain rate at 6GHz with MP DSD.

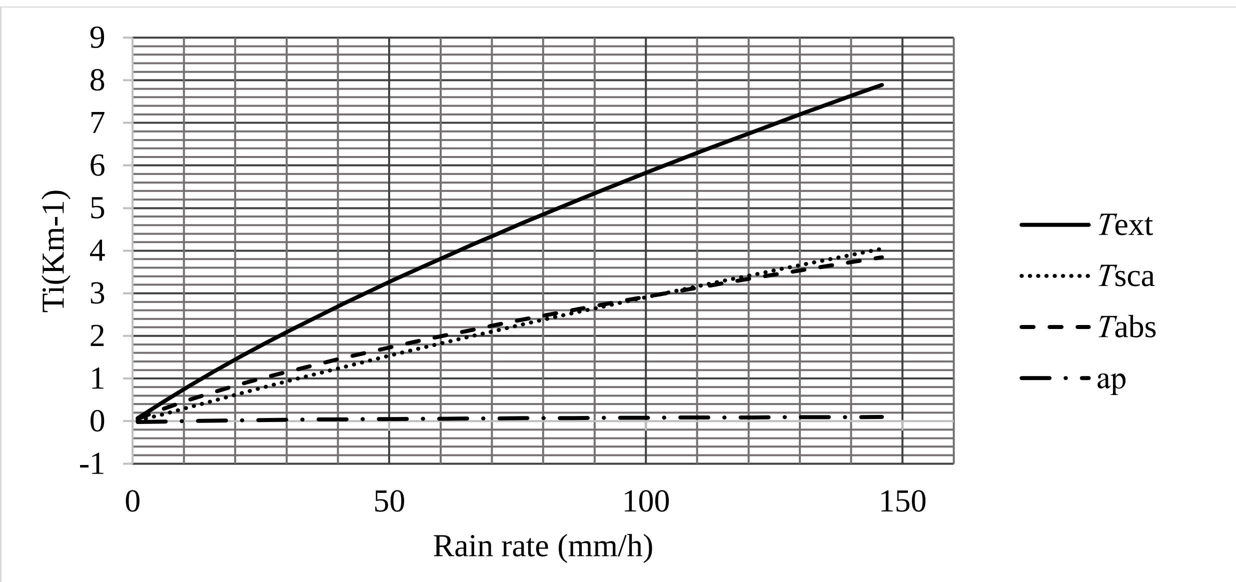

Figure 4-24. *T*i vs rain rate at 38GHz with MP DSD.

From the above Figure 4-23, and Figure 4-24 it can be seen how the rain rate affects the propagation constants. The extinction coefficient, *T*ext, which indicates the level of power loss from both scattering and absorption, is around 0.27 at the highest rain rate, 146mm/h at 6GHz. The increase in attenuation at 38GHz is more than 13dB.

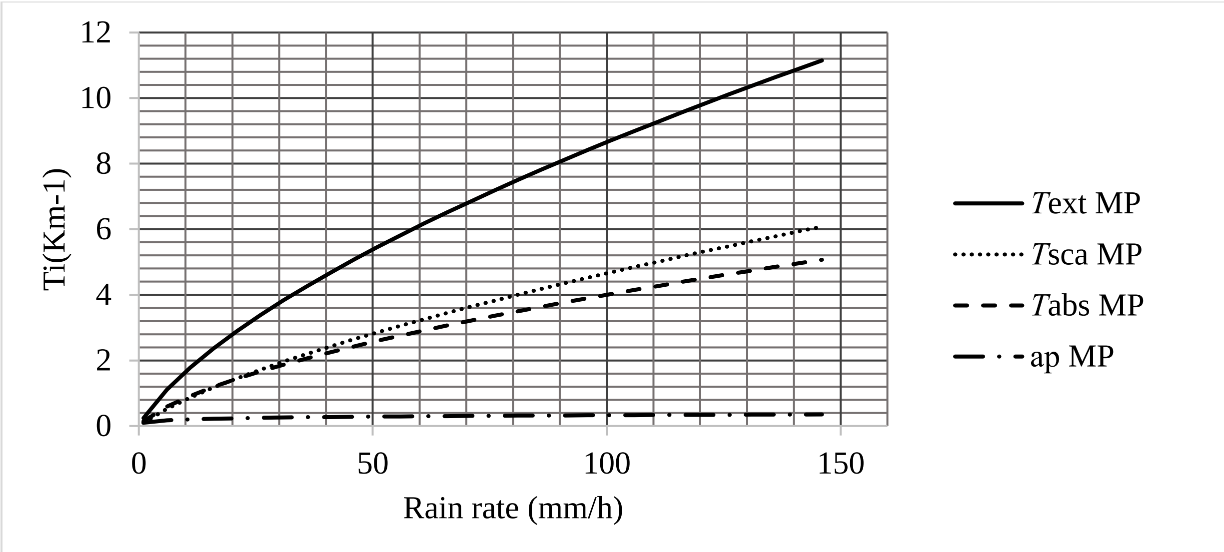

Figure 4-25. T_i vs rain rate at 75GHz with MP DSD.

The increase in extinction coefficient looks abated moving from 38GHz to 75GHz. The increase is only around 1.4dB. This is further confirmed in the calculation of the specific attenuation in the next section.

Lest now take a look at how the different modified DSD models established to describe the rain event across the tropical region of Africa work. First the Ile Ife model devised by Ajayi and Olsen [43].

The instant observation from Figure 4-26 is that the propagation coefficients are lower than those obtained using the MP DSD. In section 3.4 it was revealed that the MP DSD is a monotonically decreasing function of drop diameter. It was also stated that it doesn't represent the measured drop size concentration, in the small diameter region especially. It indeed gives that highest importance to small diameter droplets when in fact in the modified lognormal [43] and modified lognormal [42] models the concentration of droplets in the lower diameter class tends to be zero.

Figure 4-27 shows how the MP and the lognormal DSD compare in terms of contribution to *T*i. Once again lets to go back to Figure 4-14 of section 4.5 to explain the observed mismatch between the MP and lognormal DSD. In the figure it is seen that the MP DSD model over emphasizes the importance of small diameter droplets. The concentration of rain drops with diameter less than 0.8mm is in the thousands and reaches up to ten thousand for even smaller ones.

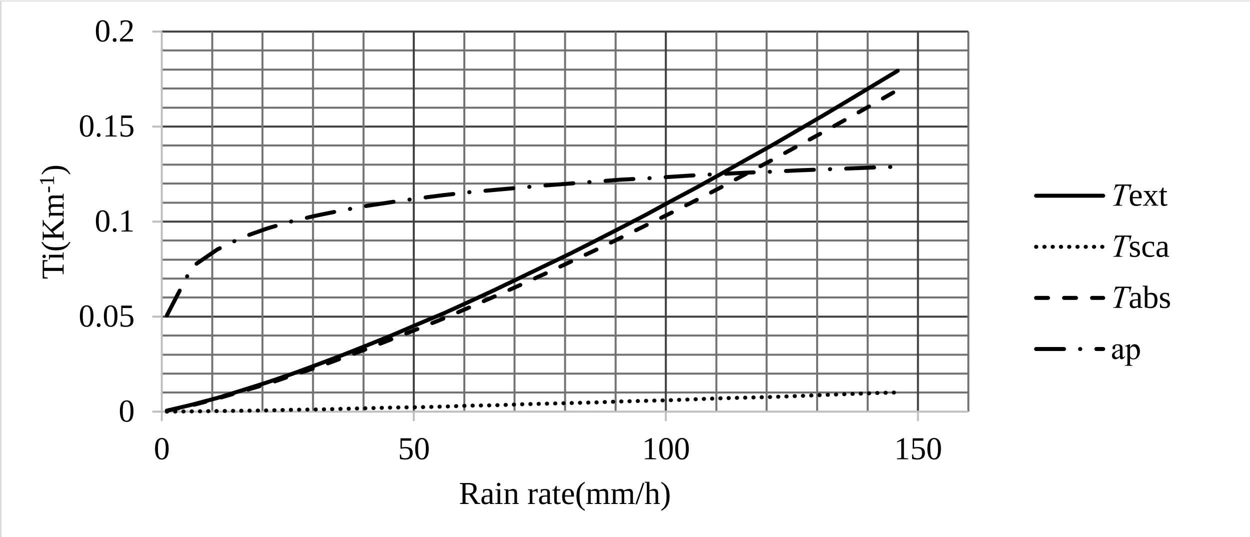

Figure 4-26. T_i vs rain rate at 6GHz with Ajayi's lognormal DSD.

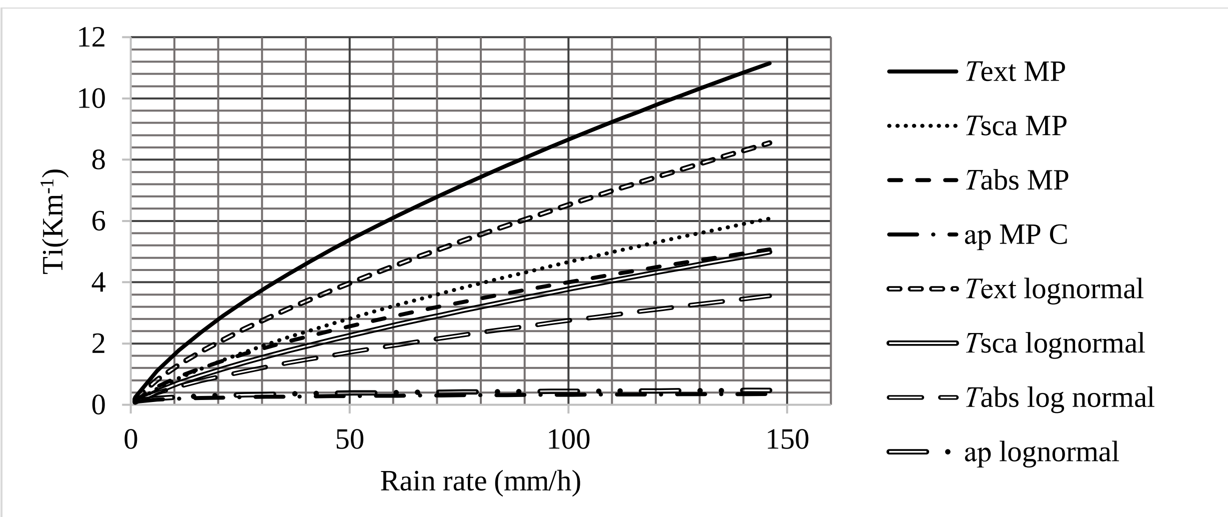

Figure 4-27. Comparison of MP and lognormal DSD models at 75GHz

In contrast the concentration of this region on the lognormal DSD could only barely counts 300 and it gets fewer and fewer for smaller diameters. When the think about the integration interval the effect of large number of smaller diameter drops gets even bigger as can be seen in Figure 4-27. Figure 4-28 and Figure 4-29 show comparison of MP to lognormal DSD and lognormal to modified lognormal DSDs, respectively. It is no wonder to see similarities between the two tropical -region DSD models when the researchers compared with the MP DSD show huge disparity.

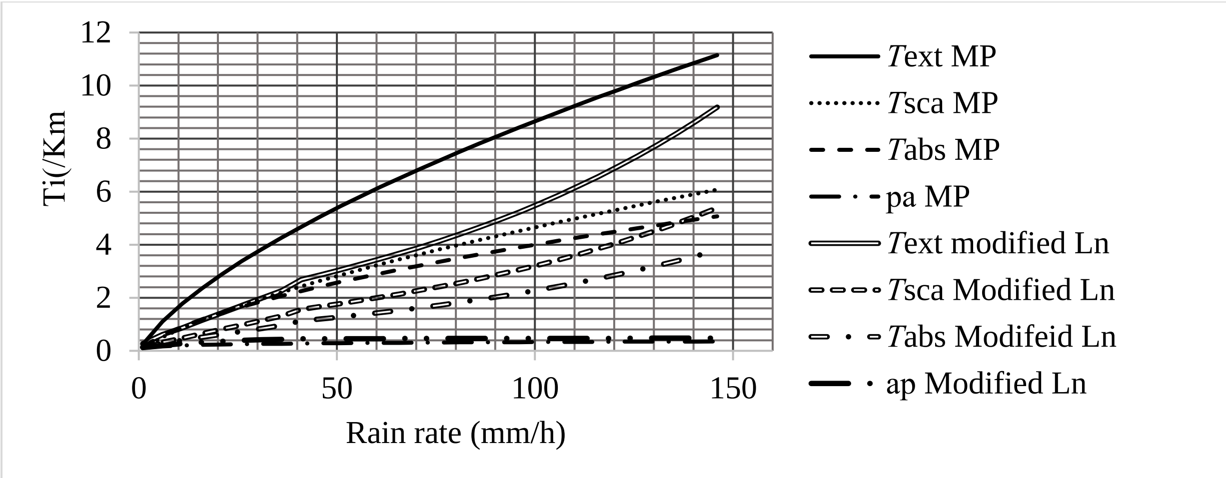

Figure 4-28. Comparison of MP and modified lognormal distribution.

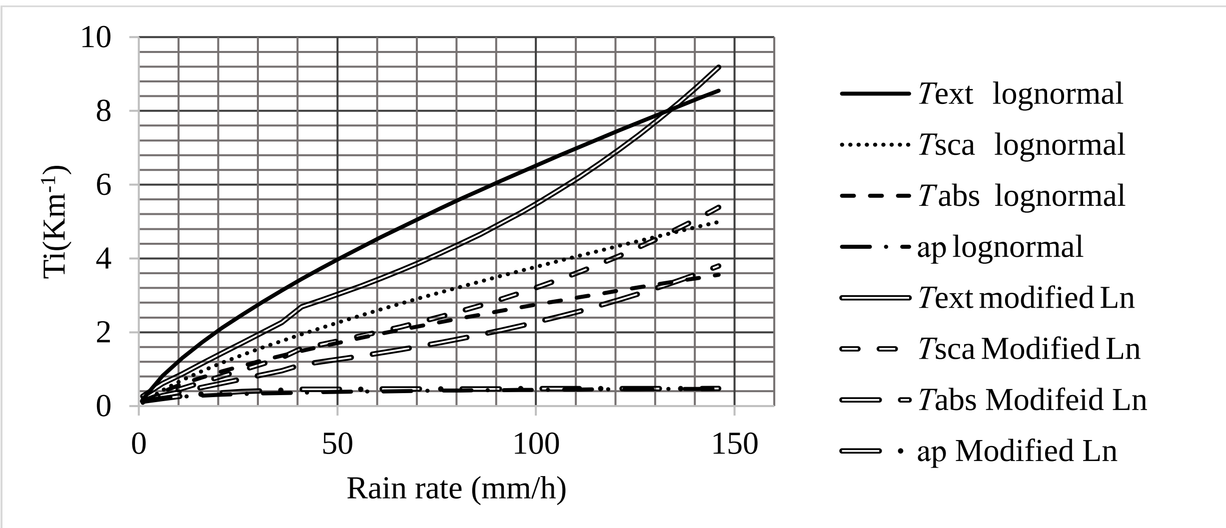

Figure 4-29. T_i vs rain rate comparison of modified-lognormal and lognormal DSD at 75GHz

4.6.3. T_{i} vs frequency

This is the last section in a series of demonstrations to show how the propagation coefficients change as a function of system parameter . The frequency , by which it is inevitably meant the wave length plays important role in the magnitude of interaction of droplets with transmitting wave . As the size of the droplets becomes comparable to the wavelength the attenuation and other effects increase . This is illustrated in the next figures which show the variability of propagation constant at different rain rates versus frequency . Figure 4-30 shows the huge difference in *T*i values that follows the increase in rain rate. Next the research investigated the lognormal DSD at the same rain rates. The next Figure 4-31 lognormal DSD at different frequency and its contribution to *T*i. The next section deals with the calculation of specific attenuation . The dependence of attenuation calculations on DSD model being used is clearly illustrated.

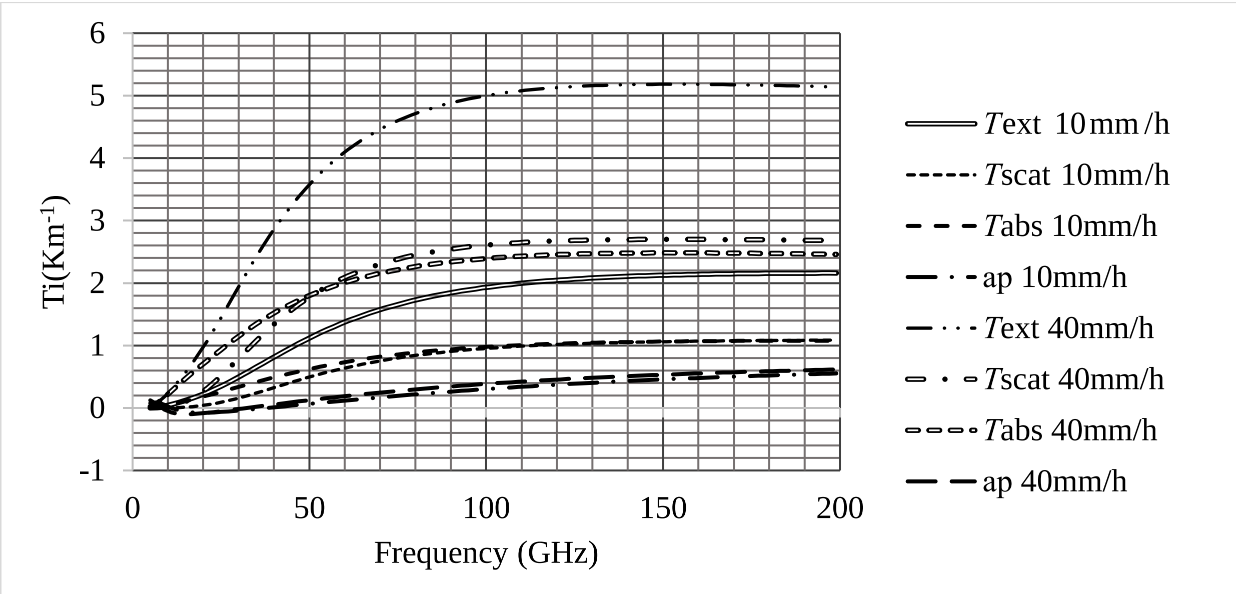

Figure 4-30. T_i vs frequency at 10 and 40mm/h with MP DSD.

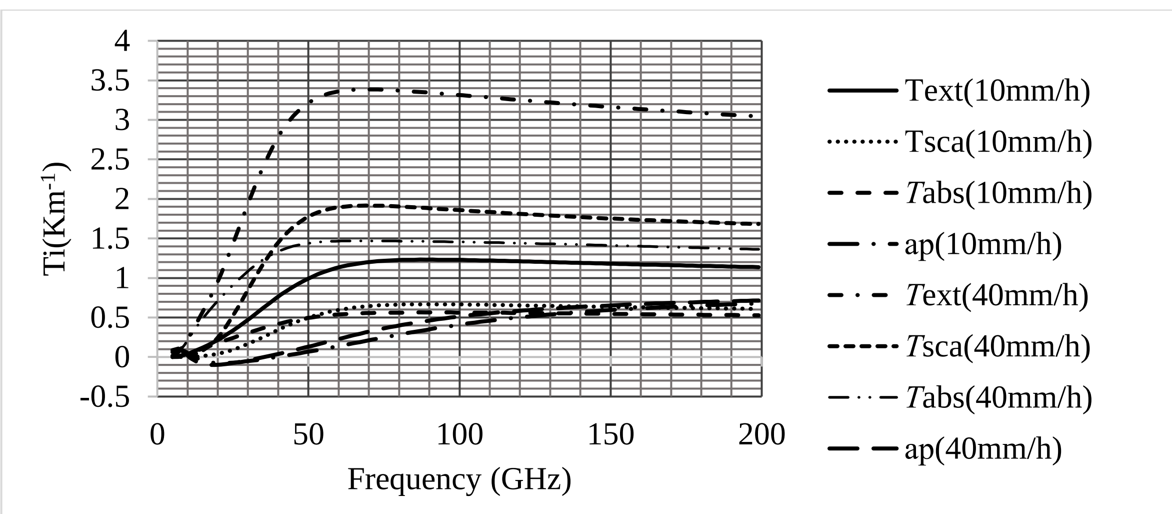

Figure 4-31. *Ti* vs frequency at 10 and 40mm/h with the lognormal DSD.

4.6.4. Specific attenuation

In this section, the specific attenuation calculations using two approaches are presented. As discussed in the literature review section 2.5.2 ITU R-P530-16 [2] provides specific attenuation calculation complete with rain rate $R_{0.01\%}$ prediction method. This procedure is detailed in section 2.5.2. Comparison of this approach is made with the method employing the forward scattering function described in 3.5. Series of figures are presented here illustrating the results of different approach specific attenuation calculations. First the specific attenuation calculated using ITU's recommended method together with [52] predicted $R_{0.01\%}$. This is shown in Figure 4-32. To start with, the $R_{0.01\%}$ value is far from what to be expected considering Ethiopian climate. Jimma, for example, with the highest $R_{0.01\%}$ of all with 84.77mm/h is not accurately represented with this figure. As described in section 4.2, the $R_{0.01\%}$ value obtained from measurement data is around 122.9mm/h. So, it is imperative to devise a more reliable means of calculating the specific attenuation.

Figure 4-33 shows the difference in specific attenuation values obtained by using rain rate values predicted by the method introduce in this research work based on measured data from Jimma. For the sake of clearer comparison only five cities are presented. From Figure 4-32 and Figure 4-33 it is clear to see that the prediction method employed by [51],[52] and [2] underestimates the attenuation values. Taking Jimma for instance, the specific attenuation at 50GHz is 23.8dB/Km

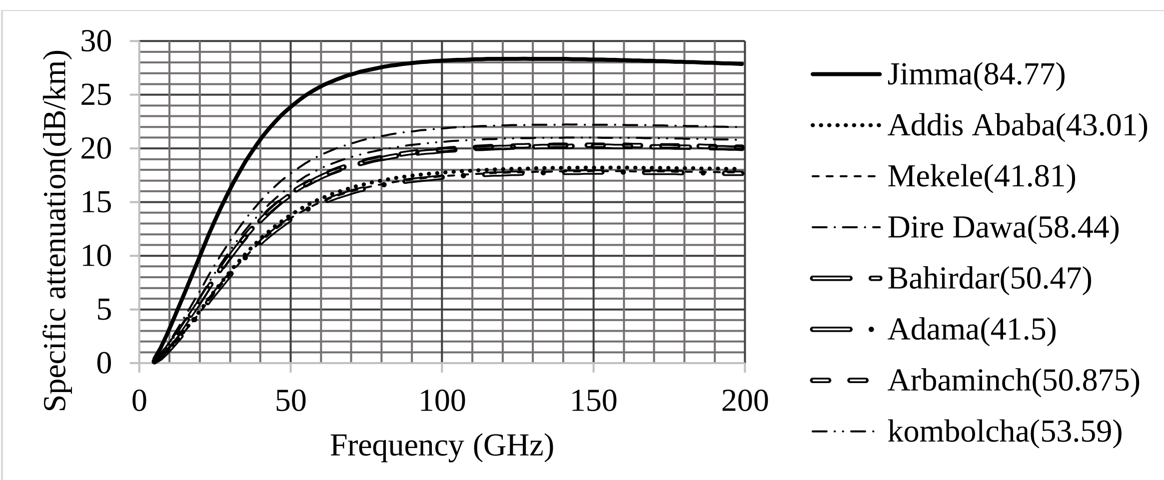

Figure 4-32. ITU R-P.838-3 [2]specific attenuation prediction for 8 cities in Ethiopia. Shown in brackets are the estimated $R_{0.01\%}$ rain rate values.

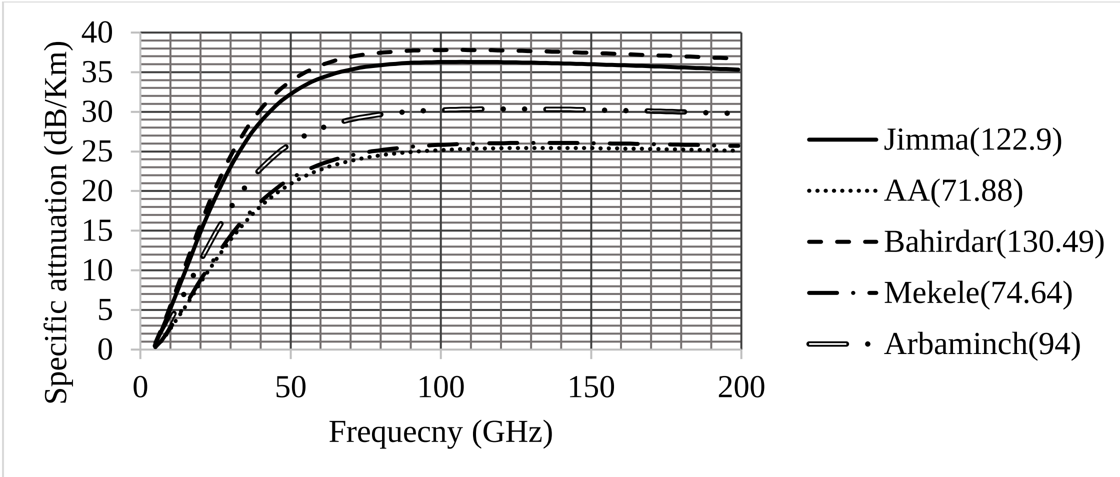

Figure 4-33. New Specific attenuation for five sites with $R_{0.01}$in mm/h.

and 33 dB /km with the ITU -R.P837 -7 rain rate prediction and the new prediction method respectively . There is a difference of about 15 dB /km which is significant considering communication distance. The situation is worse for Bahirdar that was predicted to have lower rain rate than Jimma in the on previous but actually receives a slightly higher rain rate, if not the highest as confirmed by this research work paper and [7]. The next two tables Table 4-5 and Table 4-6 show the mismatch of specific attenuation values at selected frequencies.

Table 4-5. ITUR- P.838-3 predicted specific attenuation ITUR-P.837-7 rain rate estimation.

Frequency (GHz)	Specific attenuation (dB/km)				
	Jimma	Addis Abab	Bahirdar	Mekele	Arbaminch
5	0.404428	0.12788	0.121885	0.167786	0.170047
21	10.67003	5.251933	5.098947	6.207767	6.259148
41	21.20813	11.82855	11.544	13.57516	13.66764
61	25.91169	15.45031	15.12071	17.45449	17.55976
101	28.18686	17.76514	17.4264	19.8088	19.91542
121	28.34567	18.07317	17.73712	20.09734	20.20279
141	28.32553	18.18915	17.85623	20.19243	20.2967
161	28.21362	18.20079	17.87108	20.18344	20.28658
181	28.04694	18.15012	17.82367	20.11237	20.21441
199	27.86647	18.07049	17.74699	20.0144	20.11547

Table 4-6. ITUR- P.838-3 predicted specific attenuation values with proposed rain rate estimation

F(GHz)	Specific attenuation(dB/km)				
	Jimma	Addis Abab	Bahirdar	Mekele	Arbaminch
5	0.759578	0.305692	0.840882	0.325875	0.481958
21	15.72848	8.981088	16.74463	9.34166	11.88661
41	29.19524	18.40178	30.74024	19.0082	23.18073
61	34.38931	22.85105	35.99618	23.51669	28.03505
101	36.29045	25.1948	37.80058	25.849	30.24017
121	36.26445	25.40813	37.73492	26.05113	30.35699
141	36.09798	25.43399	37.53812	26.06735	30.30261
161	35.86495	25.36184	37.28065	25.98676	30.16174
181	35.59189	25.23125	36.98657	25.84845	29.96923
199	35.32305	25.08144	36.70051	25.69203	29.76705

Table 4-7. Difference in specific attenuation prediction in four cities

F (GHz)	Jimma	Addis Abab	Bahirdar	Mekele	Arbaminch
5	0.36	0.18	0.72	0.16	0.31
21	5.06	3.73	11.65	3.13	5.63
41	7.99	6.57	19.20	5.43	9.51
61	8.48	7.40	20.88	6.06	10.48
81	8.33	7.50	20.78	6.11	10.49
101	8.10	7.43	20.37	6.04	10.32
121	7.92	7.33	20.00	5.95	10.15
141	7.77	7.24	19.68	5.87	10.01
161	7.65	7.16	19.41	5.80	9.88
181	7.54	7.08	19.16	5.74	9.75
199	7.46	7.01	18.95	5.68	9.65

From the two tables the huge estimation error attributed to erroneous rain rate prediction is seen. Relatively speaking, from Table 4-7 the least affected location appears to be Mekele with the least and biggest mismatch amounting to 0.16 and 6.11dB/km at 5 and 81GHz respectively.

Bahirdar, on the other hand, suffers the biggest estimation errors with the difference in prediction amounting to as much as a huge 19dB/km. Attenuation calculation using forward scattering amplitude given in equation (2-40) is presented in Figure 4-34.

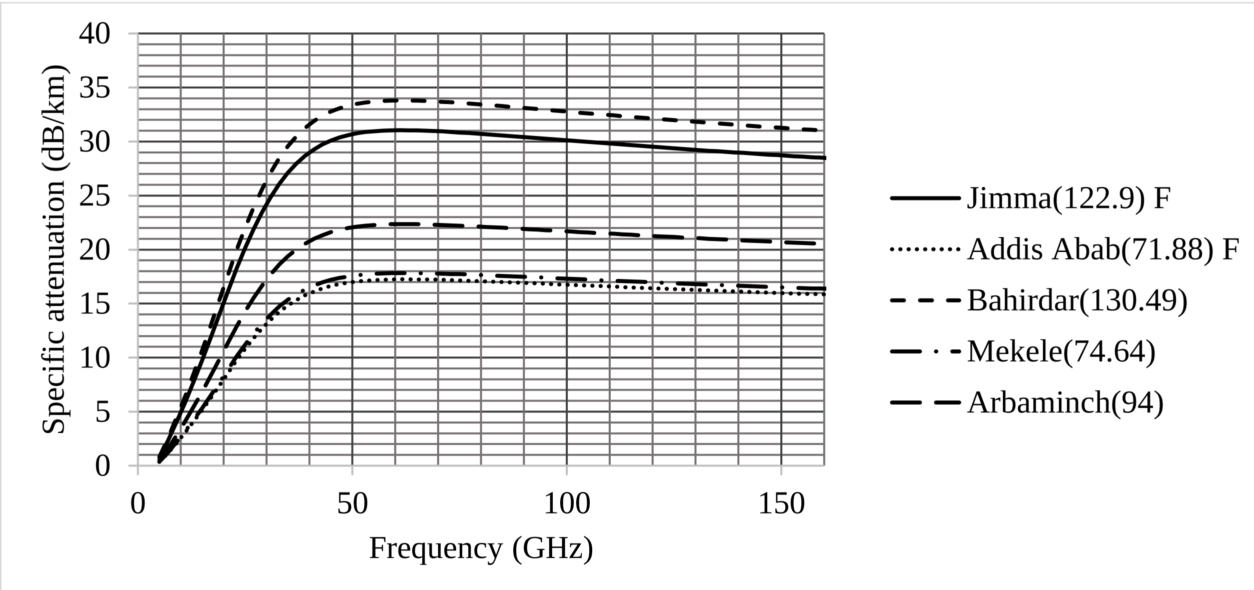

Figure 4-34. Specific attenuation calculation based on Mie forward scattering function.

In Figure 4-35 the results of ITUR-P.838-3 [2] and the other approach using the forward scattering method are compared. It is shown in Figure 4-35 how the two approaches fare in Jimma and Addis Ababa. The two approaches are in good agreement up to around 40GHz. After that the former continues to rise steadily before it enters a no-change region after about 90GHz. Second pair of line plotted by the Mie forward scattering function seem to attain a decreasing trend after they peaked at about 50GHz. The latter approach portrays what actually happens in the mechanism of absorption and scattering by rain droplets. As the frequency increases from 5GHz above the wave length and drop sizes become more and more comparable. This favors attenuation mechanisms, thus the rapid increase in the specific attenuation. This will not continue indefinitely though as the wave lengths become smaller and smaller, the amount of direct interaction between EMW and rain drops becomes less and less. As can be seen in the figure, this boundary between linear proportionality and saturation happens to be around 50GHz (λ~ 0.006m).

The main take away point from the discussion so far has been the need to develop attenuation prediction models for Ethiopian region are necessary. Models devised using DSD models and experimental statistics of other regions of the world cannot produce reliable attenuation prediction results. This directly affects the service availability and customer experience. The network components thus designed will not be able to give the necessary service required of them.

The research work has tried to show attenuation statistics determination based on rain rate values that represent the geographic locations under investigation. The research work had tried to show the impact of three DSD models on the performance of attenuation prediction model. The need to establish DSD measurement stations in Ethiopia is undeniable. If one doesn't have as accurate a picture as possible about the rain drop concentration distribution of an area, it is difficult, erroneous at best, to design wireless communication networks that meet customer needs. In the next section the cumulative effect of all the factors discussed up to until now on the performance of MIMO links will be discussed. Performance measurement is done in terms of capacity available to the user. Continuing the trend used in the previous sections, the performance of the three DSD models are compared.

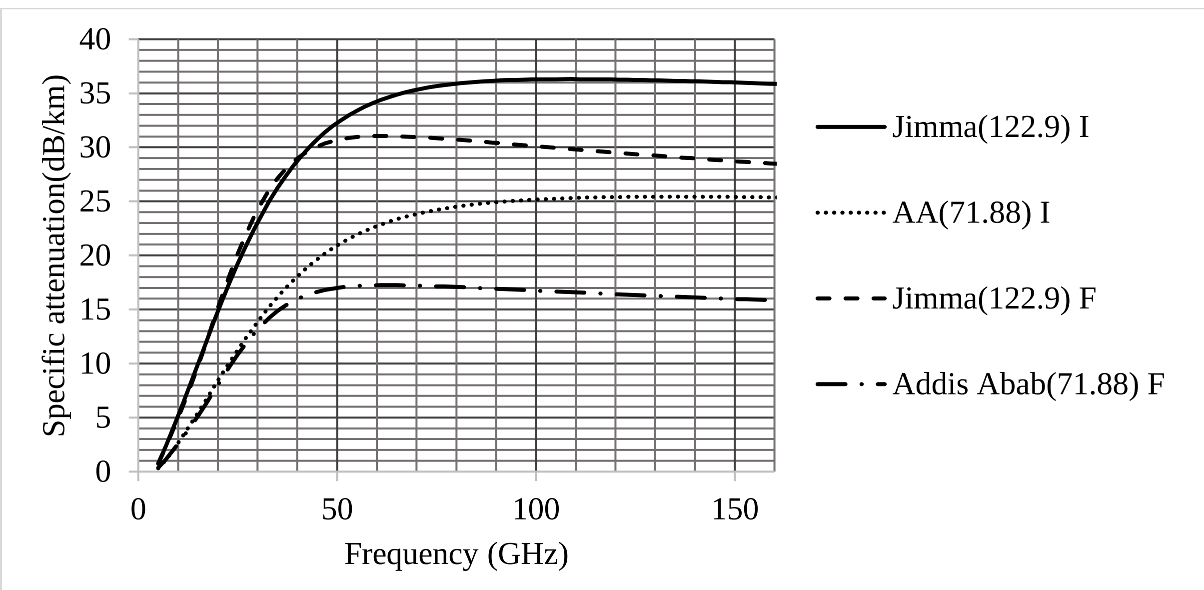

Figure 4-35. Specific attenuation comparison of ITU's method and forward scattering approach.

4.7. MIMO Channel Capacity

As discussed in section 3.8, there are basically to transmission possibilities in MIMO system. The first is the case when there is no CSIT at the transmitter where the transmitter has no option but to divide the total power into N transmit antennas equally. The capacity under this condition is given in equation (3-45). The other option is when the transmitter has channel information and evaluates the status of the channels. It refrains from assigning large power for channels known to be noisy or experiencing deep fade at the moment. This way the transmitter maximizes the channel capacity as given in equation (3-48). The simulations have been done using MATLAB routines. The capacity results you see below are result of averaging after k=1000 iterations. This approach is used because true gaussian complex number variables with N(0,1) are not generated in one trail.

4.7.1. MIMO channel capacity without CSIT

In this section the results of channel capacity under the no-CSIT assumption are illustrated with the help of figures. The contribution of the different DSD profiles are compared against one another at different frequencies starting from 6GHz in an effort made to cover the microwave and millimeter wave range. Effect of number of Tx and Rx antennas is also demonstrated by varying the SNR of the system.

We start by assessing the performance of MIMO channel assuming the MP DSD profile at various frequencies and SNRs and rain rates. We will a few of the frequencies selected for 5G technology implementation; 6, 15, 28, 38, 60, 72 and 75GHz.

The first illustration in Figure 4-36 shows channel capacity as a function of rain rate at different SNRs. There is no channel information at the transmitter and it can be imagined how the system is suffering. The maximum channel capacity for a 75GHz base MIMO system is only 9pbs/Hz at best with 30dB of SNR.

The effect of CSIT will be clear in section 4.7.2. Figure 4-36-38 show how channel capacity varies as the no of antennas increase from 51 to 101 each at the transmitter and receiver. Comparing results from Figure 4-36 and Figure 4-37 it can be seen that the increase in number of antennas has resulted capacity increase amounting to around 1bps/Hz. For easier comparison lets plot the two antenna configuration capacities at SNR of 12dB in Figure 4-38.

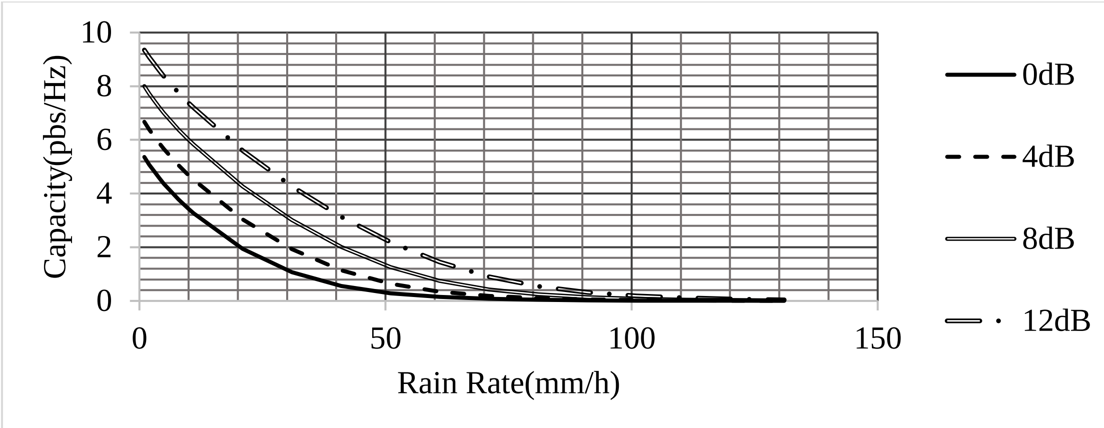

Figure 4-36. Capacity vs rain rate at different SNRs with no CSIT.M=N=51(MP DSD)

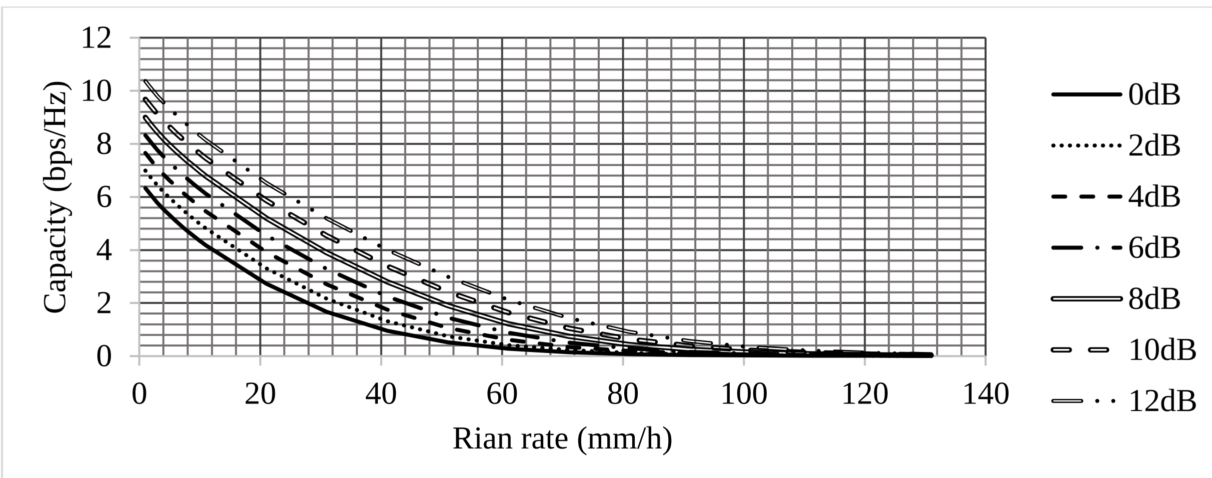

Figure 4-37. Channel capacity at 75GHz without CSIT. M=N=101.MP DSD is utilized.

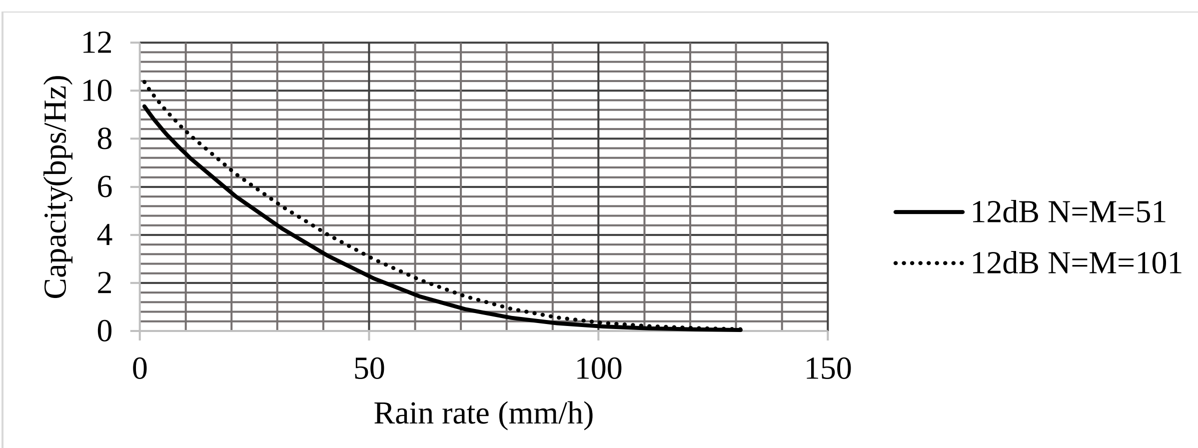

Figure 4-38. Channel capacity at 75GHz using two antenna configuration and MP DSD.

The difference in capacity illustrated in the above Figure 4-38 is at its highest of more than 1bps/Hz at 1mm/h. Then as the rain rate increases the performance of both systems suffer from high attenuation and finally dies off.

Next the effects of the lognormal distribution by Ajayi and Olsen [43] the modified lognormal by Sumbiri et al [42] on the channel capacity are shown. Figure 4-41 reveals that the DSD models developed in the tropical Africa provide higher channel capacity than MP model. The reason for this is found in section 4.6.4. There it is shown that the attenuation prediction at frequencies above 50 GHz fall off using these modified distributions thus contributing less to signal attenuation, that means increasing channel quality. There the research has shown the attenuation prediction using these modified distributions at frequencies above 50 GHz falls off thus contributing less to signal attenuation, that means increasing channel quality.

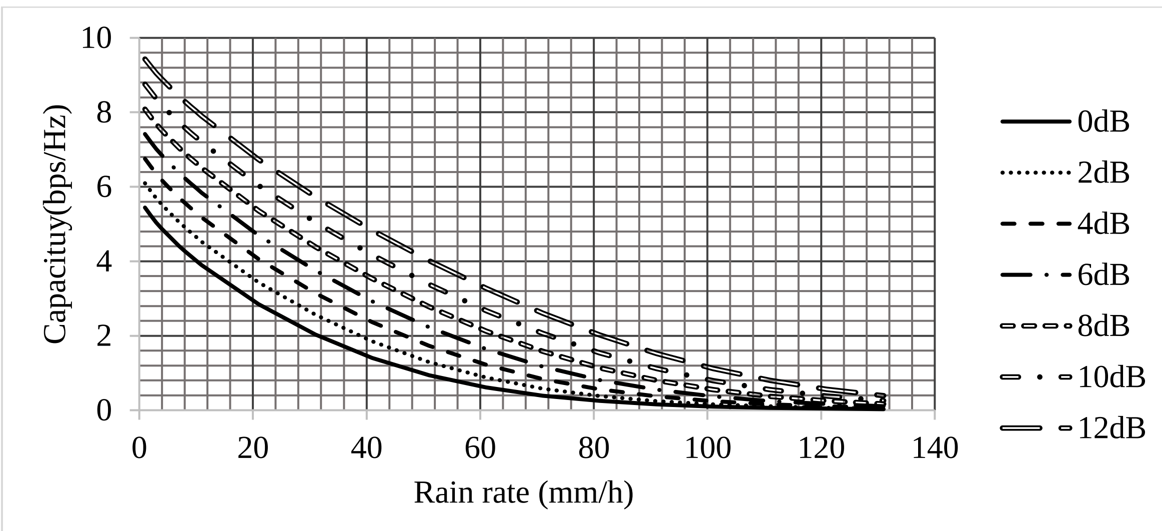

Figure 4-39. Lognormal DSD based capacity performance against rain rate at 75GHz. M=N=51.

So far, it has been shown that the system capacity falls off monotonically as the rain rate increase from zero upward . This is due to attenuation taking the upper hand in the extinction and multipath effect trade off. The given SNRs 0-12dB are not enough to compensate for attenuation and allow multiple channels to flourish. But this changes as the SNR is increased. The channel capacity increases starting from 0mm/h and attains a peak before it falls off again as the effect pf attenuation kicks in again. The rain rate where the capacity reaches maximum value depends on the type of DSD profile and the frequency in question. more than one healthy sub channels thus increasing the channel capacity. A plot of channel capacity vs SNR would reveal that phenomena

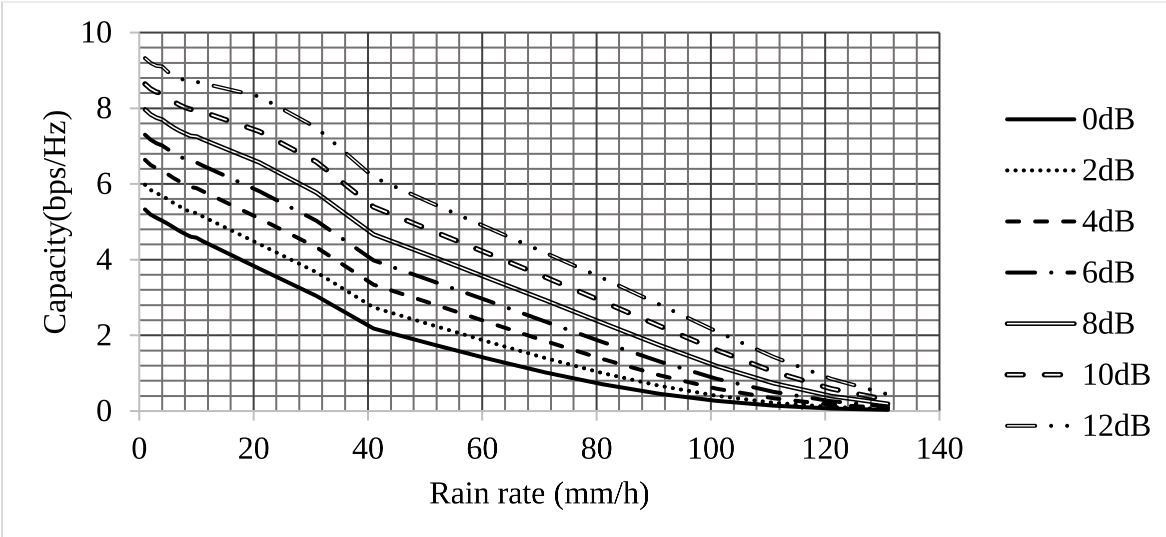

Figure 4-40. Modified lognormal DSD based capacity calculation at 75GHz. M=N=51.

This is an otherwise unexpected finding because one would assume that rain fall has capacity reducing effect. But the presence of rain drops gives the potential of

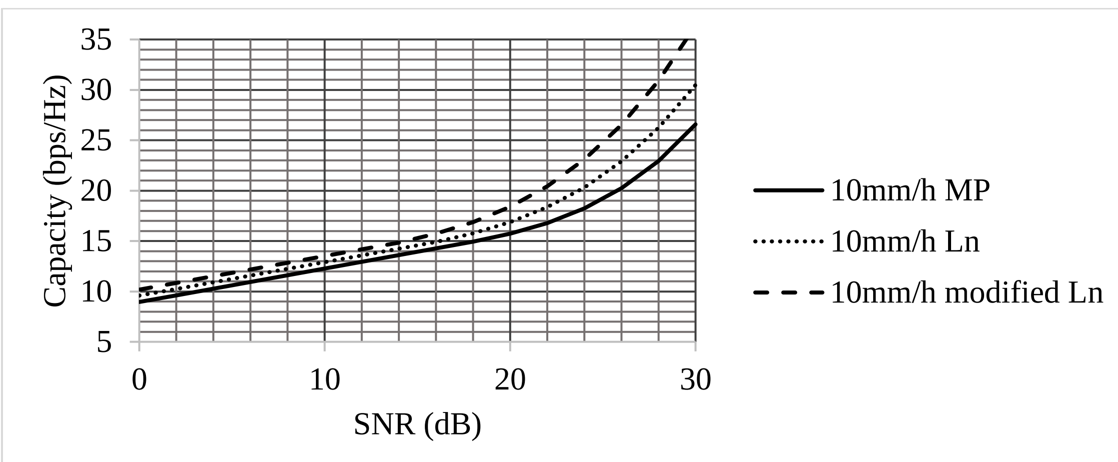

Figure 4-41. Capacity at 75GHz of the three DSD models.

In Figure 4-42 following the curves for 1mm/h and 10mm/h, it is shown that the capacity at rain rate 1mm/h remains at the top of that of 10mm/h up until around 27dB SNR. Then the 10mm/h curve suddenly finds itself on the top. The reason for this event is as explained above, the multipath effect that would normally be overshadowed by high attenuation starts to take effect at high SNR values which nullify the attenuation. The same is true for the other DSD models albeit different capacity values and "best rate" rain rate values. The same phenomena could be seen on

Figure 4-43 for lognormal and DSD and Figure 4-44 for the modified lognormal distribution.

Capacity plots as a function of rain rate at different SNR levels reveal this more clearly as shown in Figure 4-45 and Figure 4-46 for MP and lognormal DSD at 75GHz. It is evident from these figures that the increase in channel capacity happens at different rain rates and SNR values for different arrangements and DSD profiles in use. This means for a certain MIMO configuration and location of interest, there is a rain rate where the system capacity is at its maximum. This characteristic rain rate-SNR combination would be unique for the area. This can be used in fade mitigation schemes where transmission is made via the available best rate channel when other known channels are experiencing more fade. This would be an advantage

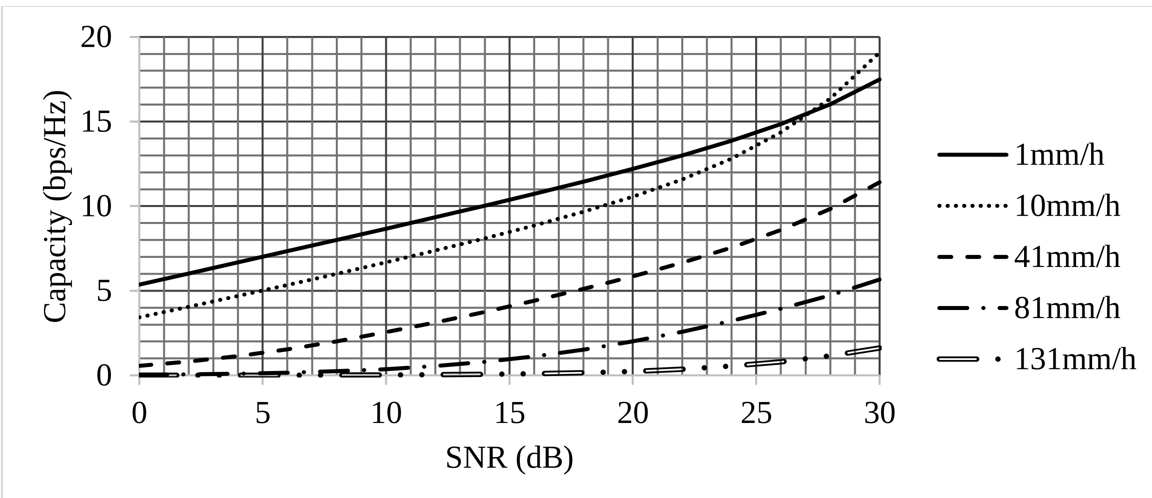

Figure 4-42. System capacity vs SNR at 75GHz using MP DSD.

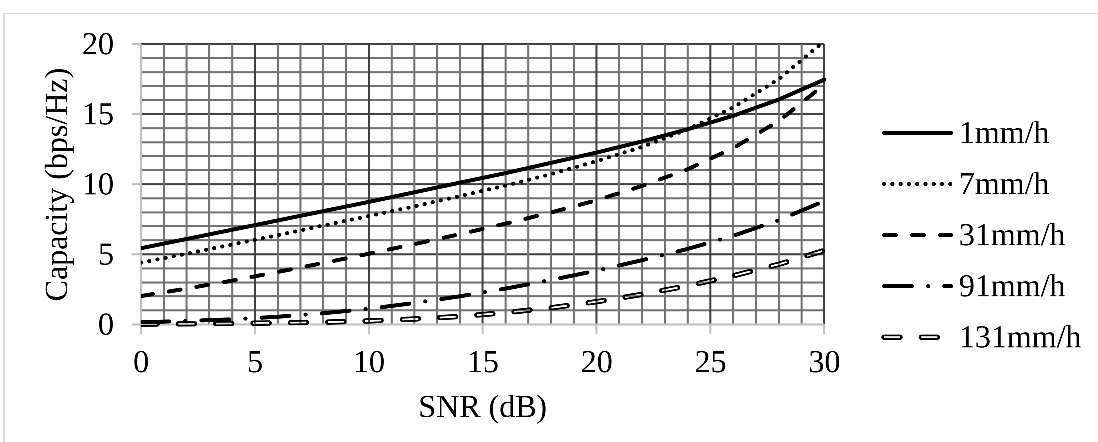

Figure 4-43. Capacity vs SNR showing increase in capacity with rain rate. f=75GHz.

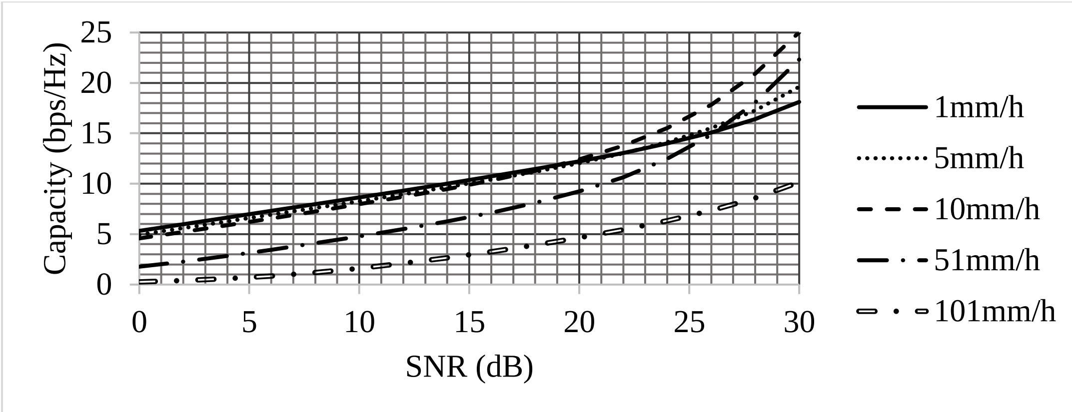

Figure 4-44. Modified lognormal distribution capacity vs SNR showing increase in capacity as rain rate increases. f=75GHz

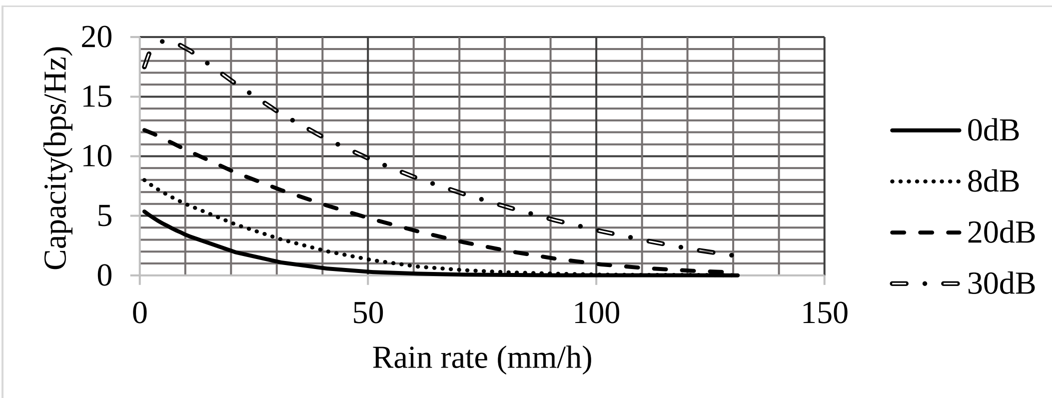

Figure 4-45. Increase in capacity with rain rate capacity. (MP DSD at f=75GHz)

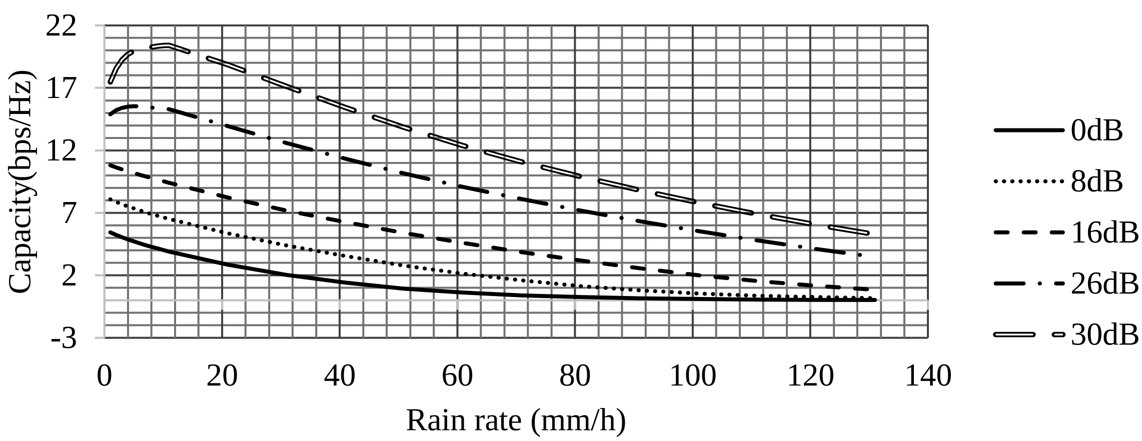

Figure 4-46. Capacity increment with rain rate. (lognormal DSD at f=75GHz)

4.7.2. MIMO channel capacity with CSIT

The calculation of channel capacity when there is perfect channel state information at the transmitter is detailed in section 3.8. The results are presented here. Let's begin this discussion by showing how the channel capacity is enhanced by taking advantage of CSIT. Since most of our discussion in section 4.7.1 was based on 75GHz, other frequencies will be used to illustrate the findings.

The increase in channel capacity due to CSIT is shown below in Figure 4-47. The increase obtained is significant. It amounts to 7bps/Hz on average. To illustrate how much this means in terms of numbers, assume band width of a channel is 2 KHz at 35GHz without CSIT the total channel capacity of the system at 10mm/h (and SNR=0 dB) is 9.3 kbps on the other hand, in case of perfect CSIT, the channel capacity is 20.53kbps, more than double the figure in no CSIT case. The increase in capacity don't appear to be dependent on the SNR and the rain rate in question, maintaining the same gap throughout. The increase of channel capacity together with the rain rate can be seen in the same figure.

Figure 4-49 below shows how the MP DSD model compares to the other two models in terms of channel capacity. Recalling Figure 4-22, it was shown that the extinction cross section is the highest at the drop diameter between 1mm and 2mm. While the two tropical models have 10s of drops in this range the MP model is in the region of thousands of drops per unit volume. The attenuation thus is highest causing faster reduction of the channel capacity in Figure 4-49 compared to the other models.

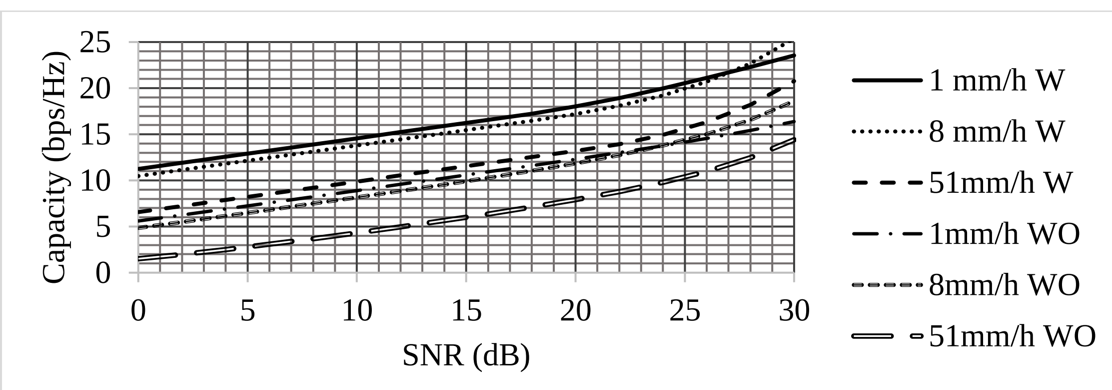

Figure 4-47. Capacity comparison with and without CSIT at f=38GHz with MP DSD

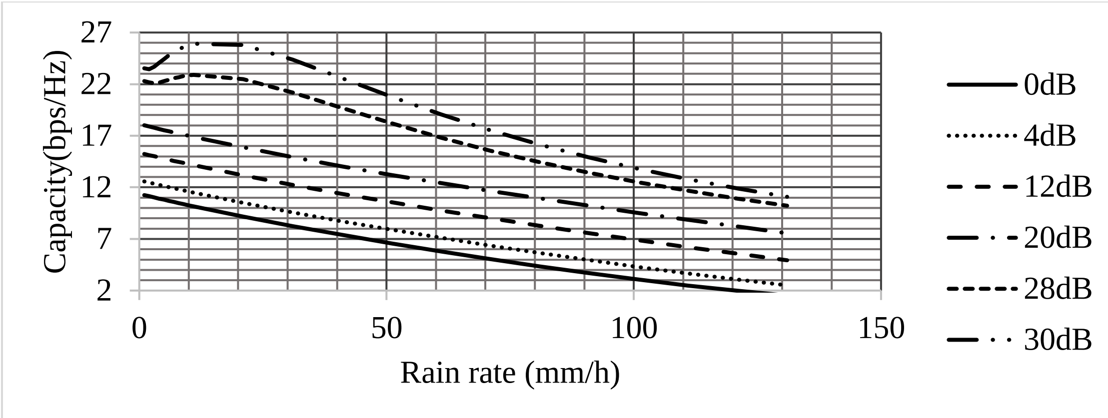

Figure 4-48. Capacity increment with rain rate at 38GHz with CISIT (MP DSD)

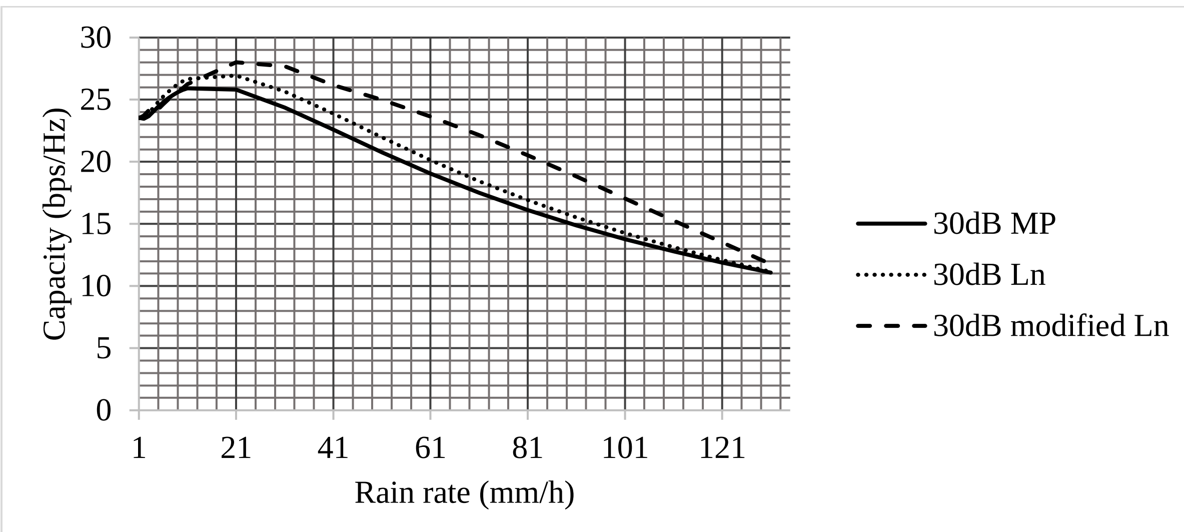

Figure 4-49. Comparison of the three DSD profiles. (f=75GHz).

CHAPTER FIVE

5. Conclusions and Recommendations

5.1. Introduction

MIMO is one of the technologies being researched for utilizing the millimeter and microwave frequency spectrum efficiently by employing the new dimension, space. However, precipitation (rain), affects this band of frequency the most. To study effect of rain an accurate prediction mechanism is necessary for both rain rate distribution and attenuation statistics. The prediction methods being used so far are based on temperate region data. As found out in this work, models constructed thus cannot produce representative data for Ethiopian locations and tropical region in general.

By accomplishing this study, the research work has introduced new approaches which can be used as a reference for future works. It has also reported interesting performance patterns of MIMO system capacity as a function of rain rate and signal to noise ratio.

The following sections summarize what has been accomplished and recommended for future works. Although the final objective of this work was the study of rain fall effects on MIMO systems, for the sake completeness, it has touched up on a lot of areas that are inputs to the work. The conclusions and recommendations listed are based on the topics that have been covered.

5.2. Conclusion

5.1.1 Determination of $R_{0.01}$

In this work, rain rate exceeded for 0.01% of the year 2017/18 has been calculated by using the procedure outlined in 3.2.2 where the collected 1-min rain data for Jimma city was statistically processed. The value obtained 122.9 mm/h has a huge difference compared to what global prediction methods would calculate. ITUR-P.837-7 [52] calculates $R_{0.01}$ for Jimma city as 84.76mm/h and R-H would make it around 76mm/h. These are discrepancies which lead to wrong design calculations if used.

For cities that don not have min measured data, integration time conversion was conducted based on Jimma data. Better prediction values were gained for these cities as well. For city of Bahirdar, for instance, ITU predicted $R_{0.01}$ was 50.6mm/h which is lower than that of Jimma when in fact it is known that Bahirdar experience the most intense of rain falls out of the major cities in Ethiopia. According to the conversion procedure used by this research work, the new $R_{0.01}$ value is 130.49mm/h. Similar results are calculated for other major cities as well.

5.1.2. Rain cell size determination

Equally important as the intensity of rain is the spatial extent of coverage. The amount of link distance that is traversed by rain events determines the level of fade experienced by transmissions. The research work has used statistical procedure described to calculate the rain cell size that accompany intense rain events around Jimma. At the rain rate $R_{0.01}$ the rain cell extension was calculated to be around 1Km.

The rain cell size statistics could not be determined for other locations due to lack of 1 min integrated rain rate time series data. However, the procedure demonstrated could be applied to any location, given proper time series rain rate data are available.

5.1.3. Drop size distribution

In this section of the research work three main DSD models have been discussed. The models have been compared by researching the nature of data from measurement campaigns used inother works. The research work has shown that the widely used MP distribution fails to capture drop size distribution patterns seen in tropical regions of Africa. Thus, it has been ruled out of use which this work has confirmed in other sections as well. The other two models by Ajay and Ofoche [43] and Sumbiri et al [42] show relatively closer profiles with measured data. The later model, however, seems to extend to regions of drop diameters that are known to be physically unstable. The effect of these DSD models has been shown in the attenuation calculations and performance evaluation of effect of rain on MIMO capacity.

5.1.4. Specific attenuation

Two approaches were compared to calculate the specific attenuation of major cities. The first approach is recommended by ITU in ITUR-P.838-3 [2] which is the standard approach for attenuation statistics determination. The second approach involves determination of propagation coefficients using the Mie scattering theory. Calculation of propagation coefficient for millimeter and microwave-based MIMO system have been extensively shown. The dependence of these parameters on the DSD profile of choice and system constants like frequency and temperature has been described and illustrated.

Similar to the case with rain rate prediction, the attenuation statistics was found to be inaccurate and improved calculation results have been found by this research work. The new attenuation statistics shown in Table 5-2 can be used as reference points by designers and academicians alike.

Table 5-1. Specific attenuation prediction by ITUR-P.838-3[2]

Frequency (GHz)	Specific attenuation (dB/km)				
	Jimma	Addis Abab	Bahirdar	Mekele	Arbaminch
5	0.404428	0.12788	0.121885	0.167786	0.170047
41	21.20813	11.82855	11.544	13.57516	13.66764
101	28.18686	17.76514	17.4264	19.8088	19.91542
141	28.32553	18.18915	17.85623	20.19243	20.2967
181	28.04694	18.15012	17.82367	20.11237	20.21441

Table 5-2. New specific attenuation calculation results.

F(GHz)	Specific attenuation(dB/km)				
	Jimma	Addis Abab	Bahirdar	Mekele	Arbaminch
5	0.759578	0.305692	0.840882	0.325875	0.481958
41	29.19524	18.40178	30.74024	19.0082	23.18073
101	36.29045	25.1948	37.80058	25.849	30.24017
141	36.09798	25.43399	37.53812	26.06735	30.30261
181	35.59189	25.23125	36.98657	25.84845	29.96923

5.1.5. MIMO channel capacity

The research work has demonstrated the channel capacity under varying circumstances. The effect of rain rate, DSD profile, and SNR has been shown. An important finding about the potential of rain to enhance system capacity has been communicated. The rise in channel capacity as rain rate increase has been shown to be dependent SNR and particular DSD model employed.

The "best rate" rain rates usually occur at lower rates (<30mm/h) with variations depending on DSD profile. The research work, thus, concluded that besides its negative effect of sever attenuation in the millimeter and microwave ranges, rain can increase channel capacity. The research work has indicated that the increase in capacity due to rain is a result of competition of two forces in the MIMO arrangement. The first is attenuation which is sever given the short wavelengths that are comparable to droplets. The second is formation of strong parallel sub channels due to presence of scatters in the form of rain drops. It has been shown that at low SNR values the attenuation takes the upper hand and it is not possible to get multiple strong subchannels. As the SNR increased the attenuation is counteracted and the scattering starts taking full effect which shows up as increase in capacity. But it also has been shown that this won't last forever as the rain rate increase, the number of drops increase which sways the balance back to attenuation thus showing sharp decrease in system capacity.

The research work has also showed that, under similar rain rate and SNR level, the two models from Africa's tropical region produce better channel capacity results than the DSD model formulated based on temperate climates.

5.3. Recommendations for future work

The following list contains the areas that could be pursued in future research endeavors.

- The determination of rain rate profile of an area is important part of propagation studies concerned with rain. Without proper rain data and processing tools, it is impossible to design reliable communication links. Due to unavailability of measured 1-minute rain data for most of sites except Jimma, the research work has employed the best rain rate integration time conversion method from among the number of approaches. The conversion was based on 1-min and 15-min measured data collected for Jimma town. The approach could be used by the other researchers seeking to get1-min rain rate from 15-min integration rain rate data that is available from NMA. The researcher also believes the conversion mechanism can be improved if 1-min data could be collected for more sites than just Jimma. So, future researchers, in a view to find better rain rate predictions, should base their studies on measured 1-min rain rate data.

- The research paper had used DSD models in almost all parts of the research. Although the DSD models by Ajayi and Olsen [43] could be a more fitting DSD to locations in Ethiopia, it cannot accurately describe the rain phenomena as a measurement-based model would. Considering this, to be able to accurately evaluate the propagation impairment, or enhancement for that matter, caused by rain fall, the researcher suggests, even though this might be beyond one's capacity, for stake holders in telecommunication industry in Ethiopia to collaborate in installation of state of the art distrometers all over the country. This would aid all parties, be commercial service providers or private academicians in coming up with better DSD models.
- There are factors which change the shape of droplets while they fall through to the ground. The resulting non sphericity of droplets affects the polarization of wave propagation. This in turn will affect system performance. Similar future works should consider the effect of non-sphericity of droplets on signal polarization.
- When MIMO modeling approach is chosen according to Kronecker method, it was under the assumption that the transmit antennas do not affect the receive array and vice versa. Antennas placed a certain distance apart (usually more than half the wavelength) could be considered free of linking thus validating the choice by this research work so that focus can be geared toward effects of rain on propagation. However, it is not possible to avoid linkage between antennas. So, the effect of antennal linkage should be investigated by future researchers.
- The specific attenuation and other propagation coefficients calculations have been done considering the limiting case scenario. For instance, in the calculation of specific attenuation at a certain rain rate $R_{0.01\%}$ it is assumed that the rain rate is constant over the link distance considered. This works well for availability determination calculations but it is only rarely the case and rain cells otherwise could be composed of more than one peak and different distribution around these peaks. So, for a fine-tuned calculation results, the variability rain rate within the cell should be considered by future researchers.
- The attenuation statistics reported by this work should be strengthened by experimental setup.

- Finally, the research work has shown the effect of rain on MIMO system capacity isn't necessarily a negative one. Depending on the DSD profile and the rain rate the presence of rain fall on a link path can actually increase channel capacity by means of creating more independent and parallel sub channels. This means each subregion within a collection of wireless links has different characteristic "best rate" rain rate.

  This idea could be used to mitigate effect of rain fall by redirecting transmission through a link known to be experiencing the "best rate" rain rate. This, of course, is assuming that the channel state information which is determined by the propagation parameters, can be sampled and reported in real time to the transmitter.

6. References

[1] G. Ajayi and E. Ofoche, "Some tropical rainfall rate characteristics at Ile-Ife for microwave and millimeter wave applications," *Journal of Climate and Applied Meteorology,* vol. 23, no. 4, pp. 562-567, 1984.

[2] P. Series, "Specific attenuation model for rain for use in prediction methods," *Recommendation ITU-R,* pp. 838-3, 2003.

[3] O. W. Chun and J. S. Mandeep, "Empirical methods for converting rainfall rate distribution from several higher integration times into a 1-minute integration time in Malaysia," *Geofizika,* vol. 30, no. 2, pp. 119-141, 2013.

[4] S. Salous *et al.*, "Millimeter-Wave Propagation: Characterization and modeling toward fifth-generation systems.[Wireless Corner]," *IEEE Antennas and Propagation Magazine,* vol. 58, no. 6, pp. 115-127, 2016.

[5] J.-H. Lee, Y.-S. Kim, J.-H. Kim, and Y.-S. Choi, "Empirical conversion process of rain rate distribution for various integration time," in *2000 Asia-Pacific Microwave Conference. Proceedings (Cat. No. 00TH8522)*, 2000, pp. 1593-1597: IEEE.

[6] P. A. Owolawi, "Characteristics of rain at microwave and millimetric bands for terrestrial and satellite links attenuation in South Africa and surrounding islands," 2010.

[7] F. D. Diba, "Radio wave propagation modeling under precipitation and clear-air at microwave and millimetric bands over wireless links in the horn of Africa," 2017.

[8] F. Diba, T. Afullo, and A. Alonge, "Rainfall Rate and Attenuation Performance Analysis at Microwave and Millimeter Bands for the Design of Terrestrial Line-of-Sight Radio Links in Ethiopia," *SAIEE Africa Research Journal*, vol. 107, no. 3, pp. 177-186, 2016.

[9] D. Sumbiri, T. J. Afullo, and A. Alonge, "Rain attenuation prediction for terrestrial links at microwave and millimeter bands over Rwanda," in *2016 Progress in Electromagnetic Research Symposium (PIERS)*, 2016, pp. 4233-4236: IEEE.

[10] A. A. Alonge and T. J. Afullo, "Rainfall time series synthesis from queue scheduling of rain event fractals over radio links," *Radio Science,* vol. 50, no. 12, pp. 1209-1224, 2015.

[11] M. Odedina and T. Afullo, "Determination of rain attenuation from electromagnetic scattering by spherical raindrops: Theory and experiment," *Radio Science,* vol. 45, no. 1, 2010.

[12] J. S. Ojo, M. O. Ajewole, and S. K. Sarkar, "Rain rate and rain attenuation prediction for satellite communication in Ku and Ka bands over Nigeria," *Progress in Electromagnetics Research,* vol. 5, pp. 207-223, 2008.

[13] P. Series, "Characteristics of precipitation for propagation modelling," *Recommendation ITU-R*, pp. 837-6, 2013.

[14] R. Crane, "Prediction of attenuation by rain," *IEEE Transactions on communications,* vol. 28, no. 9, pp. 1717-1733, 1980.

[15] L. D. Emiliani, L. Luini, and C. Capsoni, "Analysis and parameterization of methodologies for the conversion of rain-rate cumulative distributions from various integration times to one minute," *IEEE Antennas and Propagation Magazine,* vol. 51, no. 3, 2009.

[16] C. Capsoni and L. Luini, "1-min rain rate statistics predictions from 1-hour rain rate statistics measurements," *IEEE transactions on antennas and propagation,* vol. 56, no. 3, pp. 815-824, 2008.

[17] P. Rice and N. Holmberg, "Cumulative time statistics of surface-point rainfall rates," *IEEE Transactions on Communications,* vol. 21, no. 10, pp. 1131-1136, 1973.

[18] E. Dutton and H. Dougherty, "Year-to-year variability of rainfall for microwave applications in the USA," *IEEE Transactions on Communications,* vol. 27, no. 5, pp. 829-832, 1979.

[19] D. 3J, "Description of the method adopted for the update of Rec. ITU-R P.837-5, Annex 3," *SG3 Report*, pp. TEMP/XX-E, 24 October 2011.

[20] J. Lavergnat and P. Golé, "A stochastic raindrop time distribution model," *Journal of Applied Meteorology,* vol. 37, no. 8, pp. 805-818, 1998.

[21] J. Chebil and T. Rahman, "Rain rate statistical conversion for the prediction of rain attenuation in Malaysia," *Electronics Letters,* vol. 35, no. 12, pp. 1019-1021, 1999.

[22] F. Moupfouma, "Improved rainfall-rate distribution for radio system design," in *IEE Proceedings*, 1993, vol. 134, no. 6, pp. 527-537.

[23] F. Moupfouma, "Rainfall-rate distribution for radio system design," in *IEE Proceedings*, 1987, vol. 134, no. 6, pp. 527-537.

[24] P. Akuon and T. Afullo, "RAIN CELL SIZING FOR THE DESIGN OF HIGH CAPACITY RADIO LINK SYSTEMS IN SOUTH AFRICA," *Progress In Electromagnetics Research B,* vol. 35, 2011.

[25] P. Series, "Mean surface temperature," *Recommendation ITU-R*, pp. 1510-1, 2017.

[26] B. Segal, "The influence of Raingage Integration Time on Measured Rainfall-intensity Distribution Functions," *J. Atmos-pheric and Oceanic Technology*, p. 10, 3, December 1986.

[27] C. Capsoni, F. Fedi, C. Magistroni, A. Paraboni, and A. Pawlina, "Data and theory for a new model of the horizontal structure of rain cells for propagation applications," *Radio Science*, vol. 22, no. 03, pp. 395-404, 1987.

[28] L. Féral, H. Sauvageot, L. Castanet, and J. Lemorton, "HYCELL—A new hybrid model of the rain horizontal distribution for propagation studies: 1. Modeling of the rain cell," *Radio Science*, vol. 38, no. 3, 2003.

[29] J. Goldhirsh, "Two-dimension visualization of rain cell structures," *Radio Science*, vol. 35, no. 3, pp. 713-729, 2000.

[30] C. Capsoni and L. Luini, "A physically based method for the conversion of rainfall statistics from long to short integration time," *IEEE Transactions on Antennas and Propagation*, vol. 57, no. 11, pp. 3692-3696, 2009.

[31] P. Akuon and T. Afullo, "Rain cell size statistics from rain gauge data for site diversity planning and attenuation prediction," in *Proc. of SATNAC*, 2011, pp. 213-216.

[32] O. Fiser, "The role of dsd and radio wave scattering in rain attenuation," in *Geoscience and Remote Sensing New Achievements*: IntechOpen, 2010.

[33] J. O. Laws and D. A. Parsons, "The relation of raindrop‐size to intensity," *Eos, Transactions American Geophysical Union*, vol. 24, no. 2, pp. 452-460, 1943.

[34] R. Gunn and G. D. Kinzer, "The terminal velocity of fall for water droplets in stagnant air," *Journal of Meteorology*, vol. 6, no. 4, pp. 243-248, 1949.

[35] J. S. Marshall and W. M. K. Palmer, "The distribution of raindrops with size," *Journal of meteorology*, vol. 5, no. 4, pp. 165-166, 1948.

[36] C. W. Ulbrich, "Natural variations in the analytical form of the raindrop size distribution," *Journal of climate and applied meteorology*, vol. 22, no. 10, pp. 1764-1775, 1983.

[37] A. Ishimaru, *Wave propagation and scattering in random media*. Academic press New York, 1978.

[38] A. Ishimaru, S. Jaruwatanadilok, and Y. Kuga, "Multiple scattering effects on the radar cross section (RCS) of objects in a random medium including backscattering enhancement and shower curtain effects," *Waves in random media*, vol. 14, no. 4, pp. 499-512, 2004.

[39] A. Ishimaru, R. Woo, J. Armstrong, and D. C. Blackman, "Multiple scattering calculations of rain effects," *Radio Science*, vol. 17, no. 6, pp. 1425-1433, 1982.

[40] Y.-P. Zhang, P. Wang, and A. Goldsmith, "Rainfall effect on the performance of millimeter-wave MIMO systems," *IEEE Transactions on wireless communications*, vol. 14, no. 9, pp. 4857-4866, 2015.

[41] H. Jiang, M. Sano, and M. Sekine, "Weibull raindrop-size distribution and its application to rain attenuation," *IEE Proceedings-Microwaves, Antennas and Propagation*, vol. 144, no. 3, pp. 197-200, 1997.

[42] D. Sumbiri, T. J. Afullo, and A. A. Alonge, "Modelling of rain drop size distribution for microwave and millimiter wave in Central Africa," in *2017 Progress in Electromagnetics Research Symposium-Fall (PIERS-FALL)*, 2017, pp. 2398-2404: IEEE.

[43] G. O. Ajayi and R. L. Olsen, "Modeling of a tropical raindrop size distribution for microwave and millimeter wave applications," *Radio Science*, vol. 20, no. 2, pp. 193-202, 1985.

[44] W. C. Gibson, *The method of moments in electromagnetics*. Chapman and Hall/CRC, 2007.

[45] D. Cermak, O. Fiser, Z. Nemec, and V. Schejbal, "Study of electromagnetic scattering by rain drops," in *10th International Conference on Mathematical Methods in Electromagnetic Theory, 2004.*, 2004, pp. 592-594: IEEE.

[46] T. Oguchi, "Scattering from hydrometeors: A survey," *Radio Science*, vol. 16, no. 5, pp. 691-730, 1981.

[47] J. Chebil, "Rain rate and rain attenuation distribution for microwave propagation study in Malaysia," UTM, 1997.

[48] E. Salonen and J. P. Baptista, "A new global rainfall rate model," in *Tenth International Conference on Antennas and Propagation (Conf. Publ. No. 436)*, 1997, vol. 2, pp. 182-185: IET.

[49] R. Crane, A. W. Dissanayake, "ACTS propagation experiment: Attenuation distribution observations and prediction model comparison," *Proceedings of the IEEE*, vol. 85, p. 14, 1997.

[50] E. J. Dutton, "Microwave terrestrial link rain attenuation prediction parameter analysis," *US Department of Communications, National Telecommunications and Information Administration (STIA) Tech. Rep.* , p. 65, 1984.

[51] P. Series, "Propagation data and prediction methods required for the design of terrestrial line-of-sight systems," *Recommendation ITU-R*, pp. 530-16, 2015.

[52] P. Series, "Characteristics of precipitation for propagation modelling," *Recommendation ITU-R*, pp. 837-7, 2017.

[53] S. Shrestha and D.-Y. Choi, "Rain attenuation statistics over millimeter wave bands in South Korea," *Journal of Atmospheric and Solar-Terrestrial Physics,* vol. 152, pp. 1-10, 2017.

[54] A. Abdulrahman, T. A. Rahman, S. K. A. Rahim, M. R. Islam, and M. Abdulrahman, "Rain attenuation predictions on terrestrial radio links: differential equations approach," *Transactions on Emerging Telecommunications Technologies,* vol. 23, no. 3, pp. 293-301, 2012.

[55] L. da Silva Mello and M. Pontes, "A Unified Method for the Prediction of Rain Attenuation in Slant Paths and Terrestrial Links Using the Full Rainfall Rate Distribution," *CLIMDIFF*, 2008.

[56] L. D. S. Mello, M. Pontes, R. De Souza, and N. P. Garcia, "Prediction of rain attenuation in terrestrial links using full rainfall rate distribution," *Electronics Letters*, vol. 43, no. 25, pp. 1442-1443, 2007.

[57] F. Moupfouma and L. Martin, "Modelling of the rainfall rate cumulative distribution for the design of satellite and terrestrial communication systems," *International Journal of Satellite Communications,* vol. 13, no. 2, pp. 105-115, 1995.

[58] A. Hirata *et al.*, "Effect of rain attenuation for a 10-Gb/s 120-GHz-band millimeter-wave wireless link," *IEEE Transactions on Microwave Theory and Techniques,* vol. 57, no. 12, pp. 3099-3105, 2009.

[59] A. K. Baldotra and I. Hudiara, "Rain attenuation statistics over terrestrial microwave link at 19.4 GHz at Amritsar," *IEEE Transactions on Antennas and Propagation,* vol. 52, no. 6, pp. 1505-1508, 2004.

[60] Z. Zhou, L.-W. Li, T.-S. Yeo, and M.-S. Leong, "Cumulative distributions of rainfall rate and microwave attenuation in Singapore's tropical region," *Radio Science,* vol. 35, no. 3, pp. 751-756, 2000.

[61] M. Sekine, S. Ishii, S. Hwang, and S. Sayama, "Weibull raindrop-size distribution and its application to rain attenuation from 30 GHz to 1000 GHz," *International Journal of Infrared and Millimeter Waves,* vol. 28, no. 5, pp. 383-392, 2007.

[62] T. A. Wysocki, A. Mertins, and J. Seberry, *Complex orthogonal space-time processing in wireless communications*. Springer Science & Business Media, 2007.

[63] W. C. Chan, *Performance Limits of MIMO Wireless Communications*. ProQuest, 2006.

[64] K. I. Pedersen, J. B. Andersen, J. P. Kermoal, and P. Mogensen, "A stochastic multiple-input-multiple-output radio channel model for evaluation of space-time coding algorithms," in *Vehicular Technology Conference Fall 2000. IEEE VTS Fall VTC2000. 52nd Vehicular Technology Conference (Cat. No. 00CH37152)*, 2000, vol. 2, pp. 893-897: IEEE.

[65] Yong Soo Cho, Jaekwon Kim, Won Young Yang, and C. G. Kang, *MIMO-OFDM WIRELESS COMMUNICATIONS WITH MATLAB*. IEEE, 2000.

[66] B. Clerckx and C. Oestges, *MIMO wireless networks: channels, techniques and standards for multi-antenna, multi-user and multi-cell systems*. Academic Press, 2013.

[67] W. Weichselberger, M. Herdin, H. Ozcelik, and E. Bonek, "A stochastic MIMO channel model with joint correlation of both link ends," *IEEE Transactions on Wireless Communications,* vol. 5, no. 1, pp. 90-100, 2006.

[68] C.-X. Wang, S. Wu, L. Bai, X. You, J. Wang, and I. Chih-Lin, "Recent advances and future challenges for massive MIMO channel measurements and models," *Science China Information Sciences,* vol. 59, no. 2, pp. 1-16, 2016.

[69] Werner Weichselberger, Markus Herdin, Hüseyin Özcelik, and E. Bonek, "A Stochastic MIMO Channel Model With Joint Correlation of Both Link Ends," *IEEE TRANSACTIONS ON WIRELESS COMMUNICATIONS,* vol. 2, no. 1, p. 11, 1, JANUARY 2006.

[70] K. Yu, M. Bengtsson, B. Ottersten, D. McNamara, P. Karlsson, and M. Beach, "Modeling of wide-band MIMO radio channels based on NLoS indoor measurements," *IEEE Transactions on Vehicular Technology,* vol. 53, no. 3, pp. 655-665, 2004.

[71] J.-P. Kermoal, L. Schumacher, K. I. Pedersen, P. E. Mogensen, and F. Frederiksen, "A stochastic MIMO radio channel model with experimental validation," *IEEE Journal on selected areas in Communications*, vol. 20, no. 6, pp. 1211-1226, 2002.

[72] D.-S. Shiu, G. J. Foschini, M. J. Gans, and J. M. Kahn, "Fading correlation and its effect on the capacity of multielement antenna systems," *IEEE Transactions on communications*, vol. 48, no. 3, pp. 502-513, 2000.

[73] K. Yu, M. Bengtsson, and B. Ottersten, "MIMO channel models," 2005.

[74] M. T. Ivrlac, W. Utschick, and J. A. Nossek, "Fading correlations in wireless MIMO communication systems," *IEEE Journal on selected areas in communications*, vol. 21, no. 5, pp. 819-828, 2003.

[75] E. Bonek, "Experimental validation of analytical MIMO channel models," *e & i Elektrotechnik und Informationstechnik*, vol. 122, no. 6, pp. 196-205, 2005.

[76] D. P. McNamara, M. A. Beach, and P. N. Fletcher, "Spatial correlation in indoor MIMO channels," in *The 13th IEEE International Symposium on Personal, Indoor and Mobile Radio Communications*, 2002, vol. 1, pp. 290-294: IEEE.

[77] R. W. Heath Jr, A. M. Sayeed, Z. Hong, and K. Liu, "Spatial multiplexing in correlated fading via the virtual channel representation," 2003.

[78] H. Ozcelik, M. Herdin, W. Weichselberger, J. Wallace, and E. Bonek, "Deficiencies of'Kronecker'MIMO radio channel model," *Electronics Letters*, vol. 39, no. 16, pp. 1209-1210, 2003.

[79] Y. Zhou, M. Herdin, A. M. Sayeed, and E. Bonek, "Experimental study of MIMO channel statistics and capacity via the virtual channel representation," *Univ. Wisconsin-Madison, Madison, WI, USA, Tech. Rep*, vol. 5, pp. 10-15, 2007.

[80] R. Mahey and J. Malhotra, "On MIMO channel modeling for the mobile wireless systems," *International Journal of Future Generation Communication and Networking. INDIA*, vol. 8, no. 5, pp. 23-38, 2015.

[81] D. Bacon, "Modelling rain rate maps for fixed-link frequency Assignment procedures," *Ofcom contract*, no. 796, 2012.

[82] www.tpub.comneetsbook1040j.htm, ed.

[83] C. F. Bohren and D. R. Huffman, *Absorption and scattering of light by small particles*. John Wiley & Sons, 2008.

[84] M. Ajewole, L. Kolawole, and G. Ajayi, "Theoretical study of the effect of different types of tropical rainfall on microwave and millimeter‐wave propagation," *Radio Science,* vol. 34, no. 5, pp. 1103-1124, 1999.

[85] H. J. Liebe, "MPM—An atmospheric millimeter-wave propagation model," *International Journal of Infrared and millimeter waves,* vol. 10, no. 6, pp. 631-650, 1989.

[86] F. F. Amrullah, E. Setijadi, and G. Hendrantoro, "Computation of rain attenuation in tropical region with multiple scattering and multiple absorption effects using exponential drop size distribution," in *2011 XXXth URSI General Assembly and Scientific Symposium*, 2011, pp. 1-4: IEEE.

[87] R. Olsen, D. V. Rogers, and D. Hodge, "The aR b relation in the calculation of rain attenuation," *IEEE Transactions on antennas and propagation,* vol. 26, no. 2, pp. 318-329, 1978.

[88] C. Mätzler, "MATLAB functions for Mie scattering and absorption, version 2," *IAP Res. Rep,* vol. 8, no. 1, p. 9, 2002.

[89] T. M. Cover and J. A. Thomas, *Elementary of Information*

Theory. John Wiley & Sons, New York, 1991.

[90] E. Telatar, "Capacity of multi‐antenna Gaussian channels," *European transactions on telecommunications,* vol. 10, no. 6, pp. 585-595, 1999.

[91] A. Goldsmith, *Wireless communications*. Cambridge university press, 2005.

[92] P. Rayi and S. C. Ch, "Performance evaluation of channel capacity in MIMO system," *International Journal of Engineering Research and Applications (IJERA),* vol. 1, no. 4, pp. 1871-1878, 2008.

[93] V. K. Minchula and G. S. Rao, "SVD-based IWFA for next generation wireless MIMO communication," *ICT Express,* vol. 4, no. 3, pp. 171-174, 2018.

[94] A. Allam, R. M. Shubair, A. M. Hemdan, and S. Botros, "Impact of MIMO antenna design on communication channel capacity using the Kronecker model," in *2017 IEEE International Symposium on Antennas and Propagation & USNC/URSI National Radio Science Meeting*, 2017, pp. 1873-1874: IEEE.

Appendix

MATLAB functions and routines

MIMO channel matrix

```
function [H1, A, B, H, beta] = MIMO_Channel(M,N,D,freq,R)
lam = 3/(freq*10);
tc = 288;
%define constants

K = exp(-1i*2*pi/(D*1000));
d_r =lam/2;
d_t =lam/2;

Srt = pi*d_r*d_t/(lam*D*1000);
piD = 4*lam*D*1000/pi;

H_static = zeros(M,N);
for m = 1:M

    a = (((2*m-1-M)*d_r)^2)/piD;
    c = (2*m-1-M);

    for n = 1:N

    b =  (((2*n-1-N)*d_t)^2)/piD;
    d = (2*n-1-N);
    H_static(m,n) = K*exp(-1i*(a+b))*exp(1i*(Srt*(c*d/2)));

    end
end
% depths = depth2(r,freq,D);
qcoef = Mie_rain3(freq,tc, R);
% t_o = depths(1);
t_o = qcoef(2);
% t_s = depths(3);% scattering depth
t_s = qcoef(3);
% t_a = depths(2);% absorption depth
t_a = qcoef(4);
% anis = depths(4);%anisotropy factor
anis = qcoef(6);

p0 = exp(-t_o);
% free_space_loss = lam/(4*pi*D*1000); % could be ignored by normalizing
```

```
H1 = sqrt(p0)*H_static;

l0 = sqrt(3*(lam^2)*anis*(1-exp(-t_s))/(t_s*(pi^2)));
dr_l0 = (d_r/l0)^2;

beta = sqrt(exp(-t_a) - exp(-t_o));% variance of all scattered items

G_r = zeros(M,M);

for m = 1:M
     m_teta = (((2*m-1-M)*d_r)^2)/piD;
    for mp = 1:M

        mp_teta = (((2*mp-1-M)*d_r)^2)/piD;
        G_r(m,mp) = sin(Srt*N*(m-mp))*exp(-1i*(m_teta - mp_teta))/sin(Srt*(m-mp));

    end
end

% dia = min(M,N);
for dia = 1:M

    G_r(dia,dia) = 1;
end

Q_r = zeros(M,M);

for l = 1:M

    for p = 1:M

    Q_r(l,p) = exp(-1*((l-p)^2)*dr_l0);

    end
end

Hr = (Q_r .* G_r)*1/N;

G_t = zeros(N,N);
for n = 1:N
    n_teta = (((2*n-1-N)*d_t)^2)/piD;
    for np = 1:N

        np_teta = (((2*np-1-N)*d_t)^2)/piD;
        G_t(n,np) = sin(Srt*M*(n-np))*exp(-1i*(n_teta - np_teta))/sin(Srt*(n-np));
```

```
    end
end

% dia = min(M,N);
for dia = 1:N

    G_t(dia,dia) = 1 + 1i*0;
end

Q_t = zeros(N,N);

for l = 1:N

    for p = 1:N

    Q_t(l,p) = exp(-1*((l-p)^2)*dr_l0);

    end
end

Ht = G_t.*Q_t*1/M;

A = sqrtm(Hr);
B = sqrtm(Ht);

% generate a complex iid variable CN(0,1)
Wn = IID(M,N);

%generate the indirctly scattered mat according to
%H2 = beta*(A*W*B)

AW = A*Wn;
AWB = AW*B;

H2 = beta*AWB;

H = H1 + H2;

end
```

Mie Scattering coefficients (a_n, b_n)

```
function result = AB(f,dm)
% a function to calculate the Qscat, Qext, Qabs, <costeta>
% f in GHz
%dr drop diameter in mm
xx = pi*f*dm/300;% xx wave no * drop size
```

```
mw = refindex2(f,20);% to be corrected with relative index of refraction against that of air medium
nmax = ceil(xx + 4*(xx^1/3) + 2) + 1;% 1 added to nmax = xx + 4*xx^1/3 + 2 for later need

mxx = mw*xx; % product mx for bessel evaluation

n = 1:nmax;

% defining bessel J functions

BJx_h = besselj(n+.5,xx);
BJmx_h = besselj(n+.5,mxx);
BJx_l = besselj(n-.5,xx);
BJmx_l = besselj(n-.5,mxx);

BYx_h = bessely(n+.5,xx);
% BYmx_h = bessely(n+.5,mxx);
BYx_l = bessely(n-.5,xx);
% BYmx_l = bessely(n-.5,mxx);

m2 = mw^2;

anN = m2*BJmx_h.*(xx*BJx_l-n.*BJx_h)-BJx_h.*(mxx*BJmx_l-n.*BJmx_h);%nominator of an
anD = m2*BJmx_h.*(xx*(BJx_l+1i*BYx_l)-n.*(BJx_h+1i*BYx_h))-((BJx_h+1i*BYx_h).*(mxx*BJmx_l-n.*BJmx_l));% denominator of an

bnN = BJmx_h.*(xx*BJx_l-n.*BJx_h)-BJx_h.*(mxx*BJmx_l-n.*BJmx_h);
bnD = BJmx_h.*(xx*(BJx_l+1i*BYx_l)-n.*(BJx_h+1i*BYx_h))-((BJx_h+1i*BYx_h).*(mxx*BJmx_l-n.*BJmx_h));

an_n = anN./anD;
bn_n = bnN./bnD;

an = an_n(1:nmax-1);
bn = bn_n(1:nmax-1);

an_1 = an_n(2:nmax);
bn_1 = bn_n(2:nmax);

nl = n(1:nmax-1);% n all but the last term

n2_1 = 2*nl+1;%2n+1 terms
n_2 = nl.*(nl+2)./(nl+1);%n(n+2)/(n+1) terms
n2_n1 = (2*nl+1)./(nl.*(nl+1));% 2n+1/(n(n+1)) terms
```

```
x2 = xx^2;

an_bn_mag= (abs(an)).^2 + (abs(bn)).^2;
an_bn_r = real(an + bn);

qsca = (2/x2)*sum(n2_1.*an_bn_mag);
qext = (2/x2)*sum(n2_1.*an_bn_r);

an_an_con = an.*conj(an_1);
bn_bn_con = bn.*conj(bn_1);

an_bn = an.*bn;

costeta = (4/(x2*qsca))*(sum(n_2.*real(an_an_con+bn_bn_con))+sum(n2_n1.*real(an_bn)));

qabs = qext - qsca;

result = [qext qsca qabs costeta];

end
```

Cross sections

```
%calculates the Mie scattering cross sections for a given temperature for %rain rate values 1-150mm/h
function result = Mie_R(TK)

fGHz = [6 15 18 28 38 60 72 75 100 150];
R = 1:5:150;

result = zeros(length(R),5,length(fGHz));
for j = 1:length(fGHz)

nsteps=500;
% Tc = TK-273.15;

m=sqrt(epswater(fGHz(j), TK)); % calls on complex refractive index of water
% m = refindex2(fGHz,Tc);

N0=0.08/10000;             % constant in teh MP DSD/mm^4


nx=(1:nsteps)';
c0=299.793;

for t = 1:length(R)
   dD=0.01*R(t)^(1/6)/fGHz(j)^0.05;
```

```
    D=nx*dD;

    x=pi*D*fGHz(j)/c0;

    sigmag=pi*D.*D*(10^-6)/4;
    loc = find(D>7);% index of drop diameters >7mm
%     LA=4.1/R(t)^0.21;

%     NMP=N0*exp(-LA*D);
% introducing the modified lognormal distribution
  Nln = zeros(1,length(D));
for k = 1: length(D)
%    Nln(k) = ileife(R(t),D(k));
%     Nln(k) = gamma_dsd(R(t),D(k));
% % % %introducing the butare distribution
 Nln(k) = butare(R(t),D(k));

end
 Nln(loc) = 0;% remove drop diameters >7mm
%     NMP(loc) = 0;
%     sn=sigmag.*NMP*1000000;

Nln = Nln';
sn = sigmag.*Nln*1000;% drop concentration/1Km

    for jk = 1:nsteps

        a(jk,:)=Mie(m,x(jk));

    end;

    b(:,1)=D;

    b(:,2)=a(:,1).*sn;

    b(:,3)=a(:,2).*sn;

    b(:,4)=a(:,3).*sn;

    b(:,5)=a(:,4).*sn;

    b(:,6)=a(:,2).*a(:,5).*sn;

    gext= sum(b(:,2))*dD;

    gsca= sum(b(:,3))*dD;
```

```
    gabs= sum(b(:,4))*dD;

%     gb = sum(b(:,5))*dD;

    gteta=sum(b(:,6))*dD/gsca;

    res(t,:) =[R(t) gext gsca gabs gteta];
end
result(:,:,j)=res;
end
end
```

I. I. D variable generator

```
function W = IID2(M,N)
%generated an MxN matrices with iid elements of N(0,1)
nsample = 1000;
rng(0,'twister');% fix the random number generator

a1 = randi(1000);

% a complex random number generator with CN(0,1)
Wsample = (randn(M, N, nsample) + 1i * randn(M, N, nsample)) / sqrt(2);
W = Wsample(:,:,a1);
end
```

DSD models

```
% the Marshall-Palmer distribution
function N = mp(r,D)
%r the rain rate
%D the drop diameter
    N0 = 8000;% constant in mm^-1m^-3
    l = 4.1/(r^.21);
    N = N0*exp(-D*l);

End
function N = butare(r,dD)
% returns the drop size distribution
% according to modified lognormal distribution of butare, Rwanda by Alonge, Sumbiri
C = 2.93;%normalization constant
if r < 5
    mu = -.01053 + .1754*log(r);
    stdd = .1095 + .0172*log(r);
```

```
    a = 2.8875*(r^.1504);
end
if (r>=5) && (r<10)

    mu = -.1785 + .26974*log(r);
    stdd = .1128 + -.017*log(r);
    a = 2.2146*(r^.4247);
end
if (r>=10) && (r<40)

    mu = -.232 + .2869*log(r);
    stdd = .0817 + -.002*log(r);
    a = 1.2755*(r^.6425);
end
if r >= 40

    mu = .6065 + .0599*log(r);
    stdd = .1067 +.008*log(r);
    a = 8.5443*(r^.1477);
end
N0 = [137.227 157.525 165.48 293.384];
Ra = [4.95 9.9 27.7 75.28];
NT = pchip(Ra,N0,r); % extra ploation

fDi = exp((-1*(log(dD)-mu)^2)/(2*stdd))*(1 + a*exp(-dD))/(dD*sqrt(2*pi*stdd));

N = NT*fDi;
% index0 = find(N <=.01);
% N(index0) = 0;
end
```

Attenuation

```
%calculates the attenuation as per given in ITUR-P.530-16 and 838-3 for specific atenuation
d = input('Enter the distance in Km: ');
f = 120;
r01 = [84.77 43.01 41.81 58.44 50.47522229 41.501868 50.87505189 53.59338645];% r001
values according to itur 837-7
p0 = [10 1 .9 .8 .5 .1 .09 .08 .05 .03 .02 .009 .008 .005 .003 .002 .001];

y001 = zeros(1,length(r01));
a001 = zeros(1,length(r01));
a_per = zeros(length(r01),length(p0));

for j = 1:length(r01)
```

```
    aad = Rec838_3(f,0,0,r01(j));
    y001(j) = aad(3);
    a = aad(1);
    k = aad(2);
    red_fac = 1/(.477*d^.633*r01(j)^(.073*a)*f^.123-10.579*(1-exp(-.024*d)));
     if red_fac < .4
     red_fac = 2.5;
     end
     d_eff = d*red_fac;
   a001(j) = y001(j)*d_eff;

end

for v = 1:length(a001)
   for n = 1:length(p0)
      a_per(v,n) = a001(v)*att_p(p0(n),f);
   end
end

% calculate the specific attenuation by using the extinction coefficient
function resul = specific_extinction(tk)
fG = 5:2:199;
r01 = [122.9 71.88 130.49 74.64 94.00];
resul = zeros(length(fG),length(r01));
N0 = 8000;
for jk = 1:length(r01)


for j = 1:length(fG)
   m = sqrt(epswater(fG(j),tk));
   dD=0.01*r01(jk)^(1/6)/fG(j)^0.05;
   nstep = 500;
   D = (1:nstep)*dD;
   % exclude drop sizes largr than 7mm for physical reason
   pin = find(D>7);
   c0=299.793;

   x=pi*D*fG(j)/c0;

   d_area = (10^-6)*pi*D.*D/4;
   N = zeros(1,nstep);
%     ex = 4.1/(r01(j)^.21);
   q = zeros(1,nstep);
   for t = 1:nstep
%        N(t) = N0*exp(-ex*D(t)); % calling on the MP DSD
```

```
%        N(t) = ileife(r01(j),D(t));% calling the ileife DSD
         N(t) = butare(r01(jk),D(t));% % calling the modified lognormal DSD
         kol = Mie(m,x(t)) ;
         q(t) = kol(1) ;

         end

         N(pin) = 0;
         hg = N*dD*4.343;
         dfd = (d_area.*q);
         u = dfd.*hg;
         resul(j,jk) = 1000*sum(u);
end

end
```

Capacity calculation

```
function [Cw, Cwo]= capa_snr(fGHz,R)
%Parameter
% fGHz frequency in GHz
% R is the rain rate
             % rain rate value vector
Mt=51;                  % Number of transmit antennas
Mr=51;                  % Number of receive antennas
D = 1;
% [a1 a2 a3 a4 a5] = MIMO_Channel()
K= 100;                 % Number of iteration
EsN0dB=0:2:30;          % Average signal-to-noise ratio in dB scale
EsN0=10.^(0.1*EsN0dB);  % Average signal-to-noise ratio in linear scale

for ind=1:length(EsN0dB)    % loop for rain rate
    [a1, a2, a3, a4, a5] = MIMO_Channel(Mr,Mt,D,fGHz,R);

    Cwo_temp=0;            %Initial value
    Cw_temp=0;             %Initial value

    for k=1:K              %loop for K sample per SNR

        %Generating channel channel matrix H ~ZMCSCG AWGN
        W=(1/sqrt(2))*(randn(Mr,Mt)+ 1i*randn(Mr,Mt));
        a2w=a2*W;
        a2wa3=a2w*a3;
        H = a1 + a5*a2wa3;
        lamda=sort(eig(H*H'),'descend');    % eigenvalue of H*H'
        r=rank(H);             % rank of H matrix
```

```
    % Waterfilling algorithm
        p=1;
    while 1
        inv_lamda=zeros(1,r);   % initialize invert lamda vector
        for n=1:r-p+1
          inv_lamda(n)=1/lamda(n); %invert lamda vector
        end
        %Evaluate micro value
        mic = (Mt/(r-p+1))*(1+ (1/EsN0(ind))*sum(inv_lamda));
        %Evaluate gamma value based on micro
        for n=1:r-p+1
             gamma(n)= mic - Mt*(inv_lamda(n))/EsN0(ind);
        end
        %Making decision for gamma(r-p+1) and p
        if(gamma(r-p+1)<0)
           gamma(r-p+1)=0;
           p=p+1;
        else
          break; %Stop the loop if gamma(r-p+1) is non-negative
        end
    end

  temp1=0;
  temp2=0;
  for m=1:r
    % Calculating Capacity without CSIT
    temp1=temp1 + log2(1+EsN0(ind)*lamda(m)/Mt);
    % Calculating Capacity with CSIT
    temp2=temp2 + log2(1+gamma(m)*EsN0(ind)*lamda(m)/Mt);
  end
    Cwo_temp=Cwo_temp+temp1;    % Update value
    Cw_temp=Cw_temp+temp2;      % Update value
  end
  Cw(ind)=Cw_temp/K;  % Taking average value of K sample
  Cwo(ind)=Cwo_temp/K;
end
```